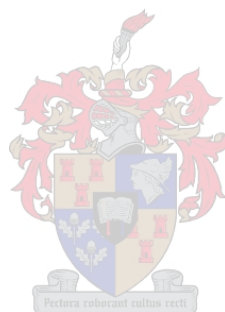


**A  $^{195}\text{Pt}$  Nuclear Magnetic Resonance and Molecular Dynamics  
Computer Simulation Study of the Solvation of Simple Platinum  
(IV) Chlorido Complex Anions in Water and Water-Miscible  
Solvent Mixtures**

By

Leon de Villiers Engelbrecht



*Dissertation presented for the degree of Doctor of Philosophy  
in the Faculty of Science at Stellenbosch University*

Promoter: Prof Klaus R. Koch

March 2017

## **Declaration**

By submitting this thesis electronically, I declare that the entirety of the work contained therein is my own, original work, that I am the sole author thereof (unless to the extent explicitly otherwise stated), that reproduction and publication thereof by Stellenbosch University will not infringe any third party rights and that I have not previously in its entirety or in part submitted it for obtaining any qualification.

Signed: .....

Leon de Villiers Engelbrecht

March 2017

Copyright © 2017 Stellenbosch University

All rights reserved

## Acknowledgements

*I would like to thank the following people*

My supervisor, Prof Klaus Koch, for his guidance and support throughout my studies, for the freedom and all the opportunities

Elsa Malherbe and Jaco Brand of the Stellenbosch University NMR lab

Technical staff at the Analytical Chemistry section: Deidre Davids, Shafiek Mohammad and Roger Lawrence

Past and present members of the PGM research group at Stellenbosch University

Aatto Laaksonen, for his support and for making available computational resources; also students at the MMK department at Stockholm University, especially Matúš Rebič and Aleksander Jaworski

Yuan Fang, Evgeny Morozov, Pavel Yushmanov and István Furó at the Physical Chemistry department at KTH for making available NMR facilities, lots of assistance with experiments and helpful discussion

Francesca Mocci and Pino Saba at the University of Cagliari for their interest, support, and friendship

The Swedish National Infrastructure for Computing (SNIC) for providing computational resources

The University of Stellenbosch, AngloPlatinum and the National Research Foundation for financial support

Eleonora for her love and motivation

My family for their love and support throughout my studies

## Publications

- I. Engelbrecht, L.; Murray, P.; Koch, K. R. *Inorg. Chem.* **2015**, *54* (6), 2752–2764.
- II. Xian, L.; Engelbrecht, L.; Barkhuysen, S.; Koch, K. R. *RSC Adv.* **2016**, *6*, 34014–34018.
- III. Koch, K. R.; Engelbrecht, L. *Dalton Trans.* **2016**, submitted.

## Conference Proceedings

<i>INORG2013</i> South African Chemical Institute Durban, South Africa, 2013	Poster presentation
<i>Analitika 2014</i> Parys, South Africa, 2014	Poster presentation
<i>Multiscale Modelling of Materials and Molecules 2016</i> eSSSENCE Meeting Uppsala, Sweden, 2016	Poster presentation

---

## Abstract

A combined  $^{195}\text{Pt}$  NMR spectroscopy and Molecular Dynamics (MD) computer simulation study of the solvation of the octahedral Pt(IV) complex  $[\text{PtCl}_6]^{2-}$  in binary mixtures of water and the fully water-miscible organic solvents methanol, 2-methoxyethanol and 1,2-dimethoxyethane has been carried out. A recent  $^{195}\text{Pt}$  NMR chemical shift-trends study indicated a preferential solvation of the aforementioned platinum complex by the organic solvent component in such solvent mixtures. The solvent dependence of the intrinsic  $^1\Delta^{195}\text{Pt}(^{37/35}\text{Cl})$  NMR isotope shifts of  $[\text{PtCl}_6]^{2-}$  in pure solvents indicate a slight increase in magnitude  $\sim 7$  ppb in the order water < methanol < 2-methoxyethanol < 1,2-dimethoxyethane. In selected equimolar binary mixtures of water and organic solvents,  $^1\Delta^{195}\text{Pt}(^{37/35}\text{Cl})$  is found to be similar in magnitude to that in the pure *organic* solvents, supporting the proposed preferential solvation of the platinum complex.  $^{195}\text{Pt}$  NMR  $T_1$  spin relaxation times and pulsed gradient spin echo (PGSE) translational diffusion measurements were performed for  $[\text{PtCl}_6]^{2-}$  in selected solvents and binary mixtures. The results were interpreted in the context of hydrodynamic continuum models of molecular diffusion; while these were found to be not strictly appropriate, the rotational and translational dynamics results appear to be notionally consistent with the preferential solvation phenomenon as indicated. A series of classical MD computer simulations were performed for  $[\text{PtCl}_6]^{2-}$  in these equimolar binary solvent mixtures, using a recently revised force field developed by Naidoo *et al.* The results using the standard force field indicate a strong preference for *water* in the primary solvation shell region of the complex in all solvent mixtures studied. A similar result is obtained for  $[\text{PtCl}_4]^{2-}$  in an equimolar water–methanol mixture. Simulations were repeated with ionic charges scaled according to the recently developed Molecular Dynamics in Electronic Continuum (MDEC) theory, which is intended to account for the dielectric screening of charges in condensed phases. In these MDEC simulations, a significant reduction in the contribution of water to the primary solvation shells of both complexes is observed; this is particularly evident in the solvation shell of  $[\text{PtCl}_6]^{2-}$  in mixtures of water with 2-methoxyethanol and 1,2-dimethoxyethane, for which a strong preferential solvation by the organic components has been indicated. Dynamic properties were also computed from MD trajectories, and are qualitatively consistent with experimental trends, but deviate due to the solvent model combination. Finally, an interpretation of the fascinating  $^{35/37}\text{Cl}$  and  $^{16/18}\text{O}$  isotope-induced fine structure in the  $^{195}\text{Pt}$  NMR spectra of complexes of the type  $[\text{PtCl}_n(\text{OH})_{6-n}]^{2-}$ ,  $n = 0-5$ , is

presented, based on the expected *trans*-influence series of ligands for Pt(IV)  $\text{OH}^- > \text{Cl}^- > \text{H}_2\text{O}$  in aqueous solution.

---

## Opsomming

'n Gekombineerde  $^{195}\text{Pt}$  KMR spektroskopie en Molekulêre Dinamika (MD) rekenaarsimulasie studie van die solvasie van die oktahedriese Pt(IV) kompleks  $[\text{PtCl}_6]^{2-}$  in binêre mengsels van water en volledig water mengbare organiese oplosmiddels metanol, 2-metoksiëtanol en 1,2-dimetoksiëtaan is uitgevoer. 'n Onlangse studie van  $^{195}\text{Pt}$  KMR chemiese verskuiwings (frekwensies) het 'n voorkeur solvasie vir solvasie van die platinum kompleks deur die organiese komponent in sulke mengsels aangedui. Die  $^1\Delta^{195}\text{Pt}(^{37/35}\text{Cl})$  KMR isotoopverskuiwing van  $[\text{PtCl}_6]^{2-}$  in suiwer oplosmiddels toon 'n relatief klein toename van  $\sim 7$  ppb in die orde van oplosmiddels, water < metanol < 2-metoksiëtanol < 1,2-dimetoksiëtaan. Die  $^1\Delta^{195}\text{Pt}(^{37/35}\text{Cl})$  verskuiwing gemeet in sekere ekwimolare binêre mengsels van water en organiese oplosmiddels is soortgelyk in grootte aan die verskuiwing in die suiwer organiese oplosmiddel, in ooreenkoms met die voorgestelde voorkeur vir die organiese komponent.  $^{195}\text{Pt}$  KMR  $T_1$  kenmerkende tye en translasionele diffusiekoëffisiente m.b.v. die gepulste gradient spin-echo (PGSE) tegniek, is ook gemeet vir  $[\text{PtCl}_6]^{2-}$  in geselekteerde oplosmiddels en binêre mengsels. Die resultate word geïnterpreteer in die konteks van hidrodinamiese modelle van molekulêre diffusie, en alhowel daar gevind word dat sulke modelle nie geskik is vir hierdie doel, word getoon dat die resultate nietemin algemeen konsistent is met die voorgestelde oplosmiddelvoorkeur, soos aangedui. 'n Reeks klassieke MD rekenaarsimulasies van  $[\text{PtCl}_6]^{2-}$  in binêre oplosmiddelmengsels is uitgevoer deur gebruik te maak van 'n onlangs-hersiene model wat deur Naidoo *et al.* ontwikkel is. Die resultate van simulasies, wat met die standaard model vir die platinum kompleks uitgevoer is, toon 'n sterk voorkeur vir *water* in die onmiddellike omgewing van die kompleks in alle gebestudeerde mengsels. 'n Soortgelyke resultaat is verkry vir die vierkantig-planêre  $[\text{PtCl}_4]^{2-}$  in 'n ekwimolare water–metanol mengsel. Die simulasies is herhaal deur ioniese ladings aan te pas volgens die onlangs ontwikkelde Molekulêre Dinamika in Elektroniese Kontinuum (MDEK, oorspronklik *MDEC*) teorie, wat deels voosiening maak vir die diëlektriese afskerming van gelaaiede partikels in gekondenseerde fases. In hierdie MDEK simulasies word 'n merkbare afname in die bydrae deur water tot die primêre oplosmiddel omgewing van beide komplekse waargeneem: die effek is veral ooglopend in die geval van  $[\text{PtCl}_6]^{2-}$  in mengsels van water met 2- metoksiëtanol en 1,2-dimetoksiëtaan, waarin 'n sterk voorkeur vir die organiese komponent eksperimenteel waargeneem is. Dinamiese inskappe is ook van MD trajekte bereken, en toon tendense soortgelyk aan eksperimentele waardes, maar wyk af weens die oplosmiddelmodel. Verder is 'n interpretasie van die fassinerende

---

$^{35/37}\text{Cl}$  en  $^{16/18}\text{O}$  isotoopgeïndusseeerde fynstruktuur in die  $^{195}\text{Pt}$  KMR spektra van komplekse met vorm  $[\text{PtCl}_n(\text{OH})_{6-n}]^{2-}$ ,  $n = 0-5$ , voorgestel, gebaseer op die verwagte *trans*-invloedreeks van ligande vir Pt(IV)  $\text{H}_2\text{O} < \text{Cl}^- < \text{OH}^-$  in waterige oplossing.



---

## Table of Contents

Declaration.....	ii
Acknowledgements.....	iii
Publications and Conference Proceedings.....	iv
Abstract.....	v
Opsomming.....	vii
Table of Contents.....	ix

### Chapter 1. Introduction

1.1 General introduction and context of the study.....	1
1.2 Ion solvation.....	3
1.3 Mixed solvents and preferential solvation.....	4
1.4 NMR spectroscopy: basic concepts.....	8
1.5 Rationale and general objectives of the study.....	11
References.....	14

### Chapter 2. A study of Solvent Effects on $^{195}\text{Pt}$ NMR Isotope Shifts, and the Implications of the *trans*-influence in the $^{195}\text{Pt}$ NMR Spectra of $[\text{PtCl}_n(\text{OH})_{6-n}]^{2-}$ , $n = 1-5$ , in Aqueous Solution

Abstract.....	16
2.1 Introduction	
2.1.1 $^{195}\text{Pt}$ NMR spectroscopy: an overview.....	17
2.1.2 Solvent effects on $^{195}\text{Pt}$ NMR chemical shifts.....	18
2.1.3 Chemical speciation of platinum complexes.....	21
2.1.4 NMR isotope shifts.....	22
2.1.5 Rationale and aims.....	28
2.2 Technical information	
2.2.1 Chemical shift referencing.....	30
2.2.2 Processing of NMR data.....	33
2.2.3 Sample preparation and instrumentation.....	39
2.3 Results and discussion	
2.3.1 $^{195}\text{Pt}$ NMR isotope shifts and the <i>trans</i> -influence.....	40

---

2.3.2	Temperature dependence of $^{195}\text{Pt}$ NMR chemical shifts: some background .....	45
2.3.3	Effect of solvent on $^{195}\text{Pt}$ NMR chemical shifts of Pt complexes.....	47
2.3.4	The effect of solvent on $^{195}\text{Pt}$ NMR isotope shifts.....	50
2.3.5	Effect of partial deuteration on $^{195}\text{Pt}$ NMR chemical shifts.....	55
2.3.6	Chemical speciation .....	57
2.4	Conclusions .....	62
	References.....	64

### **Chapter 3. A Study of the Dynamic Properties of Hexachloroplatinate (IV) in Binary Mixtures of Water and Selected Organic Solvents using $^{195}\text{Pt}$ NMR Spectroscopy**

Abstract .....	67	
3.1	Introduction	
3.1.1	Molecular motion in solution: some background .....	68
3.1.2	Relaxation in NMR spectroscopy .....	70
3.1.3	Pulsed gradient spin–echo (PGSE) experiments.....	71
3.1.4	Rationale and aims .....	73
3.2	Materials and methods	
3.2.1	Sample preparation and instrumentation.....	75
3.2.2	Measurement of $^{195}\text{Pt}$ NMR relaxation times.....	75
3.2.3	Measurement of translational diffusion coefficients.....	77
3.3	Results and discussion	
3.3.1	Relaxation times and molecular rotation.....	82
3.3.2	Translational diffusion .....	90
3.4	Conclusions .....	94
	References.....	96

### **Chapter 4. Molecular Dynamics Simulation Study of the Solvation of $[\text{PtCl}_6]^{2-}$ and $[\text{PtCl}_4]^{2-}$ in Binary Solvent Mixtures**

Abstract .....	99	
4.1	Introduction	
4.1.1	Molecular Dynamics simulations: some background .....	100
4.1.2	Molecular Mechanics .....	101

---

4.1.3	More technical aspects of MD simulations .....	102
4.1.3.1	Periodic Boundary Conditions .....	102
4.1.3.2	Temperature and pressure coupling .....	103
4.1.4	Aims .....	105
4.2	Technical details	
4.2.1	Simulation details.....	106
4.2.2	Trajectory analysis .....	108
4.3	Results and discussion .....	112
4.3.1	Solvation shell structure.....	112
4.3.2	Rotational motion.....	125
4.3.3	Translational motion .....	127
4.4	Summary and concluding remarks.....	129
	References.....	131
<b>Chapter 5.</b>	<b>General Discussion and Conclusions .....</b>	<b>134</b>

## **Appendix**

# 1. Introduction

## 1.1 General introduction and context of the study

The platinum group metals (PGMs) platinum (Pt), palladium (Pd) and rhodium (Rh) are used extensively as automobile emission control catalysts (“autocatalysts”).<sup>1</sup> These metals are also used as supported catalyst in other industries, e.g. naphtha reforming.<sup>2</sup> In the case of platinum specifically, the former accounts for about half of the annual platinum demand, and autocatalyst demand has increased in recent years. Other significant contributions are jewellery, owing to the high corrosion resistance and shine of the metal, and as investment in the form of exchange-traded products (ETFs) as well as physical bars and coins, notably by Japanese investors.<sup>1</sup> South Africa produces about three quarters of the annual global platinum supply, and also has by far the largest estimated reserves (Fig. 1.1).<sup>3</sup> Recovery, or recycling, of platinum from used autocatalysts in particular has also increased in recent years.<sup>1</sup>

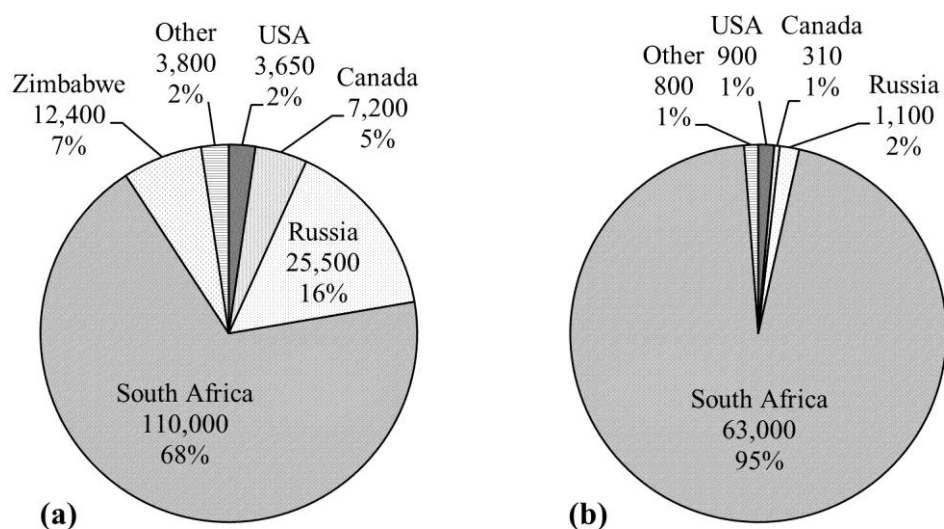


**Figure 1.1** (a) Platinum mine production in kilograms in 2014, and (b) estimated PGM reserves by country in tonnes (1000 kg).<sup>3</sup>

The PGMs are often found closely associated, also with other elements e.g. gold and various base metals, and are dissolved by oxidation (typically with chlorine, or other oxidising agents e.g. sodium chlorate and/or bromate) in highly acidic chloride-rich aqueous solutions, where they are then present as anionic chlorido-complexes,  $[MCl_n]^{n-x}$ , where  $x$  is the oxidation state and  $n$  the coordination number (typically 4 or 6) of the metal  $M$ .<sup>4</sup> Modern industrial separation of these anionic complexes may be achieved by a combination of techniques, but



## 1.2 Ion solvation

The nature of hydration (solvation by water) of ions has been studied extensively for more than a century.<sup>8</sup> Interactions between ions and water molecules determine their solubility and affect chemical reactions in aqueous solution, also in biological media; on the other hand, studies of the effect of ions on the structure of water, which itself is complex and the subject of continued scientific interest, has led to classification of ions as water structure “makers” or “breakers”, based on several observable properties.<sup>9,10</sup> A key feature of the hydration of ions is the local ordering, or reorientation, of the polar water molecules in the electric field of the ion, which is, of course, different for cations and anions.<sup>9</sup> The effect of ions on the orientation and dynamic characteristics of water molecules naturally is also dependent on the distance from the ion, and the notion of concentric spherical layers of water molecules, or hydration shells, surrounding simple monoatomic ions is well-established in general chemistry, especially in the case of cations (Fig. 1.3). Another recurring theme in studies of the hydration of such monoatomic ions, is that of cations, like sodium, being more strongly hydrated than anions, like chloride and the other halide anions, i.e. hydration shells are more rigid with longer residence times of the water molecules in the vicinity of the cation.<sup>9</sup>

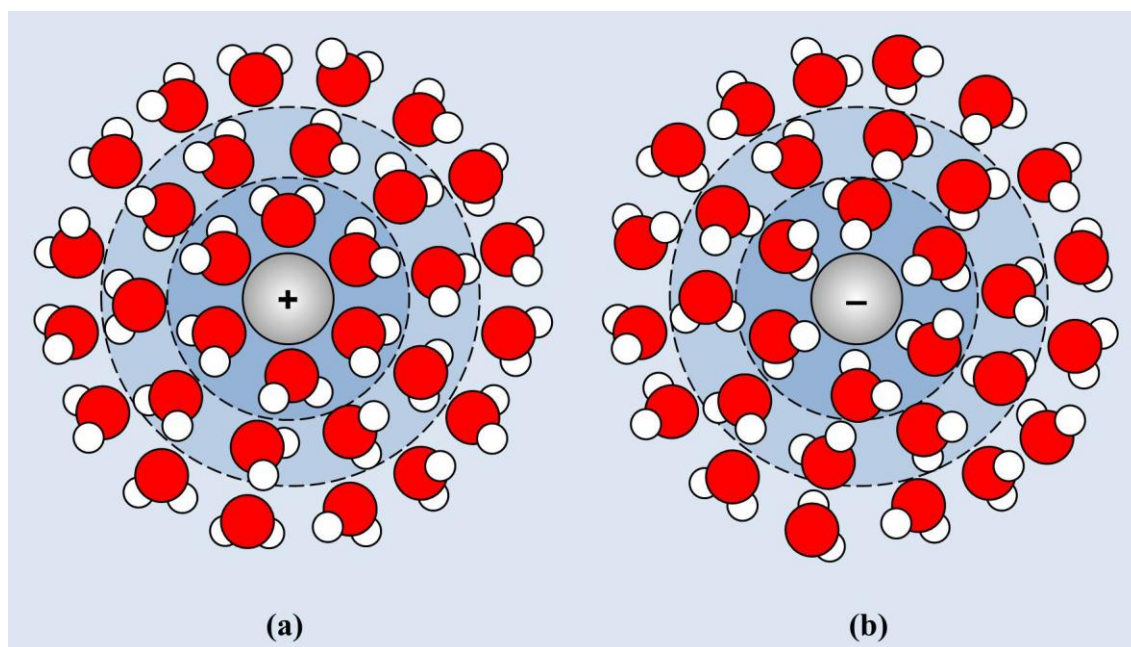


**Figure 1.3** Schematic representations of conceptual concentric hydration shells of simple cations and anions. Water molecules shown in red (O) and white (H).

Experimental studies of the hydration structure of ions, in particular, make use of both scattering methods, e.g. X-ray, electron and neutron diffraction methods, and spectroscopic techniques, which include X-ray absorption (extended X-ray absorption fine structure, EXAFS, and X-ray absorption near edge structure, XANES, methods), vibrational (infra-red and Raman) and nuclear magnetic resonance (NMR) spectroscopy.<sup>11</sup> The experimental technique of choice depends upon the particular system studied, and may provide information regarding the number and orientation of water molecules interacting with ions in solution, including geometric information (often by scattering techniques) and dynamic characteristics, e.g. translational and reorientational motions of water molecules or ions (usually by NMR). Additionally, computational methods, specifically *ab initio* electronic structure calculations (e.g. based on Density Functional Theory, DFT) and Molecular Dynamics (MD) and Monte Carlo (MC) computer simulations, have provided valuable insights regarding the nature of ion hydration, often in combination with experimental results.<sup>11,12</sup>

The solvation of ions in solvents other than water, on the other hand, has been less extensively studied in general,<sup>8,9</sup> but is also of considerable fundamental and practical importance; consider, for example, battery electrolytes and solvent extraction processes in the precious metal refining industry mentioned above. A notable exception is the numerous studies of the nature of solvation of monoatomic ions in *solvent mixtures*, particularly binary mixtures of water and organic compounds, where preferential solvation of the ion by one of the solution components may occur.<sup>13</sup>

### 1.3 Mixed solvents and preferential solvation

Preferential solvation of a solute in a multicomponent solvent mixture refers essentially to a difference between the solvent composition in the immediate vicinity of the ion (local composition) compared to that of the bulk solvent mixture, i.e. a relative excess of one solvent component in the vicinity of the ion (its solvation environment, or solvation shells).<sup>14</sup> Theoretical treatments of the problem of preferential solvation have been presented, notably by Marcus<sup>15</sup> and Ben-Naim,<sup>14</sup> and make use of the local mole fraction of a solvent in the vicinity of the solute, the formal definition of which will be given at a later stage, but is illustrated in Fig. 1.4. In particular, these considerations require knowledge of the solvation number(s) of the solute, which can be determined from pair correlation, or more commonly, radial distribution functions (RDFs).<sup>14</sup> RDFs describe the average radial distribution of



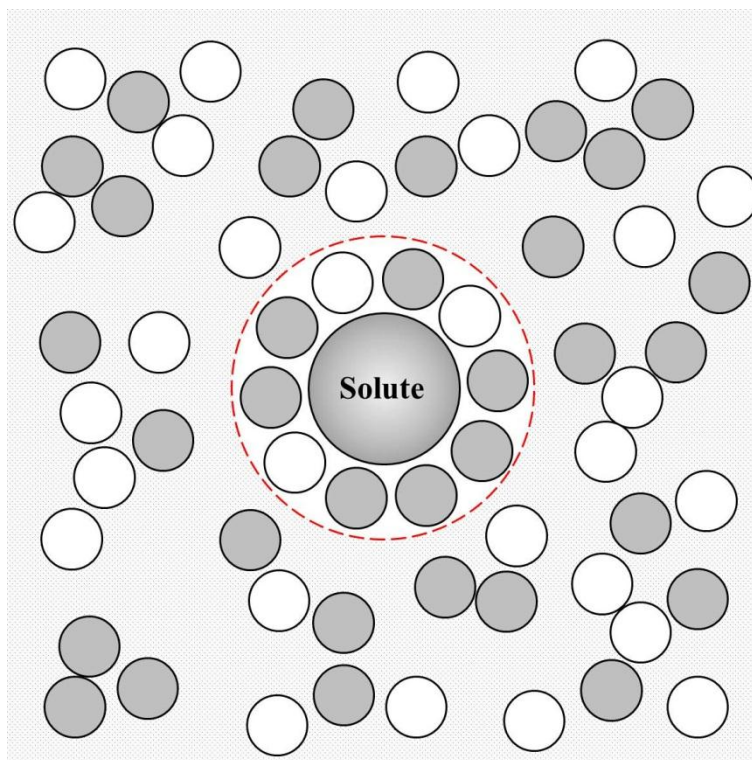


**Figure 1.4** Scheme illustrating preferential solvation of a simple solute (e.g. an ion) in a binary solvent mixture, the components of which are grey and white spheres. The composition of the primary solvation shell (7 grey and 3 white particles), the boundary of which is indicated in red, differs from that of the surrounding bulk solvent mixture (equal amounts grey and white solvent particles).

particles in liquids and solution, characterising their static structures; information regarding these functions may be obtained experimentally from scattering methods (e.g. X-ray diffraction), or, more commonly, from MD computer simulations. A simple drawing showing the characteristic features of a typical RDF,  $g(r)$ , of a pure liquid is shown in Fig. 1.5 (a), based on a similar scheme by Ben-Naim.<sup>14</sup> Maxima, or peaks, in the function indicate the positions of solvation shells, the closest being the primary shell which is in direct contact with the solute, while the minima correspond to their approximate boundaries. Note that at distances greater than a few particle (molecular) diameters,  $\sigma$ , the function attenuates to unity: this feature results from the normalisation of the function to the bulk density of the particle under consideration, i.e. average bulk solution structure resumes.<sup>14</sup> Technical aspects of the evaluation of RDFs from the results of computer simulations will be presented in Chapter 4.

While preferential solvation of a solute by a particular component in a solvent mixture may be expected intuitively to result from a competition between the different solvent components, where one interacts intrinsically more favourably with the solute, this is not

necessarily the case and the underlying reason for the observed preference is not known in general, resulting from a delicate balance of solvent–solvent and solvent–solute interactions which may be dependent possibly upon several factors e.g. mixed solvent composition and temperature. Indeed, such solvent mixtures may have complex microscopic structures and other anomalous properties which themselves have been extensively and actively studied by experimental and computational techniques.<sup>16,17</sup> Of particular interest are binary mixtures of water and polar organic compounds; classic examples include methanol,<sup>17</sup> acetonitrile<sup>18</sup> and dimethyl sulfoxide (DMSO).<sup>19</sup> Finally, solvation phenomena are expected to be much more complex for polyatomic solutes containing atomic groups with different properties, specifically organic compounds, as has been demonstrated e.g. for phenol and carbohydrates in mixed solvents.<sup>20,21</sup>

Experimental studies of preferential solvation of simple solutes in binary solvent mixtures typically involve measurements of solute properties that are expected to be dependent on the nature of the local solvation environment of the solute.<sup>14</sup> In the case of monoatomic ions, specifically, NMR spectroscopy has been used extensively, where the ion nucleus (e.g. <sup>23</sup>Na) NMR frequency, or chemical shift  $\delta$ , is measured at various bulk mixed solvent compositions, ideally at low salt concentration.<sup>13</sup> The variation of such properties with bulk

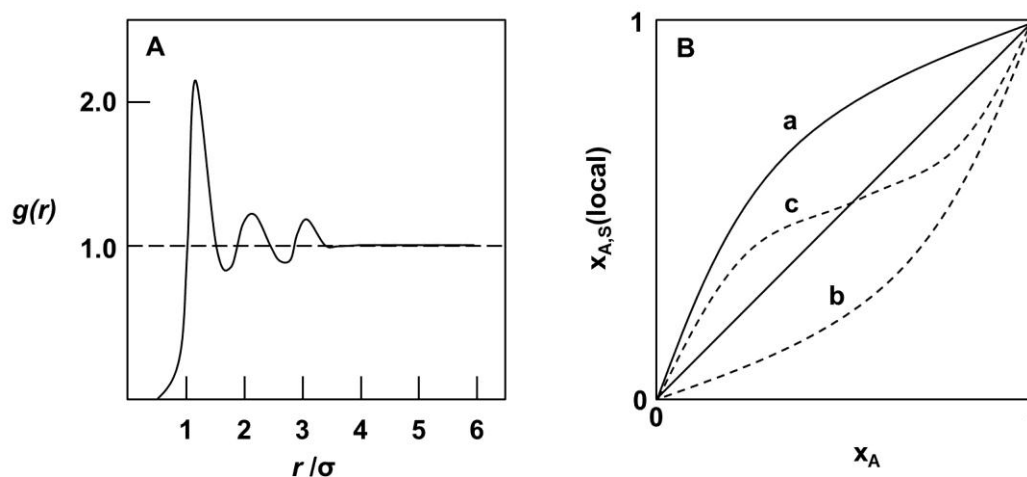


**Figure 1.5** Schematic representations of (a) typical features of the radial distribution function,  $g(r)$ , of a pure liquid, with distance  $r$  between solvent particles given in units of the solvent diameter ( $\sigma$ ); (b) plot showing variation in local solvent composition (fraction A) in the vicinity of solute S as a function of bulk solvent composition (mole fraction A,  $x_A$ ): lines a and b indicate positive and negative preferential solvation of S by A, while c shows a scenario where the sign of preferential solvation changes with  $x_A$ . Adapted from Ben-Naim.<sup>14</sup>

solvent composition is assumed to reflect changes in the solvent composition of the primary (closest) solvation shell of the ion; examples of typical cases are shown in Fig. 1.5 (b), a reproduction of a scheme by Ben-Naim,<sup>14</sup> for a solute S dissolved in a binary mixture of solvents A and B. Here, the local solvent composition in the vicinity of S, given as a contribution by component A (the local mole fraction of A,  $x_{SA}$ ) is shown as a function of the bulk mixed solvent composition (bulk mole fraction of A,  $x_A$ ). Here, of course, a mole fraction A of 0 indicates pure solvent component B, while a value of 1 corresponds to pure component A. However, as noted by the Ben-Naim, the approach described above may be an approximation only, since there is, in general, no theoretical support that the property ( $\delta$ ) should necessarily be a local composition-weighted average of the same property measured in the pure solvent components, e.g. that in the absence of preferential solvation, where the local composition changes linearly with bulk composition (straight solid diagonal line in Fig. 1.5 (b)), the measured property  $\delta$  should *necessarily* follow a similar trend. This effect may additionally dependent on the particular solute property measured.<sup>14</sup>

Models for the interpretation of specifically solute NMR chemical shift data related to preferential solvation of monoatomic ions in binary solvent mixtures have been presented e.g. by Covington and co-workers,<sup>22</sup> and require, among other conditions, that the total number of solvent molecules (A + B) surrounding the solute, the solvation number, remains constant over the entire bulk solvent composition range. In the next section, a brief introduction to the fundamental aspects of NMR spectroscopy is presented, specifically the definition of the NMR chemical shift.

## 1.4 NMR spectroscopy: basic concepts

Many atomic nuclei, or specific isotopes of chemical elements, possess a property called spin, denoted  $I$ , as does many other subatomic particles e.g. electrons and other fundamental particles.<sup>23</sup> Particles can have either half-integer (fermions) or integer spin (bosons); in the context of NMR spectroscopy, nuclei with spin  $1/2$  are particularly important (since these include  $^1\text{H}$  and  $^{13}\text{C}$ , the most frequently studied isotopes) and are commonly referred to as dipolar nuclei; nuclei with spin  $> 1/2$  (half-integer or integer) are called quadrupolar nuclei, for reasons described below. Associated with this intrinsic spin property, is a nuclear magnetic moment,  $\mu$ , which enables magnetic interactions of the nucleus. The relationship between the nuclear spin (angular momentum property) and the associated magnetic moment for a particular nucleus is described by its magnetogyric ratio,  $\gamma$ .

$$\mu = \gamma I \quad (1.1)$$

When a nucleus having non-zero spin is placed in an external (or “applied”) magnetic field, as is done in an NMR experiment, its magnetic moment interacts with the external field; this is known as the Zeeman interaction. The result of this Zeeman interaction is that the energy of a nuclear spin in the presence of an external magnetic field is quantised, i.e. only specific orientations of the magnetic moment are allowed, each with defined energy. In the case of a dipolar (spin  $1/2$ ) nucleus, two nuclear spin energy levels exist in an external magnetic field: one with magnetic moment aligned with the external magnetic field vector, the other opposing it, the latter being the higher-energy orientation. In the case of quadrupolar nuclei, a greater number of energy levels exist, specifically  $2I + 1$ . The difference in energy between such nuclear spin energy levels is dependent on the strength of the applied magnetic field, and increases in magnitude with increasing external magnetic flux density,  $B_0$  (tesla, T). When an ensemble of identical nuclei with non-zero spin are placed in the applied magnetic field, the nuclei distribute among energy levels, and the occupancies of these are very nearly equal, with a slight excess in the lower level. The small difference in occupancy is due to the fact that the energy difference between the nuclear spin energy levels is extremely small, even at high magnetic fields, and only this small excess nuclei residing in the lower level is observed in an NMR experiment.

When electromagnetic radiation of frequency matching the nuclear spin energy level difference (Larmor, or resonance frequency, in the radio-frequency range) is applied to a nuclear ensemble in an external magnetic field, transitions between the nuclear spin energy levels can be induced, a condition referred to as resonance. Following the perturbation of the equilibrium distribution of nuclear spins (which is temperature dependent), a slow thermal re-equilibration period follows during which the nuclei exchange energy with their surroundings, eventually re-establishing the equilibrium distribution. Depending on the nature of the sample studied, this process, known as nuclear spin relaxation, can require up to several tens of seconds. It is during this thermal re-equilibration process that the NMR signals are detected, and the nuclear spin relaxation characteristics can provide important information regarding the environment of the nuclei, particularly when these are located in molecules (i.e. information regarding molecular structure and motion). More information on nuclear spin relaxation will be provided at a later stage, and the interested reader is referred to NMR textbooks for a detailed description of the various pathways, or relaxation mechanisms, by which nuclei interact with their environment.<sup>24,25</sup>

Nuclei studied by NMR spectroscopy are situated in atoms and molecules, where they are surrounded by electrons. When placed in an external magnetic field, electronic motions are induced which, in a simplified picture, act to produce an induced magnetic field which opposes the static external field.<sup>26</sup> Nuclei situated in such electronic environments, then, do not experience the full strength of the external magnetic field, but rather an effective field, which is the sum of the external and induced fields. This effective magnetic field is weaker than the external field, with magnetic flux densities  $B_{\text{eff}} < B_0$ ; the phenomenon is known as nuclear magnetic shielding, or simply shielding, with the effective magnetic field given by  $B_{\text{eff}} = B_0(1 - \sigma)$ , where  $\sigma$  is a small dimensionless constant known as the magnetic shielding (usually reported in parts per million, ppm). The resonance frequency, typically tens to hundreds of MHz, of a nucleus shielded by electrons is given by:

$$\nu = \frac{\gamma}{2\pi} B_0(1 - \sigma) \quad (1.2)$$

Naturally, the amount of magnetic shielding, i.e. the magnitude of  $\sigma$  that a particular nucleus experiences in, for example, a molecule, depends on the nature of its electronic environment, and in general  $\sigma$  is a second-rank tensor, varying with orientation of the molecule in the external magnetic field (this is averaged by rapid molecular tumbling in mobile solutions)

and consisting of shielding contributions from different physical phenomena.<sup>23</sup> However, the net effect is that identical nuclei, say  $^1\text{H}$ , fixed in the same molecule, but in different electronic environments have different resonance frequencies in the same external magnetic field. This phenomenon is known as the chemical shift. The existence of the chemical shift, originally referred to as the chemical effect, is what makes the NMR phenomenon useful in chemistry, particularly in the characterisation of chemical compounds in solution.<sup>27</sup> The proposed definition of the chemical shift,  $\delta$ , also expressed in ppm, is given by:<sup>23</sup>

$$\delta_{\text{X,sample}}/\text{ppm} = \frac{(\nu_{\text{X,sample}} - \nu_{\text{X,reference}})/\text{Hz}}{\nu_{\text{X,reference}}/\text{MHz}} \quad (1.3)$$

Here, the subscript X refers to the particular nucleus studied (observed), e.g.  $^1\text{H}$ , and  $\nu_{\text{X,reference}}$  the resonance frequency of nucleus X located in a specified reference compound or sample. Recommended methods for practical NMR chemical shift referencing will be described in Chapter 3.

The many technical aspects of modern NMR spectroscopy cannot be presented in this brief introduction, and will be introduced as required in subsequent sections of this work. The interested reader is referred to textbooks for the fascinating history, fundamental aspects and technical details of NMR spectroscopy.<sup>24</sup>

## 1.5 Rationale and general objectives of the study

While a large number of NMR studies of preferential solvation of monoatomic ions in binary solvent mixture have been reported over several decades, few have considered the solvation of complex ions of transition metals.<sup>13</sup> Westra,<sup>28</sup> only relatively recently, reported  $^{195}\text{Pt}$  NMR chemical shift measurements for simple, but industrially relevant platinum complexes,  $[\text{PtCl}_6]^{2-}$  and to a lesser extent  $[\text{PtBr}_6]^{2-}$ , in binary mixtures of water and selected organic solvents and found that, in all mixtures studied, the variation of  $^{195}\text{Pt}$  chemical shifts with solvent composition appears to be consistent with a preferential solvation of the platinum complex by the *organic* solvent component over the entire mixed solvent composition range. However, as pointed out by Ben-Naim,<sup>14</sup> the interpretation of such NMR chemical shift trends in the context of preferential solvation may be complicated, since the variation in this property may not necessarily parallel changes in the composition of the primary solvation shell of the solute.

Additionally, the platinum complexes mentioned above are known to undergo chemical speciation reactions in aqueous solution, in which ligands (halide ions) are displaced by water molecules to form aquo- or hydroxido-complexes of the form  $[\text{PtCl}_n(\text{H}_2\text{O})_{6-n}]^{4-n}$  and  $[\text{PtCl}_n(\text{OH})_{6-n}]^{2-}$  respectively, where  $n = 0-5$ , depending on various factors including concentration, and the presence of excess chloride ion and other chemical species.<sup>7,29</sup> Moreover, different geometrical isomers may be present in solution. The characterisation of such complexes by  $^{195}\text{Pt}$  NMR chemical shift measurements has been demonstrated, e.g. by Kramer and Koch, however this method is not necessarily reliable or applicable in view of the sensitivity of  $^{195}\text{Pt}$  NMR chemical shift to factors such as temperature and solvent composition.<sup>29</sup> In this context, Koch and co-workers have demonstrated how the study of intrinsic  $^{35/37}\text{Cl}$  and  $^{16/18}\text{O}$ -induced isotope effects, or “isotope shifts”, in the  $^{195}\text{Pt}$  NMR spectra of the aquo-complexes introduced above can be applied for their unambiguous characterisation in aqueous solution.<sup>30,31</sup>

Initial work in the present study involved the interpretation of apparently similar isotope effects observed in the  $^{195}\text{Pt}$  NMR spectra of the related hydroxido-complexes  $[\text{PtCl}_n(\text{OH})_{6-n}]^{2-}$ ;<sup>32</sup> however, interesting differences in the detailed isotope-induced fine structure are observed when compared with that in the  $^{195}\text{Pt}$  spectra of the corresponding aquo-complexes

described above, which are shown to result from the geometric effects of the Pt(IV) ligand *trans*-influence series  $\text{OH}^- > \text{Cl}^- > \text{H}_2\text{O}$  in these aqueous solutions.

The effect of solvent on the intrinsic NMR isotope shifts of solute nuclei in general has not been studied in detail, particularly in solvent mixtures where preferential solvation of solutes may occur.<sup>33</sup> In view of the proposed preferential solvation of  $[\text{PtCl}_6]^{2-}$  in binary mixtures of water and certain water-miscible organic compounds, an important aim of this study was to determine the effect of solvent and solvent composition on the well-known  $^{35/37}\text{Cl}$  isotope-induced  $^{195}\text{Pt}$  NMR fine structure of this octahedral complex dissolved in selected organic solvents methanol, 2-methoxyethanol and 1,2-dimethoxyethane, and their binary mixtures with water. These related solvents were studied by Westra and suggested to preferentially solvate the complex to different degrees in their mixtures with water, while maintaining similar functional groups in the organic solvents; the phenomenon is described in detail in Chapter 2. The investigation additionally requires knowledge of chemical speciation reactions occurring in these solutions, which has not been studied in detail for  $[\text{PtCl}_6]^{2-}$  in non-aqueous solvents and solvent mixtures.

The dynamic properties of solutes, which include their rotational and translational motions, are also expected to depend upon the nature of their immediate solvation environment.<sup>34</sup> The  $^{195}\text{Pt}$  NMR  $T_1$  spin relaxation times of  $[\text{PtCl}_6]^{2-}$  were measured and used to determine reorientational correlation times of the complex, describing its rotational motion in the solvent mixtures, while  $^{195}\text{Pt}$  pulsed gradient spin-echo (PGSE) experiments were performed with the intention of determining translational diffusion coefficients. The results of these measurements are interpreted in the context of hydrodynamic models of molecular diffusion with the aim of obtaining additional, independent information regarding the nature of the solvation environment of the complex.

Finally, a series of Molecular Dynamics (MD) computer simulations of representative systems are performed using a platinum complex force field recently presented by Naidoo and co-workers.<sup>35</sup> The computational study is performed specifically with the aim of determining detailed solvation shell compositions of  $[\text{PtCl}_6]^{2-}$  and, to some extent square-planar  $[\text{PtCl}_4]^{2-}$ , in the binary solvent mixtures, and also to compute dynamic properties that may be directly compared with the results of the NMR experiments described above.

The specific aims of the study can be summarised as follows:



1. The full assignment and interpretation of the isotope-induced fine structure in the  $^{195}\text{Pt}$  NMR spectra of the complexes  $[\text{PtCl}_n(\text{OH})_{6-n}]^{2-}$ ,  $n = 0-5$ , both in normal and  $^{18}\text{O}$ -enriched aqueous solutions. This work is presented in Chapter 2.
2. The accurate measurement of the intrinsic  $^1\Delta^{195}\text{Pt}(^{37/35}\text{Cl})$  NMR isotope shifts in the spectrum of  $[\text{Pt}^{35}\text{Cl}_n^{37}\text{Cl}_{6-n}]^{2-}$ ,  $n = 0-6$ , in normal water, methanol, 2-methoxyethanol and 1,2-dimethoxyethane, with the aim of determining the solvent dependence of the isotope shift in these solvents (at 293 K); and similar measurements in binary mixtures of water with these organic solvents and the interpretation of the results in the context of the proposed preferential solvation on the platinum complex by the organic solvent component in these solvent mixtures. The results are also presented and discussed in Chapter 2.
3. Measurements of  $^{195}\text{Pt}$  NMR  $T_1$  spin relaxation times and pulsed gradient spin-echo (PGSE) experiments to determine respectively reorientational correlation times and translational diffusion coefficients of the complex in these solution environments, and the interpretation of the results using hydrodynamic models of molecular diffusion. This work is presented in Chapter 3.
4. Perform classical MD simulations of  $[\text{PtCl}_6]^{2-}$  in the solvent mixtures described in aim 2, using the recently revised metal solution force field reported by Naidoo and co-workers with the specific aim of determining solvation shell compositions and dynamic properties for comparison with experimental data. These computational studies are described in Chapter 4.

## References

1. *PGM Market Report May 2016*, Johnson Matthey PLC, 2016.
2. Shelimov, B.; Lambert, J. F.; Che, M.; Didillon, B. *J. Am. Chem. Soc.* **1999**, *121*, 545–556.
3. Loferski, P. *U.S. Geological Survey, Mineral Commodity Summaries, January 2015*, 2015.
4. Berfeld, G. J.; Bird, A. J.; Edwards, R. I. *Gmelin Handbook of Inorganic Chemistry*, 8th Edition, Springer-Verlag, Berlin, 1986.
5. Bernardis, F. L.; Grant, R. A.; Sherrington, D. C. *React. Funct. Polym.* **2005**, *65*, 205–217.
6. Koch, K. R.; Burger, M. R.; Kramer, K. R.; Westra, A. N. *Dalton Trans.* **2006**, 3277–3284.
7. Kramer, J.; Koch, K. R. *Inorg. Chem.* **2006**, *45*, 7843–7855.
8. Ohtaki, H. *Monatsh. Chem.* **2001**, *132*, 1237–1268.
9. Marcus, Y. *Ion Solvation*, Wiley-Interscience, Chichester, 1985.
10. Marcus, Y. *Chem. Rev.* **2009**, *109*, 1346–1370.
11. Ohtaki, H.; Radnai, T. *Chem. Rev.* **1993**, *93*, 1157–1204.
12. Impey, R. W.; Madden, P. A.; McDonald, I. R. *J. Phys. Chem.* **1983**, *87*, 5071–5083.
13. Bloor, E. G.; Kidd, R. G. *Can. J. Chem.* **1968**, *46* (22), 3425–3430.
14. Ben-Naim, A. *Pure Appl. Chem.* **1990**, *62* (1), 25–34.
15. Marcus, Y. *J. Chem. Soc., Faraday Trans. 1* **1989**, *85*, 381.
16. Corsaro, C.; Spoooren, J.; Branca, C.; Leone, N.; Broccio, M.; Kim, C.; Chen, S. H.; Stanley, E.; Mallamace, F. *J. Phys. Chem. B* **2008**, *112*, 10449–10454.
17. Lin, B.; He, X.; MacKerell, A. D. Jr. *J. Phys. Chem. B* **2013**, *117*, 10572–10580.
18. Kovacs, H.; Laaksonen, A. *J. Am. Chem. Soc.* **1991**, *113*, 5596–5605.
19. Vishnyakov, A.; Lyubartsev, A. P.; Laaksonen, A. *J. Phys. Chem. A* **2001**, *105*, 1702–1710. See also: Luzar, A.; Chandler, D. *J. Chem. Phys.* **1993**, *98* (10), 8160–8173.
20. Dahlberg, M.; Laaksonen, A. *J. Phys. Chem. A* **2006**, *110*, 2253–2258.
21. Vishnyakov, A.; Widmalm, G.; Kowalewski, J.; Laaksonen, A. *J. Am. Chem. Soc.* **1999**, *121* (23), 5403–5412.
22. Covington, A. K.; Lilley, T. H.; Newman, K. E.; Porthouse, G. A. *J. Chem. Soc. Faraday Trans. 1* **1973**, *69*, 963–972.

23. Harris, R. K.; Becker, E. D.; Cabral de Menezes, S. M.; Goodfellow, R.; Granger, P. *Pure Appl. Chem.* **2001**, *73* (11), 1795–1818.
24. Farrar, T. C.; Becker, E. D. *Pulsed and Fourier Transform NMR*, Academic Press, New York, 1971.
25. Bakhmutov, V. I. *Practical NMR Relaxation for Chemists*, John Wiley & Sons, Ltd., Chichester, 2004.
26. Ramsey, N. F. *Phys. Rev.* **1950**, *78* (6), 699–703.
27. Proctor, W. G.; Yu, F. C. *Phys. Rev.* **1950**, *77*, 717.
28. Westra, A. N. *High Resolution NMR Studies Concerning the Solvation/Hydration and Coordination Chemistry of Pt(II/IV) Compounds*, PhD Dissertation, University, 2005.
29. Kramer, J.; Koch, K. R. *Inorg. Chem.* **2007**, *46*, 7466–7476.
30. Gerber, W. J.; Murray, P.; Koch, K. R. *Dalton Trans.* **2008**, 4113–4117.
31. Murray, P.; Gerber, W. J.; Koch, K. R. *Dalton Trans.* **2012**, *41*, 10533–10542.
32. Engelbrecht, L.; Murray, P.; Koch, K. R. *Inorg. Chem.* **2015**, *54* (6), 2752–2764.
33. Hansen, P. E. *Prog. NMR. Spectrosc.* **1988**, *20*, 207–255.
34. Chowdhuri, S.; Chandra, A. *J. Chem. Phys.* **2005**, *123*, 234501-1–234501-8.
35. Matthews, R. P.; Venter, G. A.; Naidoo, K. J. *J. Phys. Chem. B* **2011**, *115*, 1045–1055.

## 2. A Study of Solvent Effects on $^{195}\text{Pt}$ NMR Chemical Shifts

and the Implications of the *trans*-Influence in the  $^{195}\text{Pt}$  NMR Spectra of  $[\text{PtCl}_n(\text{OH})_{6-n}]^{2-}$ ,  $n = 1-5$ , in Aqueous Solution

### *Papers based on results described in this chapter (Appendix)*

1. Engelbrecht, L.; Murray, P.; Koch, K. R. *Inorg. Chem.* **2015**, *54* (6), 2752–2764.
  2. Xian, L.; Engelbrecht, L.; Barkhuysen, S.; Koch, K. R. *RSC Adv.* **2016**, *6*, 34014–34018.
  3. Koch, K. R.; Engelbrecht, L. *Dalton Trans.* **2016**, submitted.
-

## Abstract

Isotope effects in <sup>195</sup>Pt NMR spectra have been known for many years and may be used for the characterisation of platinum complexes in solution. Solvent effects on intrinsic NMR isotope shifts of molecules, on the other hand, have rarely been reported, and have not been studied systematically in general. This section of the work describes a study of the solvent dependence of the <sup>195</sup>Pt NMR isotope shift  $^1\Delta^{195}\text{Pt}(^{37/35}\text{Cl})$  in the spectrum of the complexes  $[\text{Pt}^{35}\text{Cl}_n^{37}\text{Cl}_{6-n}]^{2-}$ , where  $n = 0-6$ , dissolved in the series of solvents water, methanol, 2-methoxyethanol and 1,2-dimethoxyethane, and also in equimolar binary mixtures of water and these organic solvents, which are fully miscible. A previous <sup>195</sup>Pt NMR chemical shift study has indicated preferential solvation of the platinum complex by the organic component in such binary solvent mixtures. The solvent dependence of  $^1\Delta^{195}\text{Pt}(^{37/35}\text{Cl})$  in this complex is found to be relatively small, increasing in magnitude by  $\sim 0.007$  ppm (7 ppb) in the order, water < methanol < 2-methoxyethanol < 1,2-dimethoxyethane. This trend, and the magnitude of the isotope shifts determined in the binary solvent mixtures, are interpreted in the context of the proposed preferential solvation phenomenon and are found to be at least qualitatively consistent. The chemical speciation of the platinum complex in the various solutions was also determined using <sup>195</sup>Pt NMR spectroscopy. In water-methanol mixtures, the <sup>195</sup>Pt NMR chemical shift of the square-planar  $[\text{PtCl}_4]^{2-}$  displays a similar dependence on solvent composition suggesting that this complex, too, is preferentially solvated by methanol under these conditions. Finally, the utility of <sup>195</sup>Pt NMR isotope shifts for the characterisation of platinum complexes is illustrated by considering the signals of complexes of the type  $[\text{PtCl}_n(\text{OH})_{6-n}]^{2-}$  ( $n = 1-6$ ) in <sup>18</sup>O-enriched aqueous solutions. These spectra show exquisite fine structure as a result of the signals of both isotopologues and, in some case, isotopomers being partially resolved and may be considered unique fingerprints for the characterisation of the complexes in solution.

## 2.1 Introduction

### 2.1.1 <sup>195</sup>Pt NMR spectroscopy: an overview

The first <sup>195</sup>Pt magnetic resonance experiment was reported in 1950 by Proctor and Yu.<sup>1</sup> The measurement was made in a 6600 gauss (0.66 tesla) magnetic field on a liquid sample of platinum metal dissolved in aqua regia; the resonance frequency measurement was used to estimate the magnetic moment of the nuclide,  $\mu(^{195}\text{Pt}) = (0.6005 \pm 0.0001)\mu_{\text{N}}$ , where  $\mu_{\text{N}}$  is the nuclear magneton (IUPAC currently lists a value of  $1.0557\mu_{\text{N}}$ ).<sup>2</sup>

Von Zelewsky, in 1968, reported <sup>195</sup>Pt NMR spectra showing the signals of various octahedral Pt(IV) complexes with the general formula  $[\text{PtCl}_{6-n}\text{Br}_n]^{2-}$ , where  $n = 0-6$ , in aqueous solution.<sup>3</sup> In the same year, measurements of <sup>195</sup>Pt NMR chemical shifts of square-planar Pt(II) complexes were presented by Pidcock and co-workers and correlated with electronic absorption frequencies.<sup>4</sup> A second study of factors determining <sup>195</sup>Pt chemical shifts, by Dean and Green, was also reported.<sup>5</sup> The large chemical shift ranges of heavy nuclei such as <sup>59</sup>Co and <sup>195</sup>Pt were recognised by early workers to be determined by the paramagnetic nuclear shielding component described by Ramsey.<sup>6</sup> In this theory, the magnetic shielding,  $\sigma$ , of an atomic nucleus by electrons in the presence of an external magnetic field may be written as a sum of two contributions:

$$\sigma = \sigma_{\text{d}} + \sigma_{\text{p}} \quad (2.1)$$

Here  $\sigma_{\text{d}}$  is the diamagnetic shielding resulting from the induced motion of electrons in the ground state, while  $\sigma_{\text{p}}$  depends also on excited electronic states. More recently, the importance of a third contribution, that resulting from spin-orbit ( $\sigma_{\text{SO}}$ ) coupling, has been recognised, which is of particular importance in the magnetic shielding of heavy nuclei e.g. <sup>195</sup>Pt and other transition metals.<sup>7</sup> The SO contribution arises from electronic spin polarisation by spin-orbit coupling, which is then relayed to the resonant nucleus via the Fermi-contact interaction (similar to spin-spin, or  $J$ -coupling). The reader is referred to work by Kaupp *et al.*<sup>7</sup> and that of Ziegler and co-workers.<sup>8</sup> The paramagnetic and spin-orbit shielding contributions have been shown to determine chemical shifts of transition metal nuclei, i.e. the diamagnetic term does not change appreciably with variations in molecular structure or environment. Other factors may also affect the magnetic shielding of a nucleus to some extent, which may then be expressed generally as follows:

$$\sigma = \sigma_d + \sigma_p + \sigma_{SO} + \sigma_{\text{other}} \quad (2.2)$$

The measurement of <sup>195</sup>Pt NMR spectra has since become routine, owing to instrumental developments and the favourable magnetic properties of the nucleus (spin 1/2 with NMR receptivity relative to <sup>13</sup>C of about 20) and its compounds.<sup>2</sup> A number of review articles describing applications of <sup>195</sup>Pt NMR spectroscopy have appeared, many of which concern Pt(II) complexes in view of their biological activity as anticancer agents.<sup>9–12</sup> In this context, <sup>195</sup>Pt NMR spectroscopy has been found to be a very suitable technique with which to characterise platinum-containing compounds and study their reactions, since the chemical shift is highly sensitive to structural variations: the known <sup>195</sup>Pt NMR chemical shift range exceeds 13 000 ppm.<sup>12</sup> Spin-spin (*J*) coupling interactions involving <sup>195</sup>Pt are typically large (a <sup>1</sup>*J*(<sup>195</sup>Pt–<sup>205</sup>Tl) constant of *ca.* 78 kHz has been reported<sup>13</sup>) and have been particularly useful in establishing *trans*-influence series, notably in square-planar Pt(II) compounds.<sup>9,14</sup> More recently, solid state <sup>195</sup>Pt NMR has found application in the characterisation of supported platinum catalysts and nanoparticles.<sup>12,15</sup>

### 2.1.2 Solvent effects on <sup>195</sup>Pt NMR chemical shifts

The nature of the solvent environment of a platinum complex may affect its <sup>195</sup>Pt NMR spectrum in three ways: 1) intermolecular interactions, e.g. hydrogen-bonding interactions; 2) changes in the chemical composition of the platinum complex, also known as chemical speciation or solvolysis reactions, and 3) change in the bulk magnetic susceptibility of the sample. The first of these three effects is commonly referred to as the “solvent effect” on the chemical shift and is of particular importance in the present study;<sup>2</sup> the remaining two effects are also important in practice and will be addressed in subsequent sections.

Solvent effects on the <sup>195</sup>Pt NMR chemical shifts of simple platinum complexes were first reported by Freeman *et al.*<sup>16</sup> in 1976, and by Pesek and Mason<sup>17</sup> in 1977. The authors presented measurements for two platinum complex anions, octahedral [PtCl<sub>6</sub>]<sup>2-</sup> and square-planar [PtCl<sub>4</sub>]<sup>2-</sup> (typically as *n*-tetrabutylammonium or sodium salts), in water and selected organic solvents at room temperature, and attempted to interpret the shifts in terms of solvent properties e.g. basicity, noting also the importance of ion-ion interactions (or “ion-pairing”) in non-aqueous solvents. Pesek and Mason reported such solvent effects to be consistently smaller in the case of [PtCl<sub>4</sub>]<sup>2-</sup> (242 ppm downfield shift when substituting dimethyl

sulfoxide for water, compared with 400 ppm downfield for  $[\text{PtCl}_6]^{2-}$ , despite expected closer approach of solvent molecules to the platinum centre in the square-planar complex.

NMR chemical shift measurements have also been used to study problems of preferential or selective solvation of ions in mixed solvents, notably for monoatomic<sup>18,19</sup> (e.g. <sup>23</sup>Na in the sodium cation) and, to a lesser extent, complex ions (<sup>59</sup>Co in  $[\text{Co}(\text{CN})_6]^{3-}$ ).<sup>20,21</sup> In binary solvent mixtures, where NMR chemical shift data are collected at various solvent compositions, preferential solvation of the compound containing the resonant nucleus by one solvent component over the other is indicated by a non-first order (nonlinear) change in the chemical shift with solvent composition (see Section 1.3 for more information).<sup>22</sup>

Early work by Bloor and Kidd,<sup>16</sup> and by Popov and co-workers<sup>17</sup> on the solvent dependence of <sup>23</sup>Na NMR chemical shifts and preferential solvation of the sodium ion in binary solvent mixtures showed correlation of such shifts with solvent basicity and Gutmann donor numbers, indicating of the ability of solvents to donate electrons (the interested reader is referred to textbooks by Burgess<sup>23</sup> and Marcus<sup>24</sup>). Covington and co-workers<sup>25</sup> extensively studied solvent effects on alkali metal and halide ion NMR chemical shifts, specifically in the context of preferential solvation in mixed solvents, and presented mathematical models for calculating preferential solvation equilibrium constants. The NMR chemical shift work of Stengle and co-workers on preferential solvation of halide ions,<sup>26–28</sup> and that based on nuclear quadrupole spin relaxation time measurements by Holz and co-workers (see Chapter 3) are also relevant.<sup>29</sup>

Frankel, Stengle and Langford used <sup>59</sup>Co NMR chemical shift measurements to study preferential solvation of  $[\text{Co}(\text{acac})_3]$  in  $\text{CHCl}_3\text{--CCl}_4$  mixtures;<sup>20</sup> Eaton *et al.*<sup>21</sup> followed a similar approach in their study of the nature of hydrogen-bonding interactions of  $[\text{Co}(\text{CN})_6]^{3-}$  in binary mixtures involving water, dimethyl sulfoxide and selected carboxylic acids where, in certain mixtures, preferential solvation of the complex ion was also indicated.

More recently, Westra *et al.*<sup>30</sup> performed <sup>195</sup>Pt NMR chemical shift measurements for the  $[\text{PtCl}_6]^{2-}$  anion dissolved (as hexachloroplatinic acid,  $\text{H}_2\text{PtCl}_6$ ) in binary mixtures of water ( $\text{D}_2\text{O}$ ) and various water-miscible organic solvents. Attempts were made to correlate solvent-induced shifts with various properties of the pure solvents. In all solvent mixtures studied by these workers, the platinum complex was found to be preferentially solvated by the organic solvent component over the entire mixed solvent composition range (all solvents studied were fully miscible with water). This conclusion was based on previous studies of cation solvation



in binary solvent mixtures by NMR chemical shift measurements (see above<sup>18,19</sup> and Fig. 2.1); an explanation of the phenomenon based on properties of the mixed solvent was proposed, namely that the observed preference for the organic solvent component may result not from stronger interactions between the platinum complex and the organic molecules, but rather from a mutual exclusion of the anionic solute and organic component by strong hydrogen-bonding interactions between water molecules (see Section 1.3).<sup>30</sup>

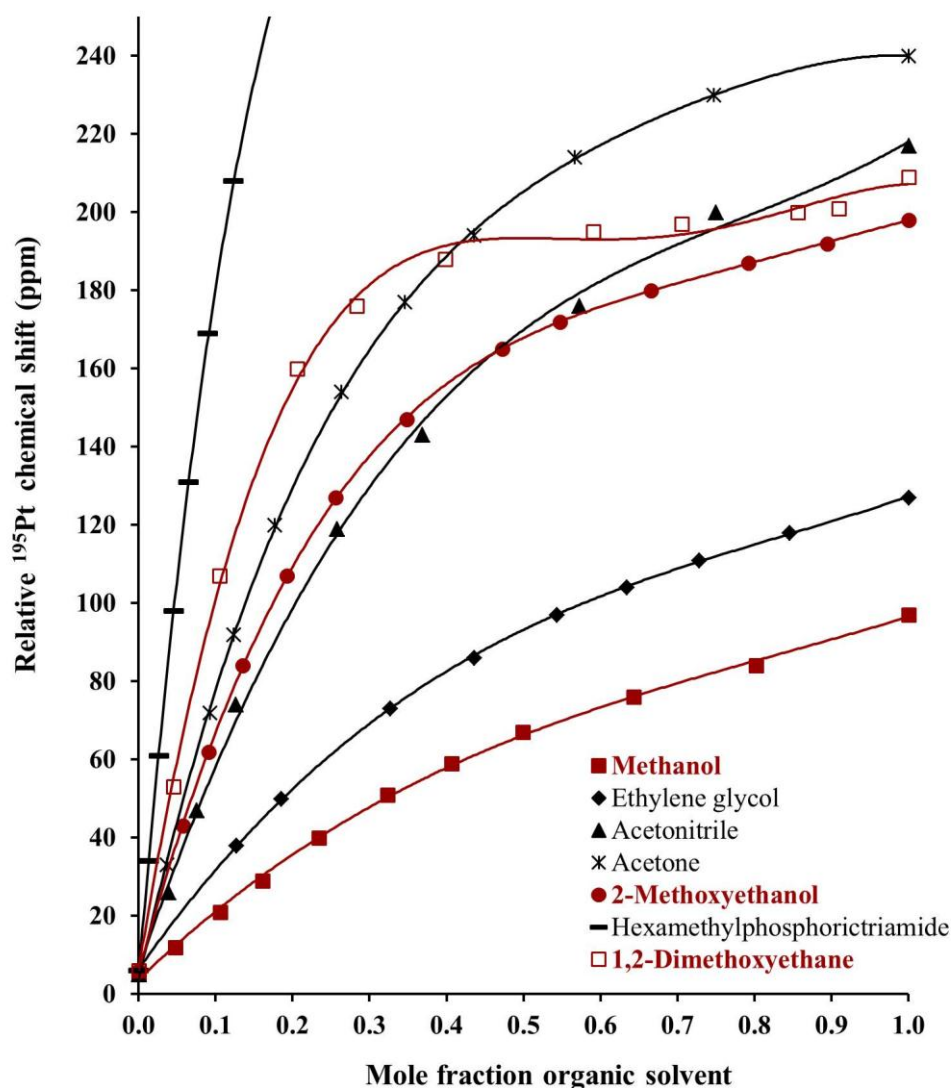


**Figure 2.1** <sup>195</sup>Pt NMR chemical shifts of [PtCl<sub>6</sub>]<sup>2-</sup> in solutions of hexachloroplatinic acid in binary mixtures of water (D<sub>2</sub>O) and various water-miscible organic solvents at 303 K; polynomial functions have been least-squares fitted to the individual datasets. Only partial data shown for hexamethylphosphoric triamide, which extends to  $\delta(^{195}\text{Pt}) \sim 400$  ppm. Mixtures studied in this work are indicated in red. Data reproduced from Westra.<sup>30</sup>

### 2.1.3 Chemical speciation of platinum complexes

The concept of “chemical speciation”, often referred to simply as “speciation”, is especially important in the chemistry of transition metal compounds, or complexes, in solution, where ligand exchange reactions can occur and transform, in part or entirely, a given metal complex to one or more complexes of different chemical composition.<sup>31</sup> The phenomenon also has a longstanding association with <sup>195</sup>Pt NMR spectroscopy,<sup>3</sup> which has been found to be an excellent tool with which to study these reactions owing largely to the fact that the products of such speciation reactions typically produce effectively single resonance signals that are well resolved due to the large chemical shift range of the nucleus.

Solvolysis reactions are a class of speciation reactions where, in the context of coordination chemistry, a solvent molecule displaces one or more ligands coordinated to the transition metal ion to form a new solvate complex; aquation/hydrolysis reactions refer to the special case where water is the coordinating solvent. In the case of simple octahedral Pt(IV) (and to some extent square-planar Pt(II)) complexes involving halide ions, aquation reactions have been extensively studied and it has been found that the extent of chemical speciation, i.e. the number of chemical species present in solution and their relative concentrations, is dependent on several factors, the most important of which are the total platinum and halide ion concentrations, the solution acidity, temperature and reaction time (which may simply be the time following dissolution of the precursor material).<sup>32–35</sup>

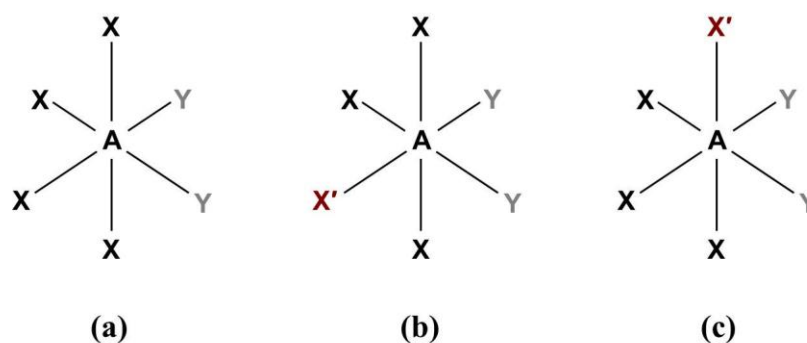
Goodfellow and co-workers used <sup>195</sup>Pt NMR spectroscopy to study the hydrolysis of  $[\text{PtCl}_6]^{2-}$  in alkaline aqueous solutions where complexes of formula  $[\text{PtCl}_n(\text{OH})_{6-n}]^{2-}$ , with  $n = 0–6$ , are formed.<sup>33</sup> It was shown for this series of hydrolysis products that the signals of species differing in the number of coordinated chloride ions (chlorido-ligands,  $n$ ) appear approximately regularly distributed with a downfield shift of about 500 ppm per substitution of a *hydroxido*- for a chlorido-ligand. Pairs of geometrical isomers *cis/trans*- $[\text{PtCl}_2(\text{OH})_4]^{2-}$ , *fac/mer*- $[\text{PtCl}_2(\text{OH})_4]^{2-}$  and *cis/trans*- $[\text{PtCl}_4(\text{OH})_2]^{2-}$  were found to be present with a chemical shift difference of *ca.* 20 ppm (this separation is not constant throughout the series, see original text for details), with substitution at positions *trans* to chlorido-ligands producing larger downfield shifts, e.g. the signal of *cis*- $[\text{PtCl}_4(\text{OH})_2]^{2-}$  appears at higher  $\delta(^{195}\text{Pt})$  than that of *trans*- $[\text{PtCl}_4(\text{OH})_2]^{2-}$ . Interestingly, the reverse order was proposed for signals of geometrical isomers of the series of *aquo*-complexes  $[\text{PtCl}_n(\text{OH}_2)_{6-n}]^{4-n}$  ( $n = 2–4$ ), formed following acidification of alkaline solution described above.

Regular, predictable changes in <sup>195</sup>Pt NMR chemical shifts following successive ligand substitution steps have also been found for other series of related platinum complexes.<sup>34,35</sup> Kramer and Koch have demonstrated the utility of a <sup>195</sup>Pt NMR chemical shift trend-analysis method, based on such regular variations, for the assignment of <sup>195</sup>Pt NMR spectra of complexes in the series  $[\text{PtCl}_{6-m-n}\text{Br}_m(\text{OH})_n]^{2-}$  ( $m, n = 0-6$ ) in aqueous solution.<sup>35</sup> While assignments based on such chemical shift trends are certainly convenient and useful, this approach may not necessarily be applicable (e.g. when only few signals are present), and the additional sensitivity of <sup>195</sup>Pt NMR chemical shifts to factors such as temperature, solvent and acidity in aqueous solutions can introduce uncertainties in assignments based on chemical shifts alone.<sup>16,17,36</sup> In this context, Gerber *et al.*<sup>37</sup> have shown that octahedral Pt(IV) complexes containing chlorido-ligands may be characterised by isotope-induced fine structure present in their <sup>195</sup>Pt NMR spectra as a result of the natural distribution of <sup>35/37</sup>Cl isotopes in their coordination spheres.

### 2.1.4 NMR isotope shifts

The effects of isotopic substitution in molecules on the NMR chemical shifts of other nuclei located in them, usually referred to simply as “isotope shifts” or “isotope effects”, have been known for many years.<sup>38,39</sup> Formally, isotope effects are classified as *intrinsic*, resulting from differences in average (by vibrational and rotational motion) electronic properties, i.e. nuclear magnetic shielding, of molecules differing in isotopic composition (*isotopologues*, see Scheme 2.1) or *equilibrium* isotope effects, where a molecule undergoes rapid exchange e.g. between two conformations, and where the populations of these two (or more) states, and hence the *average* nuclear shielding, are different for such isotopologues.<sup>40</sup> Note that, in general, isotopic substitution also affects other NMR properties of molecules e.g. *J*-coupling and spin relaxation times.<sup>41</sup>

Sadler and co-workers, in 1980,<sup>42</sup> reported intrinsic isotope effects in the <sup>195</sup>Pt NMR spectra of the complexes  $[\text{PtCl}_6]^{2-}$ ,  $[\text{PtBr}_6]^{2-}$  and  $[\text{PtClBr}_5]^{2-}$  in aqueous solution, the resonance signals of which display fine structure as a result of the natural isotopic distribution of <sup>35</sup>Cl/<sup>37</sup>Cl and <sup>79</sup>Br/<sup>81</sup>Br isotopes (Fig. 2.2). In a more recent study concerning the measurement of intrinsic isotope effects on NMR chemical shifts in the solid state, Wasylishen *et al.*<sup>43</sup> describe general features of these effects, some of which may be illustrated using the <sup>195</sup>Pt NMR spectra in Fig. 2.2.



**Scheme 2.1** Isotopologues and isotopomers. In this scheme, the labels A, X and Y indicate different chemical elements, e.g. Pt, Cl and O would be appropriate, and also refer to *specific isotopes*, in this case <sup>195</sup>Pt, <sup>35</sup>Cl and <sup>16</sup>O. The label X' in structures (b) and (c) indicate a different isotope of element X, e.g. <sup>37</sup>Cl. Structure (a) is related to structures (b) and (c) by the term *isotopologues*, while structures (b) and (c) are *isotopomers*, having the same isotopic composition, but differing in their relative positions in the molecule.

Considering a resonant (detected) nucleus A, located in a molecule containing also a nucleus X, which may be replaced by a heavier *isotope* X' (atomic masses  $m$  and  $m'$ , respectively), the NMR isotope shift resulting from this isotopic substitution is *defined* as

$$\begin{aligned} {}^n\Delta A({}^{m'/m}\text{X}) &= \sigma_A - \sigma_A^* \\ &= \delta_A^* - \delta_A \end{aligned} \quad (2.3)$$

where  $n$  denotes the number of chemical bonds between A and the position of isotopic substitution (typically  $n = 1-3$ ) and where the asterisk indicates that the property pertains to the heavier *isotopologue* (i.e. containing X'); the other symbols have their usual meaning. As listed by Wasylishen *et al.*,<sup>43</sup> the following features, or trends, are frequently found for such intrinsic isotope shifts in many chemical systems:

1. Substitution for a heavier isotope (X'), results in increased magnetic shielding of other nuclei (A) in the molecule; i.e. intrinsic isotope shifts are usually *negative* according to the above definition (note that there are exceptions to this point, including some transition metal shifts e.g. certain <sup>199</sup>Hg NMR isotope shifts<sup>44</sup>). This can be seen more clearly in the <sup>195</sup>Pt NMR spectrum of  $[\text{Pt}^{35}\text{Cl}_n{}^{37}\text{Cl}_{6-n}]^{2-}$ , where the signals of isotopologues rich in <sup>37</sup>Cl, having a lower intensity due to the lower natural abundance of this isotope compared to <sup>35</sup>Cl, appear at *lower* <sup>195</sup>Pt chemical shift.

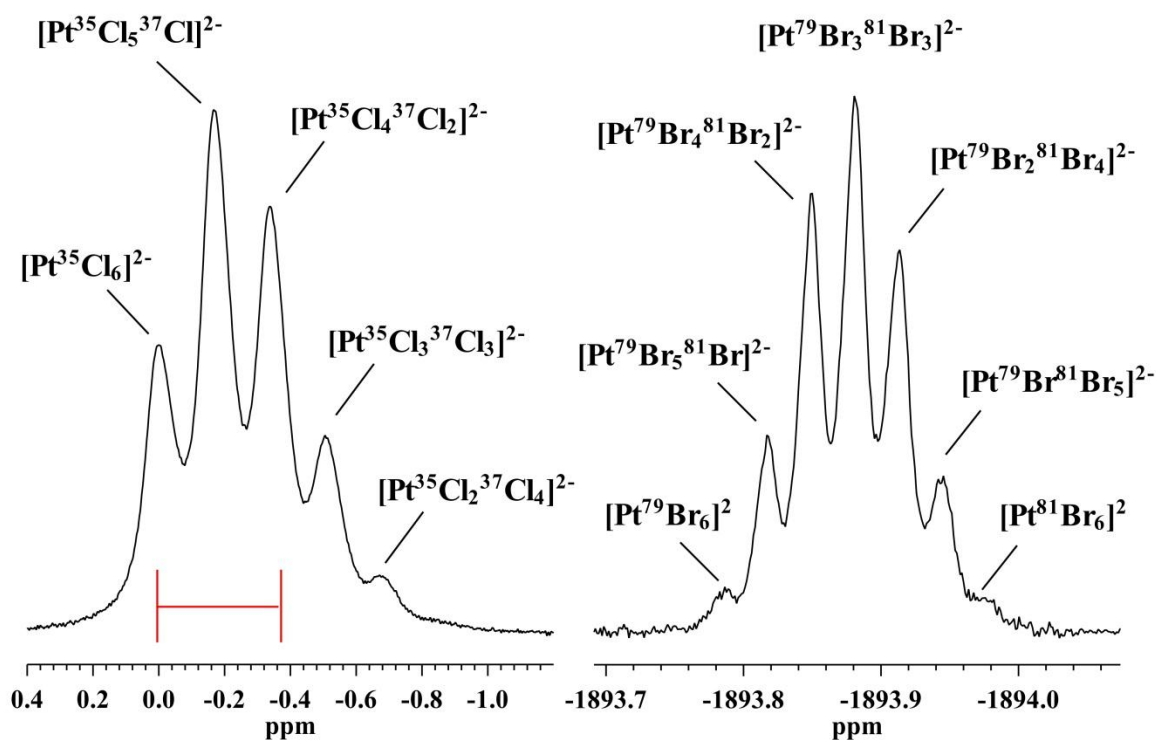


**Figure 2.2**  $^{195}\text{Pt}$  NMR spectra (*ca.* 128 MHz) of the complexes  $[\text{Pt}^{35}\text{Cl}_n^{37}\text{Cl}_{6-n}]^{2-}$  (left) and  $[\text{Pt}^{79}\text{Br}_n^{81}\text{Br}_{6-n}]^{2-}$  ( $n = 0-6$ ) (right) in aqueous solutions ( $\text{D}_2\text{O}$ ) of  $\text{H}_2\text{PtCl}_6$  and  $\text{H}_2\text{PtBr}_6$  with natural abundances of chlorine and bromine isotopes at 293 K. The red bar indicates the entire  $\delta(^{195}\text{Pt})$  range of the spectrum of  $[\text{PtBr}_6]^{2-}$  ( $\sim 0.4$  ppm).

- The magnitude of the isotope shift is proportional to the relative change in mass,  $(m' - m)/m'$ ,<sup>45</sup> i.e. isotope shifts resulting from isotopic substitution of lighter elements are often larger (in similar molecules or fragments). This is nicely illustrated by comparing the  $^{195}\text{Pt}$  NMR spectra of  $[\text{Pt}^{35}\text{Cl}_n^{37}\text{Cl}_{6-n}]^{2-}$  and  $[\text{Pt}^{79}\text{Br}_n^{81}\text{Br}_{6-n}]^{2-}$ , where  $^1\Delta^{195}\text{Pt}(^{37}/^{35}\text{Cl}) = -0.17$  ppm and  $^1\Delta^{195}\text{Pt}(^{81}/^{79}\text{Br}) = -0.03$  ppm; note that the entire expansion showing the  $[\text{Pt}^{79}\text{Br}_n^{81}\text{Br}_{6-n}]^{2-}$  signals matches the red bar (*ca.* 0.4 ppm) in the spectrum of  $[\text{Pt}^{35}\text{Cl}_n^{37}\text{Cl}_{6-n}]^{2-}$ .
- Isotope shifts are approximately additive, i.e. substitution of two isotopes X, located in chemically equivalent positions, results in an overall isotope shift in the spectrum of A that is approximately twice as large as that resulting from only one such substitution.<sup>46</sup> This feature of isotope shifts is also nicely illustrated in the  $^{195}\text{Pt}$  NMR spectra in Fig. 2.2. Note, however, that in certain literature the term “isotope shift” refers to the shift resulting from *complete* isotopic substitution of a certain element in a molecule, e.g. the  $^{13}\text{C}$  NMR chemical shift between  $\text{CH}_4$  and  $\text{CD}_4$ ; in the majority of cases, however, the

term is understood to indicate the difference resulting from a *single* isotopic substitution, i.e. per X isotope substituted, and this definition will also be used throughout the text.

4. Isotope shifts are larger for nuclei with large chemical shift ranges, e.g. <sup>195</sup>Pt.
5. The magnitude of the isotope shift decreases with increasing number of chemical bonds *n* separating the observed nucleus A and the site of a given isotopic substitution; this point is of particular importance in the case of H/D substitution in organic molecules.

The observations listed above are consistent with the extensive theoretical work of Jameson and co-workers on the origin of the isotope shift (intrinsic isotope effect) and temperature effects on NMR chemical shifts, notably in octahedral MX<sub>6</sub> molecules (with M observed) and transition metal complexes (including [PtCl<sub>6</sub>]<sup>2-</sup>).<sup>45,47,48</sup> It is shown for such molecules that these effects are related to changes in average M–X bond displacements following isotopic substitution or changes in temperature; specifically, *negative* isotope shifts result from a decrease in M–X bond displacement when a heavier isotope is substituted for X (essentially due to the lower vibrational energy of the heavier isotopologue and the effect of vibrational anharmonicity). It is proposed that changes in the paramagnetic contribution to the nuclear shielding account satisfactorily for these observations, at least for octahedral complexes of vanadium (<sup>51</sup>V) and cobalt (<sup>59</sup>Co).<sup>48</sup>

Koch and co-workers have shown that isotope shifts in the <sup>195</sup>Pt NMR spectra of complexes of the type [PtCl<sub>*n*</sub>(OH<sub>2</sub>)<sub>6-*n*</sub>]<sup>4-*n*</sup> (*n* = 2–6) can be used for their unambiguous characterisation in solution (see also Section 2.1.3).<sup>37,49</sup> For the complexes [PtCl<sub>5</sub>(H<sub>2</sub>O)]<sup>-</sup> and *cis*-[PtCl<sub>4</sub>(H<sub>2</sub>O)<sub>2</sub>], present in aqueous solutions containing [PtCl<sub>6</sub>]<sup>2-</sup>, the isotope-induced fine-structure resulting from the natural distribution of <sup>35</sup>Cl/<sup>37</sup>Cl isotopes, i.e. signals of the isotopologues [Pt<sup>35</sup>Cl<sub>*n*</sub><sup>37</sup>Cl<sub>5-*n*</sub>(H<sub>2</sub><sup>16</sup>O)]<sup>-</sup> (*n* = 0–5) and *cis*-[Pt<sup>35</sup>Cl<sub>*n*</sub><sup>37</sup>Cl<sub>4-*n*</sub>(H<sub>2</sub><sup>16</sup>O)<sub>2</sub>] (*n* = 0–4), differs from that expected based on the known spectrum of [Pt<sup>35</sup>Cl<sub>*n*</sub><sup>37</sup>Cl<sub>6-*n*</sub>]<sup>2-</sup> (*n* = 0–6) in that they contain additional, partially resolved signals, not accounted for by simply considering all possible isotopic compositions (six and five uniformly dispositioned signals, respectively) for these complexes (Fig. 2.3 (a)).<sup>37</sup> Note that <sup>17</sup>O- and <sup>18</sup>O-containing isotopologues are not detected due to the low natural abundances of these isotopes. The additional signals in these <sup>195</sup>Pt NMR spectra were shown to result from complexes having the *same* isotopic composition, but differing in the relative positions of these (<sup>35</sup>Cl/<sup>37</sup>Cl) isotopes; such compounds are known as *isotopomers* (this term is used in certain literature to refer to molecules differing in isotopic *composition*; as introduced earlier, the term *isotopologues*

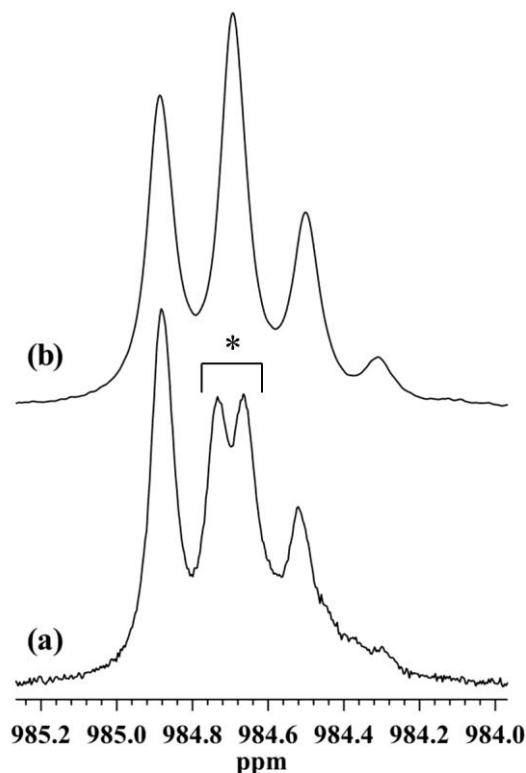


**Figure 2.3** <sup>195</sup>Pt NMR spectra (*ca.* 128 MHz) of (a) *cis*-[Pt<sup>35</sup>Cl<sub>*n*</sub><sup>37</sup>Cl<sub>4-*n*</sub>(H<sub>2</sub><sup>16</sup>O)<sub>2</sub>] in perchloric acid solution, and (b) *cis*-[Pt<sup>35</sup>Cl<sub>*n*</sub><sup>37</sup>Cl<sub>4-*n*</sub>(<sup>16</sup>OH)<sub>2</sub>]<sup>2-</sup> in strongly alkaline (NaOH) solution at 293 K. Spectra plotted on same scale (1.3 ppm) for direct visual comparison; actual <sup>195</sup>Pt chemical shift for (b) ~1276 ppm. Additional partially resolved fine structure (e.g. signals marked with \*) in (a) due to magnetically non-equivalent *isotopomers*. Spectra adapted from ref. 50.

will be used in this text when referring to such molecules; see Scheme 2.1). In the case of complexes with the isotopic formula *cis*-[Pt<sup>35</sup>Cl<sub>3</sub><sup>37</sup>Cl(<sup>16</sup>OH)<sub>2</sub>], for example, two partially-resolved signals of equal intensity are found (marked with an asterisk in Fig. 2.3 (a)). The more downfield of these signals was shown to result from the isotopomer in which two <sup>35</sup>Cl isotopes are located in the coordination positions *trans* to an oxygen atoms of one of the water molecules (*aquo*-ligands), as shown in Scheme 2.1 (b), while the more upfield signal was assigned to the isotopomer with one <sup>35</sup>Cl and one <sup>37</sup>Cl isotope in these positions (Scheme 2.1 (c)).<sup>37</sup>

The signals of isotopomers in this series of complexes are not always resolved, however: in the spectrum of [Pt<sup>35</sup>Cl<sub>*n*</sub><sup>37</sup>Cl<sub>6-*n*</sub>]<sup>2-</sup> (*n* = 0–6), for example, the signals of isotopomers are clearly not resolved (at room temperature and atmospheric pressure), as is the case for isotopomers with formula [Pt<sup>35</sup>Cl<sub>3</sub><sup>37</sup>Cl<sub>2</sub>(<sup>16</sup>OH)<sub>2</sub>]<sup>-</sup> in which a <sup>35</sup>Cl isotope is located *trans* to

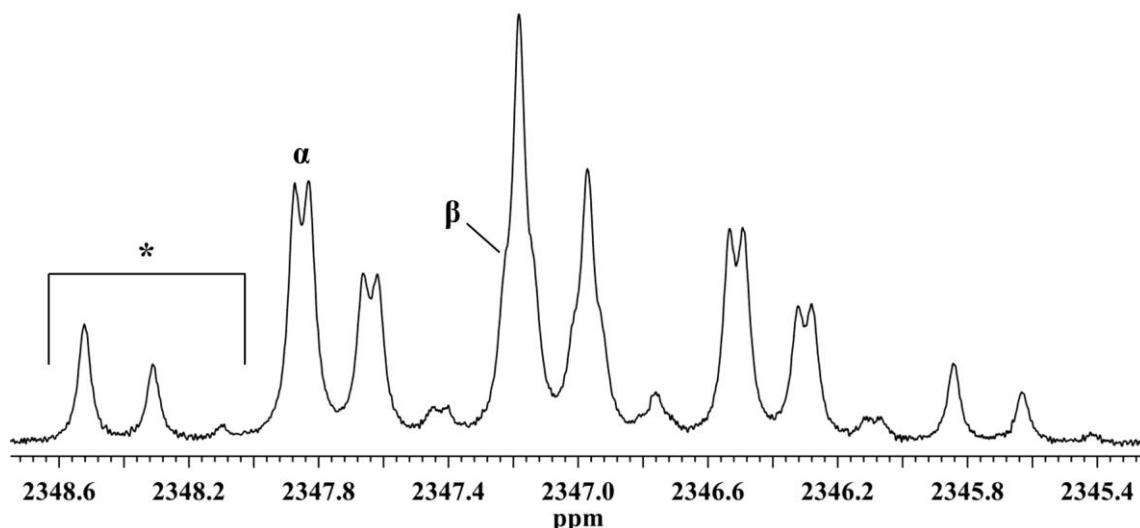


**Figure 2.4** <sup>195</sup>Pt NMR spectrum (ca. 129 MHz) of the complexes  $cis\text{-}[\text{Pt}^{35}\text{Cl}_n\text{}^{37}\text{Cl}_{2-n}(\text{}^{16}\text{OH})_m(\text{}^{18}\text{OH})_{4-m}]^{2-}$  ( $n = 0\text{--}2$ ,  $m = 0\text{--}4$ ) in a strongly alkaline solution, enriched with <sup>18</sup>O (<sup>18</sup>O-enriched water, ca. 45 %) of hexachloroplatinic acid at 293 K. Features such as those indicated, (**α**) “split” peaks and (**β**) broad peak bases, are due to unresolved signals of *isotopomers* differing in the combination of <sup>16/18</sup>O coordinated in positions *trans* to the two chlorido-ligands. Spectrum adapted from ref. 50, where a full analysis of the spectrum is presented. The asterisk (\*) shows the signals of the three isotopologues  $[\text{Pt}^{35}\text{Cl}_{2-n}\text{}^{37}\text{Cl}_n(\text{}^{16}\text{OH})_4]^{2-}$  ( $n = 0\text{--}2$ ).

the aquo-ligand (<sup>16</sup>O), i.e. the two <sup>37</sup>Cl isotopes are located in either relative *cis* or *trans* positions, but the signals of such isotopomers are not resolved.

Similarly, for the series of hydroxido-complexes  $[\text{PtCl}_n(\text{OH})_{6-n}]^{2-}$ , where  $n = 0\text{--}5$ , found in alkaline aqueous solution, Engelbrecht *et al.*<sup>50</sup> have shown that only the signals of *isotopologues* are resolved and no additional fine structure due isotopomers is observed (Figure 2.3 (b)). When solutions containing these hydroxido-complexes are enriched with the <sup>18</sup>O isotope, however, additional signals appear in the spectra of certain complexes in this series, and are shown to result from both isotopologues containing <sup>18</sup>O, as well as isotopomers differing in the combination of <sup>16</sup>O/<sup>18</sup>O isotopes located *trans* to chlorido-ligands (see Fig. 2.4, for example). The detailed assignment and interpretation of these complex <sup>195</sup>Pt NMR signal profiles formed part of an initial component of the present study and will be presented in a subsequent section.<sup>50</sup>



### 2.1.5 Rationale and aims

The solvent dependence of the intrinsic NMR isotope shift has not been studied in detail for molecules in solution. Jameson and co-workers have predicted the effect to be small in the absence of specific solvent–solute interactions, e.g. hydrogen bonding.<sup>51</sup> In the case of  $[\text{Pt}^{35}\text{Cl}_n^{37}\text{Cl}_{6-n}]^{2-}$  specifically, solvent effects on the overall (“average”) <sup>195</sup>Pt chemical shift have been studied, originally by Pesek and Mason,<sup>17</sup> and more recently by Westra,<sup>30</sup> who also reported that  $^1\Delta^{195}\text{Pt}(^{37/35}\text{Cl})$  isotope shifts could be detected in a variety of organic solvents. However, the solvent dependence of these <sup>195</sup>Pt NMR isotope shifts was not studied in detail, and also not in binary mixtures of water and the water-miscible organic solvents, where preferential solvation of the platinum complex by the organic solvent component is inferred from <sup>195</sup>Pt chemical shift measurements.<sup>30</sup>

An important aim of this component of the study was to measure high-resolution <sup>195</sup>Pt NMR spectra of  $[\text{Pt}^{35}\text{Cl}_n^{37}\text{Cl}_{6-n}]^{2-}$  in selected organic solvents (methanol, 2-methoxyethanol and 1,2-dimethoxyethane), as well as in their binary mixtures with water and, where possible, to determine accurately the  $^1\Delta^{195}\text{Pt}(^{37/35}\text{Cl})$  isotope shifts in these environments. The solvation environments of small complex anions, e.g. thiocyanate and azide, have been investigated by vibrational spectroscopy;<sup>52,53</sup> isotope shifts, similarly, are determined by differences in vibrational energy levels of isotopologues,<sup>54</sup> and such differences are expected to be dependent on the immediate solvation environment of the probe molecule. It was thus of interest to determine firstly the magnitude of the solvent effect on the  $^1\Delta^{195}\text{Pt}(^{37/35}\text{Cl})$  isotope shift of this complex and, secondly, if a study of such shifts in binary solvent mixtures could provide information regarding the primary solvation shell composition that is consistent with that inferred from <sup>195</sup>Pt NMR chemical shift measurements reported previously.

The chemical speciation of  $[\text{PtCl}_6]^{2-}$  in aqueous solutions has been investigated in detail, specifically using <sup>195</sup>Pt NMR spectroscopy.<sup>33,34</sup> Reduction reactions in methanol and other alcohols have also been studied to some extent;<sup>55</sup> however, no detailed studies of the chemical speciation of this complex in the solvents and solvent mixtures mentioned above have been reported. Certain NMR experiments, e.g. spin relaxation time or PGSE translational diffusion measurements, specifically require that the solution concentration of the analyte remain constant for the duration of the experiment, which, in this case, could be up to 20 hours. In the case of <sup>195</sup>Pt specifically, such experiments additionally require a

relatively high analyte concentration. A further aim was thus to study the platinum complex speciation in these solution using <sup>195</sup>Pt NMR spectroscopy.

Initial work concerned also the complete assignment and interpretation of isotope-induced <sup>195</sup>Pt NMR signal profiles of complexes of the type  $[\text{Pt}^{35/37}\text{Cl}_n(^{16/18}\text{OH})_{6-n}]^{2-}$ , where  $n = 0-5$ , in <sup>18</sup>O-enriched alkaline aqueous solutions, as well as isotope effects in other platinum complexes, particularly cyano-complexes. The results of these investigations were reported in a journal article, which was prepared as part of the present study, and are presented briefly to show the utility of such isotope effects for the unambiguous characterisation of certain classes of platinum complexes in solution.

## 2.2 Technical information

### 2.2.1 Chemical shift referencing

The basic theory of nuclear magnetic shielding and the definition of the chemical shift were presented in Section 1.4. In 2001, the International Union of Pure and Applied Chemistry (IUPAC) produced a report in which recommendations for NMR chemical shift referencing (and reporting of results etc.) were presented.<sup>2</sup> The primary aim of this report, which was followed by additional recommendations in 2008,<sup>56</sup> was to propose the use of a unified chemical shift scale in which *all* NMR chemical shifts are referenced to a primary reference signal, namely the <sup>1</sup>H resonance signal of tetramethylsilane (TMS) in a dilute solution in CDCl<sub>3</sub> (at room temperature and atmospheric pressure). Using this method, the convenient homonuclear reference frequencies (i.e. resonance frequency of the same nuclide as that for which the chemical shift is to be reported) proposed and used historically are related to that of the primary reference signal (<sup>1</sup>H signal of TMS), measured under the same conditions as for the sample under study, by a factor  $\bar{\epsilon}$ , expressed as a percentage and tabulated in the document along with other relevant data for each nuclide. In the case of <sup>195</sup>Pt, the value of  $\bar{\epsilon}$  is 21.496784%, as determined for a solution of Na<sub>2</sub>PtCl<sub>6</sub> (1.2 M) in D<sub>2</sub>O (presumably at 298 K). Alternatively, a fixed reference value  $\bar{\epsilon} = 21.400\ 000\%$  has been proposed for <sup>195</sup>Pt chemical shift calculations.<sup>2</sup>

The document also describes chemical shift *referencing procedures* recognised by IUPAC. As stated there, *accurate* referencing procedures are often not straightforward to implement, with all procedures listed (reproduced below) having certain advantages and disadvantages.

1. **Internal referencing.** In this procedure the appropriate reference compound is added directly to the sample being studied, i.e. mixed and in contact with sample components. This method is used in <sup>1</sup>H and <sup>13</sup>C NMR, where TMS is added directly to samples, its signals appearing in the same NMR spectrum as those of the sample components. Clearly, this method is not always applicable (e.g. where reference compounds are incompatible, i.e. interact strongly/react chemically with the *analyte*, or where addition of these compounds affect sample properties under study), may lead to uncertainty regarding specific sample effects (intermolecular interactions) on the shielding of nuclei in the reference compound, and is not necessarily consistent with the proposed use of the unified chemical shift scale (where the proposed reference compound is TMS in a dilute

solution in CDCl<sub>3</sub>). For homonuclear referencing in multinuclear magnetic resonance (not recommended by IUPAC), these points are of particular concern when considering the use of the internal referencing procedure.

- 2. External referencing.** Essentially, in this procedure the reference compound is physically separated from the sample, but their NMR spectra are acquired simultaneously, typically realised by use of a cylindrical coaxial insert placed in the sample container (cylindrical NMR tube); in principle, other reference container geometries are possible/desirable, e.g. spherical, but these are not practical. While sometimes convenient (as is the case in this work), the procedure may require corrections to measured chemical shifts due to differences in the magnetic susceptibilities of the sample and reference solutions: even though the solutions are placed in the same applied magnetic field, there may be a “local” difference in magnetic flux density/induction,  $B_0$ .
- 3. Substitution method.** Independent sample containers/NMR tubes are used for the sample and reference solutions and their NMR spectra are not acquired simultaneously, i.e. here, too, the sample and reference solutions are not mixed. When sample and reference compounds are dissolved in the same (deuterated) solvent, the <sup>2</sup>H locking feature on commercial NMR spectrometers ensures that the spectra of sample and reference are recorded under conditions of constant magnetic induction ( $B_0$ ). When different deuterated solvents are used, and the magnetic field is locked using the <sup>2</sup>H resonance of these solvents, a correction has to be applied when calculating the chemical shift so as to take account of difference in magnetic induction experienced by the compounds (this calculation requires knowledge of the <sup>2</sup>H chemical shift between the lock solvent signals, which is assumed to be identical to that between their <sup>1</sup>H signals and thus known for many solvents). Note that this procedure may not be necessary as it is often incorporated in commercial NMR spectrometers’ operating software. For a detailed description of this chemical shift correction procedure, the reader is referred to the original IUPAC document. Finally, when magnetic field locking is *not* used (“unlocked”), no modifications should be made to the *applied magnetic field* when substituting sample/reference, including changes to magnetic field homogeneity (shimming).
- 4. Referencing using lock signal.** Modern NMR spectrometers commonly monitor the <sup>2</sup>H NMR signal of the deuterated solvent to maintain a constant magnetic induction in the sample for the duration of the experiment. The lock frequency is typically fixed, and the

magnetic field is adjusted to bring the deuterons into resonance; it follows that when a field lock is established, the resonant frequency of deuterons in the known solvent are also known precisely, and the primary (and homonuclear) reference frequency can be calculated, assuming identical chemical shifts for <sup>1</sup>H and <sup>2</sup>H and using tabulated  $\mathcal{E}$  values for the nuclide of interest.

While homonuclear external chemical shift referencing, i.e. the use of a coaxial reference insert containing a recommended reference sample for a given nuclide (that of <sup>195</sup>Pt is a 1.2M solution of Na<sub>2</sub>PtCl<sub>6</sub> in D<sub>2</sub>O) is a practice not recommended by IUPAC (see above and original document)<sup>2</sup>, this procedure was nevertheless found to be particularly useful in the present work for the following reasons:

1. Addition of recommended reference compound (e.g. TMS or DSS) and deuterated solvents directly to samples was strictly not allowed since these compounds affect physical properties of the samples studied e.g. viscosity; also, in some experiments the effect of isotopic (H/D) substitution of mixed solvent components on the solute chemical shift was investigated.
2. External referencing using the recommended reference solution (TMS in CDCl<sub>3</sub>) was technically possible (and would require magnetic susceptibility corrections), but was not used since frequency ratio ( $\mathcal{E}$ ) lookup tables could not be located on operating software of all NMR spectrometers used; checks were done using a coaxial insert containing pure deuterated solvent, which was then specified in the computer interface/program used to conduct experiments, and <sup>195</sup>Pt chemical shifts were found to be different (by up to ca. 5 ppm) from those obtained when using a coaxial insert containing the reference sample indicated for <sup>195</sup>Pt by IUPAC.
3. The signals of the reference compound, which in our case is also the compound studied, appear in the same <sup>195</sup>Pt NMR spectrum as those of the sample and serve as a convenient approximation of relative concentrations of chemical species in the sample solution when spectra are compared.<sup>57</sup> The presence of a reference signal is also desirable when displaying spectra where e.g. solvent shifts are indicated.

Naturally, the homonuclear external referencing method has the same advantages (e.g. no mixing of sample and reference solutions) and disadvantages (magnetic susceptibility corrections, reduced sample volume in coil) as external referencing using the IUPAC recommended reference solution.<sup>2</sup>

## 2.2.2 Processing of NMR data

When acquiring time-domain data (free-induction decay, or FID) on a pulsed Fourier-transform (FT) NMR spectrometer, early data (i.e. acquired soon after the radio-frequency pulse) are often either missing or distorted to some extent as a result of various instrumental limitations or imperfections e.g. dead- and switching times, pulse breakthrough etc.<sup>58</sup> These effects lead to signal phase and baseline distortions, some of which may be reduced by optimization of data acquisition parameters (e.g. pre-acquisition delay times) in combination with appropriate data processing techniques i.e. linear prediction and phase/baseline correction techniques commonly available on spectrometer operating software (used for acquiring and processing/display of NMR spectra, e.g. VnmrJ, XWINNMR) or commercially available offline processing software, e.g. MestReNova (version 7.1.1 used here) or ACD/Labs software.

Additional (and optional) data processing includes application of weighting functions (“apodization”) and “zero-filling” of FID data to improve the signal-to-noise ratio or enhance certain features of the time-domain data, and to improve apparent digital resolution by simply appending zero-data to the FID. These processing techniques will not be discussed here in detail and the reader is referred to excellent NMR textbooks<sup>58</sup> or manufacturer/software distributor manuals<sup>59</sup> for more information (note that apodization and zero-filling are often applied automatically when data files are read by some processing software).<sup>60</sup> The effect of apodization (multiplication of data with an exponentially decaying function) is shown in Fig. 2.5 for <sup>195</sup>Pt NMR data (solution of Na<sub>2</sub>PtCl<sub>6</sub> in water with reference signal of same compound in D<sub>2</sub>O in a coaxial insert). While clearly improving the signal-to-noise ratio, the procedure negatively affects spectral resolution. Note that, in principle, FID data can be processed by multiplication with other functions to enhance certain features of the data, e.g. multiplication with an exponentially increasing function (positive exponential) enhances longer-time features (resolution) of the FID at the expense of signal-to-noise, a procedure known as *resolution enhancement*.

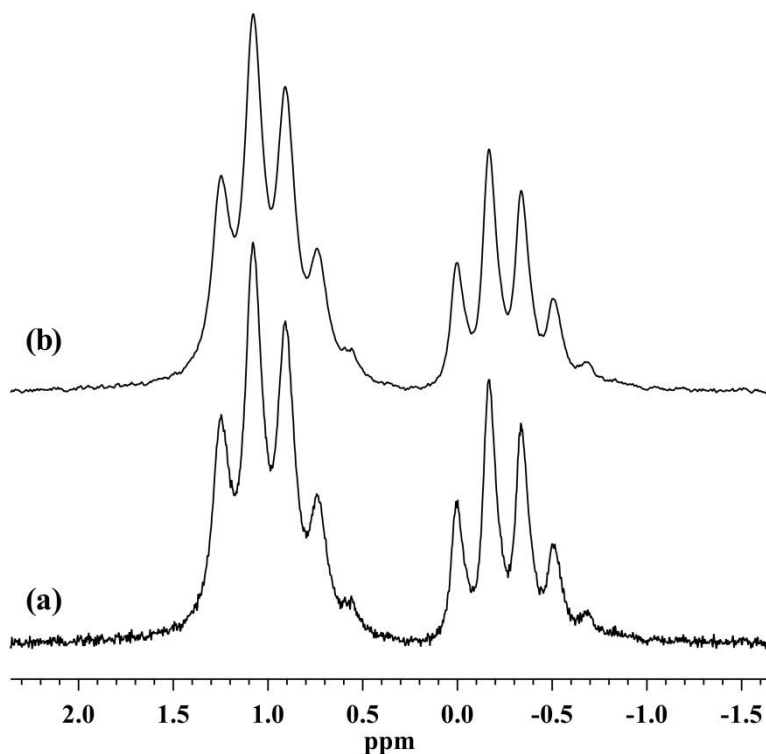


**Figure 2.5** (a) 128 MHz  $^{195}\text{Pt}$  NMR spectrum of  $[\text{Pt}^{35}\text{Cl}_n^{37}\text{Cl}_{6-n}]^{2-}$  in a solution of hexachloroplatinic acid (0.2 M) in water, with external  $^{195}\text{Pt}$  chemical shift reference solution, 1.2 M  $\text{Na}_2\text{PtCl}_6$  in  $\text{D}_2\text{O}$ , contained in coaxial capillary tube insert, at 293 K. (b) Same spectrum as above, but with FID data processed with 1 Hz exponential line-broadening (weighting).

An expansion of the signals of the  $[\text{PtCl}_6]^{2-}$  complex in water (Fig. 2.5) is shown in Fig. 2.6 (a). Note that here the FID has been processed by zero-filling from an original 25798 data points to 65536 (64K) points (this procedure is automatically applied by the processing software used here,<sup>60</sup> i.e. the data set is zero-filled to the next-higher power of two), improving the apparent digital resolution in the spectrum. Accurate determination of the  $^1\Delta^{195}\text{Pt}(^{37/35}\text{Cl})$  isotope shift in this spectrum involves fitting a model function, in this case a sum of peak functions (in principle, one peak for each of the isotopologues  $[\text{Pt}^{35}\text{Cl}_n^{37}\text{Cl}_{6-n}]^{2-}$ ,  $n = 0-6$ ), to the experimental data. MestReNova (version 7.1.1),<sup>60</sup> the commercially available spectrum processing software used in this work, includes a Line Fitting feature intended for such fitting/signal deconvolution procedures. Here the model function fitted to the experimental data is a sum of peak functions, the shape of which is Lorentzian by default, but with variable position, line width and intensity. These parameters are varied during the fitting procedure to obtain an optimal fit between the data and model function; any individual parameter may be constrained (or “locked”) to a fixed value, e.g. the width at half-height of a peak may be kept unchanged, while those of the other peaks are variable. The fitting feature

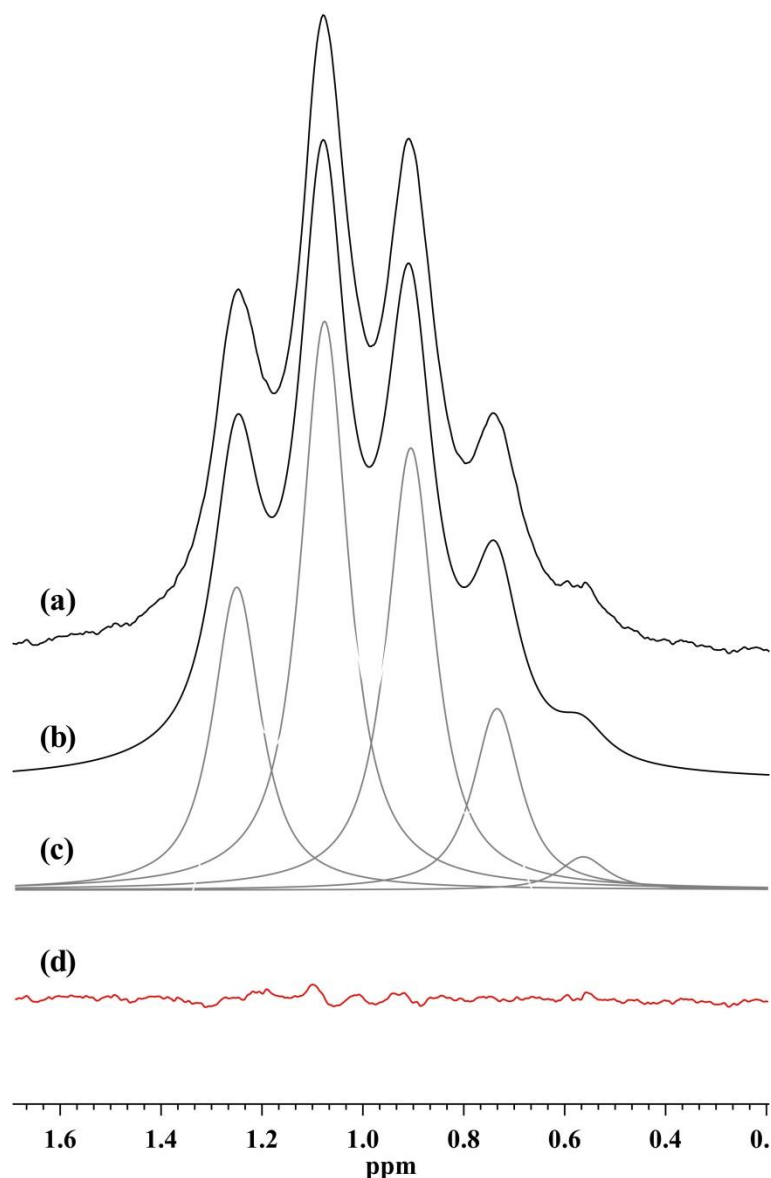


**Figure 2.6** (a) Expansion of  $^{195}\text{Pt}$  NMR signals of  $[\text{Pt}^{35}\text{Cl}_n^{37}\text{Cl}_{6-n}]^{2-}$  in water (Fig. 2.5); (b) model sum function (MestReNova 7.1.1), consisting of five peaks with “L/G” peak shape factor 0.9 and 14.5 Hz half-height width (c), fitted to the experimental spectrum; (d) residual function (difference spectrum).

also includes a peak shape parameter, or “mixing factor”, which is intended to account for deviation of peak shapes from the ideal Lorentzian shape as a result of various experimental factors (e.g. magnetic field inhomogeneity) or data processing, by introducing *Gaussian* distribution character to the peak shape. The peak shape of each component peak may be optimised or constrained individually; the default setting is fully Lorentzian peak shape for all peaks. While fully interactive and highly intuitive, the Line Fitting software does not support more sophisticated parameter constraint options, or arguments, which are highly desirable in the present case (as will be shown below).



The results of a line fitting procedure using the Line Fitting feature of MestReNova are shown in Fig. 2.6 (b–d), where the model (sum) function, the individual fitted peak functions, and the residual function (the difference of the data points and model function) are plotted below the experimental spectrum on the same chemical shift scale. The initial fitting step (itself iterative) automatically identifies a preliminary model function (e.g. number of component peaks and initial parameters) and performs a fit of this function to the data (all peak parameters, with exception of peak shape, are variable in this step). The model function may be refined in subsequent steps, e.g. peaks may be added or removed, and parameters adjusted manually or constrained, prior to initiating the next fitting cycle. In practice, an appropriate fitting strategy is required when using the Line Fitting feature: in the present case, for example, the number of peaks is known, the isotope shift is known to be additive (i.e. the isotopologue peaks are uniformly distributed) and the line widths of the peaks are known to be essentially equal/uniform for the isotopologues  $[\text{Pt}^{35}\text{Cl}_n^{37}\text{Cl}_{6-n}]^{2-}$ ,  $n = 0\text{--}6$  (not expected to be *strictly identical*;<sup>38</sup> details are given in Chapter 3). These constraint arguments cannot be provided directly or implemented in the MestReNova Line Fitting feature described above, since the isotope shift and line widths are not known accurately (the aim of the fitting procedure is to determine the constant isotope shift) and linear arguments are not supported as input e.g. that the line widths should be equal, but not defined or fixed. This limitation is particularly problematic in the case where resolution is low (e.g. Fig. 2.6), but an acceptable fit can be obtained by an iterative procedure where the line width and peak shape are adjusted manually and eventually constrained while monitoring the residual function.

The numerical results of the fitting procedure described above are given in Table 2.1; the fit can be evaluated by comparing relative peak areas to the natural abundances of corresponding isotopologues. Note that *only five peaks* are included in the model function that is fitted to the data since the signals of the isotopologues  $[\text{Pt}^{35}\text{Cl}^{37}\text{Cl}_5]^{2-}$  and  $[\text{Pt}^{37}\text{Cl}_6]^{2-}$  are not detected (natural abundances 0.38 and 0.02 %, respectively).<sup>37,42</sup> Line widths were eventually constrained to 14.5 Hz, and a uniform peak shape factor, or “L/G ratio” (a value of one corresponds to Lorentzian peak shape), of 0.9 (i.e. indicating some degree of Gaussian character) was found to yield an optimal fit. The separation between neighbouring peaks, corresponding to the  ${}^1\Delta^{195}\text{Pt}({}^{37/35}\text{Cl})$  isotope shift, obtained by this procedure is not strictly uniform or additive, and deviations typically occur between the two least intense peaks; recall that the most recent value reported for this isotope shift determined under similar physical

**Table 2.1** Results of signal deconvolution (Fig. 2.6) using the Line Fitting feature of MestReNova 7.1.1. See text for details regarding the fitting procedure. <sup>a</sup> Isotope shift refers to the separation between neighbouring peaks.<sup>43</sup>

Isotopologue	Natural abundance	Relative peak area	Isotope shift <sup>a</sup>
[Pt <sup>35</sup> Cl <sub>6</sub> ] <sup>2-</sup>	18.92	19.8	—
[Pt <sup>35</sup> Cl <sub>5</sub> <sup>37</sup> Cl] <sup>2-</sup>	36.31	36.3	-0.171
[Pt <sup>35</sup> Cl <sub>4</sub> <sup>37</sup> Cl <sub>2</sub> ] <sup>2-</sup>	29.03	28.8	-0.171
[Pt <sup>35</sup> Cl <sub>3</sub> <sup>37</sup> Cl <sub>3</sub> ] <sup>2-</sup>	12.38	12.4	-0.172
[Pt <sup>35</sup> Cl <sub>2</sub> <sup>37</sup> Cl <sub>4</sub> ] <sup>2-</sup>	2.97	3.4	-0.170
[Pt <sup>35</sup> Cl <sup>37</sup> Cl <sub>5</sub> ] <sup>2-</sup>	0.38	—	—
[Pt <sup>37</sup> Cl <sub>6</sub> ] <sup>2-</sup>	0.02	—	—

conditions is -0.171 ppm.<sup>37</sup> While generally useful and certainly convenient, the standard Line Fitting feature of MestReNova is not ideally suited for the requirements of the present investigation, specifically due to its lack of more sophisticated parameter constraint options noted above; it follows that this fitting feature was used only to obtain initial estimates of peak positions and line widths to be used as input when performing nonlinear curve fitting with the graphing software SigmaPlot 13.<sup>61</sup> It is noted, however, that in cases where experimental spectra are well resolved, line fitting with the standard MestReNova feature yields a uniform isotope shift that is entirely consistent with the value obtained using the well-documented nonlinear regression fitting of SigmaPlot 13.

SigmaPlot 13 performs nonlinear least-squares fitting of function, which may be specified by the user, to data using the Marquardt-Levenberg algorithm.<sup>62</sup> The model function used in the present study is a sum of five Lorentzian peak functions, having common width at half height. Parameters to be optimised during the fitting procedure are the common peak width and the heights and positions of the individual peaks (a total of 11 parameters to be adjusted), with the additional constraint that the peaks are uniformly distributed/dispositioned, i.e. the isotope shift is assumed to be fully additive. Initial parameter values and acceptable ranges supplied to SigmaPlot were taken from the results of the Line Fitting procedure of MestReNova, as described above. Other details of the fitting procedure, e.g. the number of fitting iterations, step size and tolerance to be satisfied were the default settings of the program. The results of line fitting of the spectrum of [Pt<sup>35</sup>Cl<sub>*n*</sub><sup>37</sup>Cl<sub>6-*n*</sub>]<sup>2-</sup> in water (Fig. 2.6)

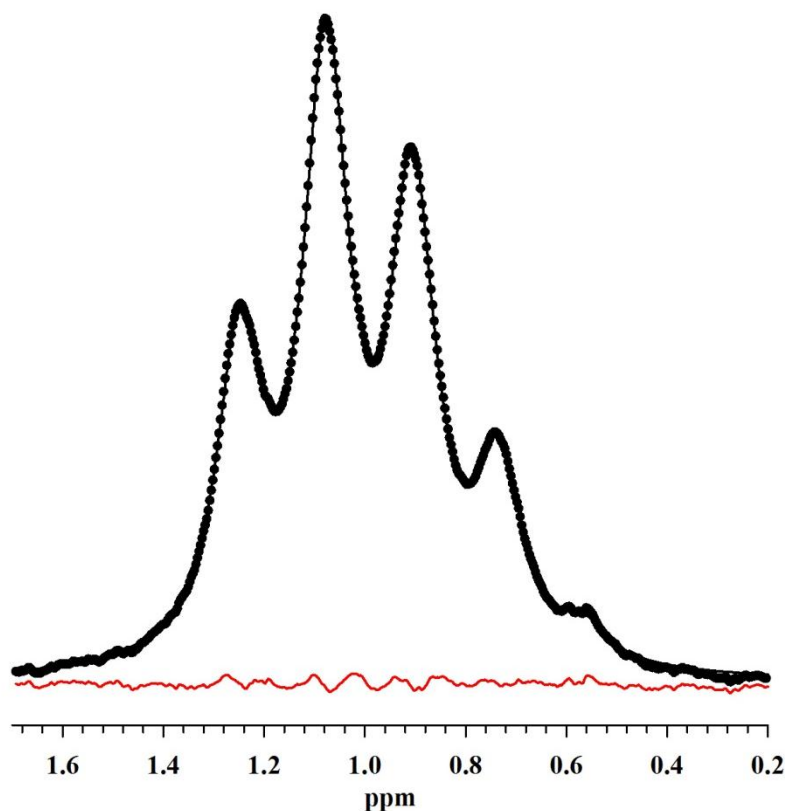


**Figure 2.7** Expansion of  $^{195}\text{Pt}$  NMR signals of  $[\text{Pt}^{35}\text{Cl}_n^{37}\text{Cl}_{6-n}]^{2-}$  in water (Fig. 2.5, black points), with least-squares fit of model function (black line) and residuals (red line) from nonlinear regression procedure of SigmaPlot 13 (see text for details).

using the nonlinear regression curve fitter of SigmaPlot 13 are plotted in Fig. 2.7; numerical results can be found in Table 2.2, along with those obtained by a similar procedure for the complexes in selected organic solvents. The fit of the model function to the data is technically not necessarily better than that possible using the Line Fitting feature of MestReNova 7.1.1. This is due in part to the fact that the Lorentzian shape of the component peaks of the model function of SigmaPlot does not account for variations from ideal NMR signal shape in the experimental spectrum.

Gerber *et al.*<sup>37</sup> reported excellent results when performing a similar line fitting procedure on a  $^{195}\text{Pt}$  NMR spectrum of the same complex in aqueous solution, using essentially the same fitting algorithm and a model function consisting of six Lorentzian peaks. The spectrum reported by these workers had a much higher signal-to-noise ratio compared that in Fig. 2.7, and also notably better spectral resolution. The first of these differences is due mainly to differences in the number of FID signals (or “scans”) acquired in the two experiments: 100 000 signals were averaged in the spectrum of Gerber *et al.*,<sup>37</sup> compared to the 2048

signals of Fig. 2.7. Moreover, while the analyte concentrations of the two samples were similar, the external referencing technique used in the current work (coaxial insert tube) reduces the active sample volume by approximately one half, further reducing sensitivity. The authors note that when only 256 FIDs were collected, a relative error below 2–3% between expected and observed signal intensities could be obtained, which is similar to that typically found in the present work. The difference in spectral resolution is inherent to the solutions studied (probe temperatures were similar), resulting from different spin relaxation behaviour in these environments (see details in Chapter 3).

The  $^1\Delta^{195}\text{Pt}(^{37/35}\text{Cl})$  isotope shift reported by Gerber *et al.* resulting in a best fit of the model function to their data is  $-0.171$  ppm.<sup>37</sup> The corresponding raw output value obtained here is  $-0.1716$  ppm, which, when considering also the variation in isotope shift values obtained by the Line Fitting feature of MestReNova ( $-0.170$  to  $-0.172$  ppm, Table 2.2), suggests that the isotope shift measured here could reasonably be reported as  $^1\Delta^{195}\text{Pt}(^{37/35}\text{Cl}) = -0.171 \pm 0.001$  ppm (assuming the isotope shift to be exactly additive).

### 2.2.3 Sample preparation and instrumentation

Varian <sup>Unity</sup>Inova 400 and 600 NMR spectrometers equipped with 5 mm <sup>1</sup>H {<sup>15</sup>N - <sup>31</sup>P} dual broadband probes (pulsed-field gradient, or PFG, probe version in the former) were used to obtain <sup>195</sup>Pt NMR spectra reported here. Probe temperatures were calibrated by a standard method based on known <sup>1</sup>H NMR chemical shifts of methanol and ethylene glycol.<sup>63</sup> After insertion of samples in the NMR probe, the sample was allowed at least 15 minutes to reach thermal equilibrium prior to starting data acquisition (<sup>195</sup>Pt NMR chemical shifts are highly temperature dependent),<sup>16,36,45</sup> and the magnetic field homogeneity was adjusted (“shimming”) by monitoring the <sup>1</sup>H NMR spectrum of the sample (shimming methods based on monitoring the <sup>2</sup>H lock signal of the deuterated solvent were found to be not ideal, since this signal reflects only the environment of nuclei contained in the coaxial insert tube containing the reference solution). Spectrometer operating/data processing software for both instruments was VnmrJ 2.1B. Standard 5 mm NMR tubes by Wilmad (PP series) and New Era (HL5) were used in all experiments, along with commercial (Wilmad) coaxial insert tubes. All chemicals used were obtained from commercial sources and were used without further purification.

## 2.3 Results and discussion

### 2.3.1 <sup>195</sup>Pt NMR isotope shifts and the *trans*-influence

<sup>195</sup>Pt NMR spectra of the series of complexes  $[\text{PtCl}_n(\text{OH})_{6-n}]^{2-}$  ( $n = 0-6$ ) found in alkaline aqueous solution were first studied by Goodfellow and co-workers.<sup>33</sup> The assignment of the signals of these complexes was based on regular chemical shift changes resulting from substitution of hydroxide for chloride ions, or chlorido-ligands, coordinated to Pt, while signals of stereoisomers (*cis/trans*, *fac/mer*) were assigned based on the known <sup>195</sup>Pt chemical shift relationship for the stereoisomer pair *cis/trans*- $[\text{PtCl}_4(\text{OH})_2]^{2-}$ . The *trans*-isomer was known to have a <sup>195</sup>Pt NMR chemical shift smaller than that of the *cis*-isomer (~20 ppm difference), and the signals of remaining stereoisomer pairs were similarly assigned, assuming that substitution of hydroxide for chlorido-ligands coordinated in a site *trans* to another chlorido-ligand produces a larger downfield <sup>195</sup>Pt chemical shift than for that *trans* to a hydroxido-ligand. The reverse assignment, or order, of stereoisomer signals was proposed for the related series of aquo-complexes  $[\text{PtCl}_n(\text{H}_2\text{O})_{6-n}]^{4-n}$  ( $n = 2-4$ ).

Following the work of Murray *et al.*<sup>37,49</sup> on  $^1\Delta^{195}\text{Pt}(^{37/35}\text{Cl})$  and  $^1\Delta^{195}\text{Pt}(^{18/16}\text{O})$  isotope shift profiles in the spectra of this aquo-series, i.e.  $[\text{PtCl}_n(\text{H}_2\text{O})_{6-n}]^{4-n}$  ( $n = 2-5$ ), it was decided to investigate these effects also in the related series of hydroxido-complexes  $[\text{PtCl}_n(\text{OH})_{6-n}]^{2-}$  ( $n = 0-5$ ), the complexes studied originally by Goodfellow and co-workers.<sup>33</sup> Murray *et al.*<sup>37,49</sup> showed that such isotope-induced profiles can be used for the unambiguous assignment of members of the series of aquo-complexes since many show unique <sup>195</sup>Pt NMR signal profiles as a result of the signals of isotopologues and, in some cases, isotopomers being partially resolved under these conditions. Note that <sup>18</sup>O-induced effects are detected only in <sup>18</sup>O-enriched samples (i.e. not in normal water), since this isotope has a low natural abundance, as does the <sup>17</sup>O isotope. Interestingly, when solutions containing the corresponding hydroxido-complexes are prepared in normal water (only <sup>16</sup>O-containing isotopologues detected), it is found that while the signals of isotopologues containing different combinations of <sup>35/37</sup>Cl isotopes are partially resolved as before, the signals of isotopomers differing in the position of these isotopes are not resolved as is the case in the <sup>195</sup>Pt spectra of the corresponding aquo-complexes.<sup>50</sup> The phenomenon is shown in Fig. 2.3, where the <sup>195</sup>Pt NMR spectrum of *cis*- $[\text{PtCl}_4(\text{H}_2\text{O})_2]$  is compared with that of *cis*- $[\text{PtCl}_4(\text{OH})_2]^{2-}$ . The most downfield signals in both spectra are due to isotopologues containing <sup>35</sup>Cl isotopes only, i.e. *cis*- $[\text{Pt}^{35}\text{Cl}_4(\text{H}_2^{16}\text{O})_2]$

and *cis*-[Pt<sup>35</sup>Cl<sub>4</sub>(<sup>16</sup>OH)<sub>2</sub>]<sup>2-</sup>, but the neighbouring signals, which are due to isotopologues containing a single <sup>37</sup>Cl isotope are clearly different. The spectrum of the aquo-complexes shows a closely-spaced pair of signals of equal intensity (“doublet” pattern, indicated in the figure by an asterisk), which is shown to be due to isotopomers differing in the combination of <sup>35/37</sup>Cl coordinated in the two sites *trans* to aquo-ligands (water molecules), the more upfield (lower chemical shift) signal corresponding to the isotopomer in which the single <sup>37</sup>Cl isotope is located in one of these *trans* positions.<sup>37</sup> This feature is not observed in the spectrum of the hydroxido-analogues, where a single signal is observed, i.e. the signals of such isotopomers are not resolved. Similar differences are found when comparing the <sup>195</sup>Pt NMR signals of other members of these series, e.g. [PtCl<sub>5</sub>(H<sub>2</sub>O)]<sup>-</sup> and [PtCl<sub>5</sub>(OH)]<sup>2-</sup>, acquired under identical conditions.<sup>50</sup>

The phenomenon is rationalised in the context of the expected Pt(IV) *trans*-influence series of ligands OH<sup>-</sup> > Cl<sup>-</sup> > H<sub>2</sub>O in aqueous solution.<sup>70</sup> The *trans*-influence of a ligand in a coordination complex is related to, but not necessarily parallel with the well-known kinetic *trans*-effect (ability of a ligand to “labialise” another ligand coordinated in a relative *trans* position), and refers to the structural influence of the ligand, specifically its ability to affect the bond displacement between the metal centre and another ligand coordinated in a relative *trans* (directly opposite) position. Such *trans*-influence series are traditionally studied in the solid state by crystallography, or in solution using NMR spin–spin coupling constants (*J*-coupling) and are strictly valid only for a particular metal and oxidation state, but are often transferable to some extent for related metal centres.<sup>70</sup> The consequence of the *trans*-influence series given above is that average Pt–Cl bond displacements *trans* to aquo-ligands are shorter than those *trans* to chlorido- or hydroxido-ligands in these octahedral Pt(IV) complexes, which is reflected in the magnitude of <sup>1</sup>Δ<sup>195</sup>Pt(<sup>37/35</sup>Cl) isotope shifts resulting from isotopic substitution/difference in these coordination sites.<sup>71,72</sup> Specifically, substitution of chlorine isotopes coordinated *trans* to aquo-ligands results in a greater (more negative) <sup>1</sup>Δ<sup>195</sup>Pt(<sup>37/35</sup>Cl) shift compared with that resulting from substitution *trans* to other chlorido-ligands, but such differences are not observed in the hydroxido-complexes, where Pt–Cl bonds *trans* to chlorido- and hydroxido-ligands are expected to be longer, as found in the solid state.<sup>71,72</sup> These observations are consistent with the work of Gombler<sup>65</sup> regarding the relationship between the magnitude of NMR isotope shifts and bond displacements in molecules, suggesting that the magnitude of the shift decreases with increasing bond displacement between observed and isotopically substituted nuclei (i.e. inverse relationship).

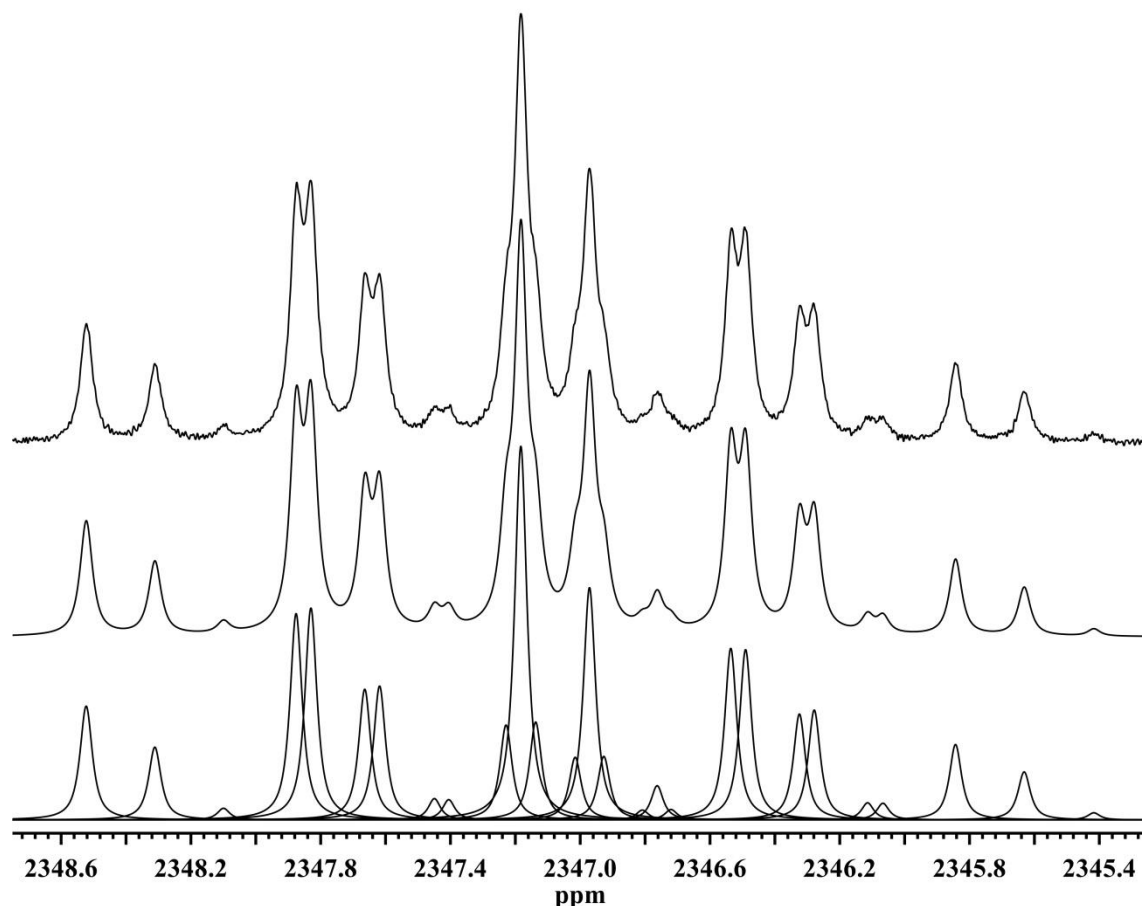


**Figure 2.8** <sup>195</sup>Pt NMR spectrum (*ca.* 129 MHz) of  $[\text{Pt}^{35/37}\text{Cl}_2(^{16/18}\text{OH})_4]^{2-}$  in alkaline aqueous solution (4 M NaOH) at 293 K (**top**). Results of a line fitting procedure (signal deconvolution) with fitted model/sum function (**middle**) and individual peaks (**bottom**) using MestReNova. Figure adapted from ref. 50.

The <sup>195</sup>Pt NMR spectra of the hydroxido-complexes *cis*- $[\text{Pt}^{35/37}\text{Cl}_2(^{16/18}\text{OH})_4]^{2-}$  and  $[\text{Pt}^{35/37}\text{Cl}(^{16/18}\text{OH})_5]^{2-}$  in an <sup>18</sup>O-enriched solution (~45%) are given in Fig. 2.8 and 2.9. In these spectra, the larger (*ca.* -0.7 ppm)  $^1\Delta^{195}\text{Pt}(^{18/16}\text{O})$  isotope shifts result essentially in a multiplication of  $^1\Delta^{195}\text{Pt}(^{37/35}\text{Cl})$  signal patterns,<sup>73</sup> however, additional, partially resolved signals are observed, e.g. the doublet “split” signals and broad bases of some signals indicated in Fig. 2.4. These additional signals are found to be due to isotopomers differing only in the combination of <sup>16/18</sup>O isotopes coordinated *trans* to chlorido-ligands. The 2.10

assignment is confirmed by comparing the relative signal intensities obtained by a signal deconvolution procedure (using MestReNova 7.1.1) with statistically expected relative abundances calculated based on the known natural abundances of chlorine isotopes and the level of <sup>18</sup>O-enrichment of the sample (numerical data in relevant research article<sup>50</sup> given in Appendix).

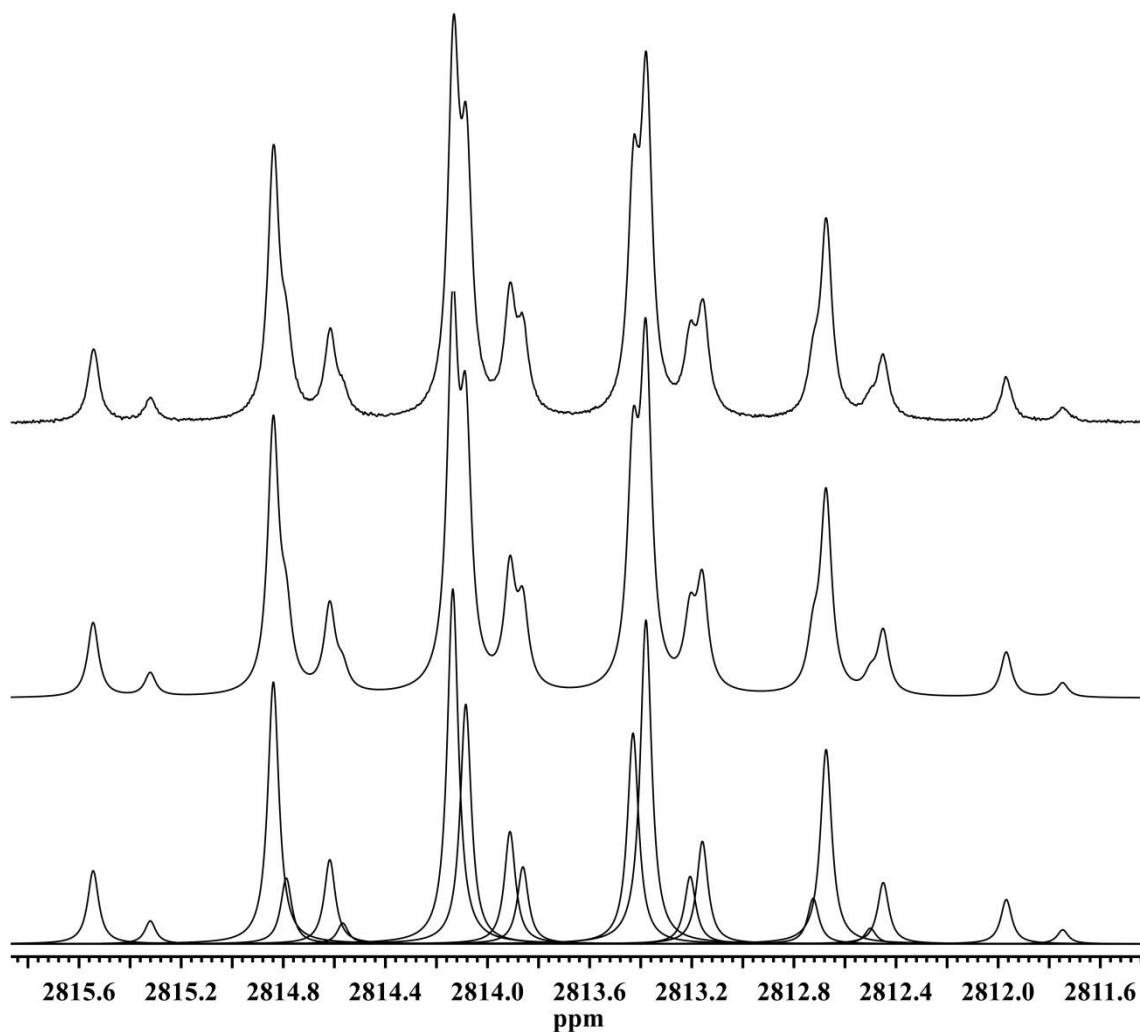


**Figure 2.9**  $^{195}\text{Pt}$  NMR spectrum (ca. 129 MHz) of  $[\text{Pt}^{35/37}\text{Cl}^{(16/18)}\text{OH}_5]^{2-}$  in alkaline aqueous solution (4 M NaOH) at 293 K (**top**). Results of a line fitting procedure (signal deconvolution) with fitted model/sum function (**middle**) and individual peaks (**bottom**) using MestReNova. Figure adapted from ref. 50.

Specifically, the spectrum of  $\text{cis-}[\text{Pt}^{35/37}\text{Cl}_2^{(16/18)}\text{OH}_4]^{2-}$  may be interpreted in a way analogous to that presented above for  $\text{cis-}[\text{Pt}^{35/37}\text{Cl}_4(\text{H}_2^{16}\text{O})_2]$ , but considering the different relative *trans*-influences of chlorido- and hydroxido-ligands: Pt–O bond displacements *trans* to chlorido-ligands are expected to be shorter than those *trans* to other hydroxido-ligands, resulting in greater absolute  $^1\Delta^{195}\text{Pt}^{(18/16)\text{O}}$  isotope shifts for the signals of isotopomers in which these positions are occupied by  $^{18}\text{O}$  compared to those having  $^{16}\text{O}$  in these sites (and  $^{18}\text{O}$  *trans* to hydroxido-ligands), resulting in the unresolved double- and triple-line patterns observed in these spectra since all such species are present in solution, i.e. their signal are



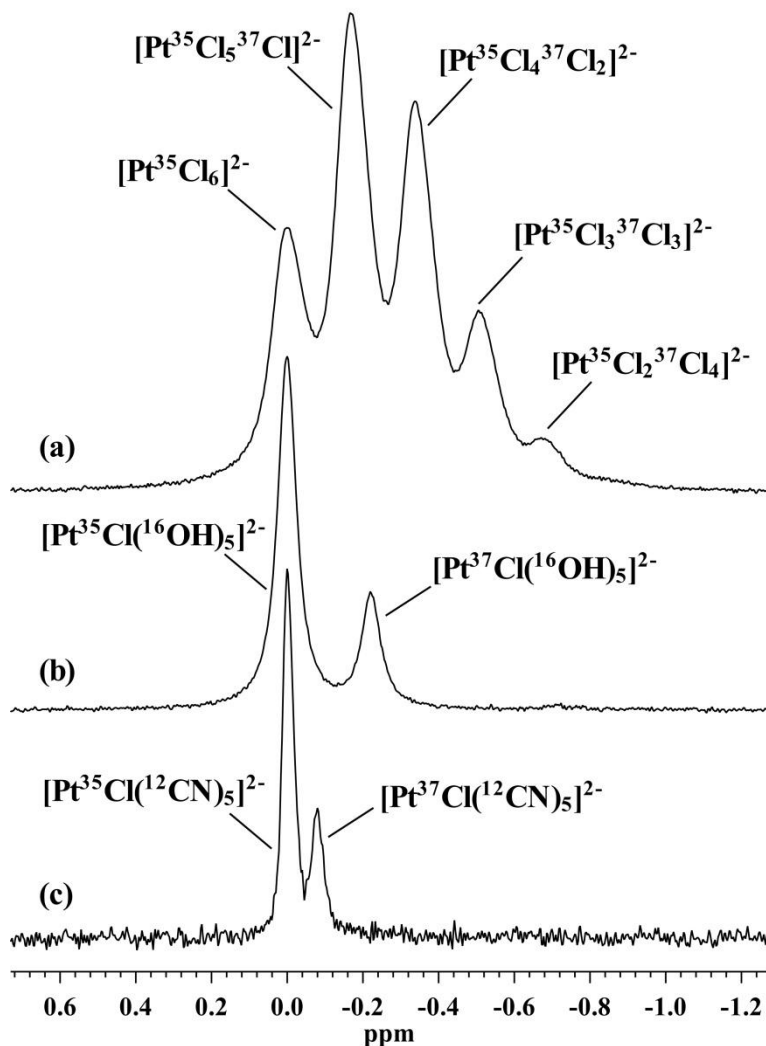


**Figure 2.10** Comparison of  ${}^1\Delta^{195}\text{Pt}({}^{37/35}\text{Cl})$  isotope shifts in platinum complexes in aqueous solution at 293 K: (a)  $[\text{PtCl}_6]^{2-}$ ; (b)  $[\text{PtCl}(\text{OH})_5]^{2-}$ ; (c)  $[\text{PtCl}(\text{CN})_5]^{2-}$ . Note the arbitrary  $^{195}\text{Pt}$  chemical shift scale; actual chemical shifts:  $\delta^{195}\text{Pt}([\text{PtCl}(\text{OH})_5]^{2-}) = 2821$  ppm,  $\delta^{195}\text{Pt}([\text{PtCl}(\text{CN})_5]^{2-}) = -3264$  ppm. Isotope labels not specified for nitrogen since no estimate of  ${}^2\Delta^{195}\text{Pt}({}^{14/12}\text{N})$  available, but due to low natural abundance<sup>2</sup> of  ${}^{14}\text{N}$ , the signals of isotopologues containing this isotope are expected to make a negligible contribution.

recorded in the same  $^{195}\text{Pt}$  NMR spectrum. This effect is particularly apparent in the spectrum of  $[\text{Pt}^{35/37}\text{Cl}({}^{16/18}\text{OH})_5]^{2-}$ , where the intensities of the signals constituting such double-line patterns are different, with intensity ratios clearly corresponding to statistically expected abundances e.g. there exist two isotopomers with the isotopic formula  $[\text{Pt}^{35}\text{Cl}({}^{16}\text{OH})_4({}^{18}\text{OH})]^{2-}$ ; one in which  ${}^{16}\text{O}$  occupies the coordination site *trans* to the chlorido-ligand and one in which  ${}^{18}\text{O}$  occupies this site, and these are expected statistically to be present in ratio 4:1 as reflected in the relative signal intensities. Note also that the latter has a slightly lower  $^{195}\text{Pt}$  chemical shift, i.e. a larger negative  ${}^1\Delta^{195}\text{Pt}({}^{18/16}\text{O})$  isotope shift

from the signal of  $[\text{Pt}^{35}\text{Cl}(\text{}^{16}\text{OH})_5]^{2-}$ , which is furthest downfield. The remaining pairs of signals may be assigned by a similar reasoning.

The implications of the *trans*-influence for NMR isotope shifts in such complexes is also illustrated by considering the <sup>195</sup>Pt NMR signals of the complexes  $[\text{PtCl}(\text{OH})_5]^{2-}$  and  $[\text{PtCl}(\text{CN})_5]^{2-}$  in aqueous solution given in Fig. 2.10. These complexes were prepared as part of an initial study intended to measure NMR isotope shifts in conceivable complexes of the type  $[\text{PtCl}_{6-m-n}(\text{OH})_m(\text{CN})_n]^{2-}$  ( $m, n = 0-6$ ) by dissolving  $\text{Na}_2\text{PtCl}_6$  in strongly alkaline (2 M NaOH) aqueous solutions containing NaCN (0.2 M). The <sup>195</sup>Pt NMR spectrum of  $[\text{Pt}^{35}\text{Cl}_n\text{}^{37}\text{Cl}_{6-n}]^{2-}$  in D<sub>2</sub>O is shown for direct comparison. The  $^1\Delta^{195}\text{Pt}(\text{}^{37/35}\text{Cl})$  isotope shifts in these spectra are clearly different: -0.171 ppm in  $[\text{PtCl}_6]^{2-}$ , to -0.22 ppm in  $[\text{PtCl}(\text{OH})_5]^{2-}$ , and only -0.08 ppm in  $[\text{PtCl}(\text{CN})_5]^{2-}$ . These observations possibly reflect differences in the dynamic properties of the Pt-Cl bonds in these complexes, as a result of a *trans*-influence series and/or differences in the nature of intermolecular interactions with surrounding water molecules, an interesting topic for a future detailed study.<sup>50</sup>

### 2.3.2 Temperature dependence of <sup>195</sup>Pt NMR chemical shifts: some background

NMR chemical shifts of molecules in solution are temperature dependent, and this is particularly evident for nuclei with large chemical shift ranges, e.g. <sup>59</sup>Co and <sup>195</sup>Pt.<sup>48</sup> The phenomenon may be due to involvement of the molecule in equilibrium processes e.g. conformational exchange, changes in intermolecular interactions (greatly affected by changes in solution density), as well as an intrinsic intramolecular component that reflects the effect of changes in molecular vibration and rotation (average geometry) on the nuclear shielding. These effects are described in detail by Jameson.<sup>64</sup> While all three effects listed may be important in general, as is the case e.g. in the temperature dependence of proton chemical shifts in many organic molecules, transition metal nuclei located at the centre of octahedral coordination complexes are different in that the intrinsic component often determines the temperature dependence, which is deshielding (downfield shift) with increasing temperature.<sup>48</sup> Intrinsic temperature shifts in transition metal complexes have been found to be approximately linear, at least over small temperature ranges, and also to be much larger than those found for many commonly measured nuclei. In the case of <sup>195</sup>Pt, few accurate measurements of chemical shift temperature coefficients (temperature dependence of

chemical shift) have been reported, but they, too, are large (*ca.* +1 ppm/K).<sup>16,36</sup> Jameson predicted the <sup>195</sup>Pt chemical shift temperature coefficient of [PtCl<sub>6</sub>]<sup>2-</sup> to be about +0.53 ppm/K using the experimental <sup>1</sup>Δ<sup>195</sup>Pt(<sup>37/35</sup>Cl) isotope shift and calculated mean bond displacements.<sup>45</sup> While this quantity has not been accurately determined (accurate measurement of the intrinsic chemical shift temperature coefficient is not straightforward in general), recent preliminary results indicate that the temperature coefficient is somewhat larger, closer to +1 ppm/K, in aqueous solution.<sup>37</sup>

As described by Jameson, the intrinsic temperature dependence of NMR chemical shift is closely related to the intrinsic isotope shift.<sup>48</sup> Isotope shifts themselves have been found to be temperature dependent, however, as shown in the work of Gombler on <sup>34</sup>S-induced isotope shifts in <sup>19</sup>F NMR spectra of chalcogen compounds.<sup>65</sup> Here the isotope shift is found to decrease (smaller negative shift) with increasing temperature; this phenomenon is attributed to vibrationally excited states of the molecules having on average longer S–F bond distances. Gombler proposes three possible explanations for the dependence of the isotope shift on bond distance:<sup>65</sup>

1. Nonlinear dependence of nuclear magnetic shielding on bond distance.
2. Decreasing (vibrational) energy difference between isotopologues (Gombler uses the term *isotopomers*) with increasing bond distance.
3. Decrease in the anharmonicity of vibrational potential with increasing bond distance.

While no detailed studies of the effect of temperature on NMR *isotope shifts* for transition metal nuclei have been reported, experiments by Gerber *et al.*<sup>37</sup> show that the <sup>195</sup>Pt NMR signals of the isotopologues [Pt<sup>35</sup>Cl<sub>*n*</sub><sup>37</sup>Cl<sub>6-*n*</sub>]<sup>2-</sup>, *n* = 0–6, in aqueous solutions are well resolved only in the temperature range *ca.* 288–298 K, with significant loss of resolution at 303 K. This phenomenon was not investigated in detail, but is due in part to broadening of the signals at higher temperatures where the spin–rotation relaxation mechanism, which is known to be important in the spin relaxation of <sup>195</sup>Pt,<sup>17</sup> becomes dominant; this phenomenon is described in detail in Chapter 3.

### 2.3.3 Effect of solvent on <sup>195</sup>Pt NMR chemical shifts of Pt complexes

Measurements of the solvent dependence of the <sup>195</sup>Pt NMR chemical shift of [PtCl<sub>6</sub>]<sup>2-</sup> dissolved in binary mixtures of D<sub>2</sub>O and selected water-miscible organic solvents were originally conducted at 303 K (Fig. 2.1).<sup>30</sup> Under these conditions, preferential solvation of the platinum complex by the organic component in the binary mixture was indicated for *all* mixtures studied and over the *entire* solvent composition range. Westra proposed a possible explanation for this phenomenon: the preference for the organic component may result from properties of the solvent mixture and not necessarily only the nature of interactions of the solvents with the platinum complex.<sup>30</sup> This conclusion was based on a computer simulation study by Hawlicka and Swiatla-Wojcik, indicating preferential solvation of chloride ion by methanol in water–methanol mixtures. The authors proposed that the phenomenon was due to a “collective exclusion” of the anion and methanol from the hydrogen-bonded structure of water, forming regions, or “clusters” as proposed also for binary mixtures of water and certain other organic compounds.<sup>66,67</sup>

An important objective of the current study was to examine the effect of solvent composition on the <sup>195</sup>Pt NMR isotope shift in the spectrum of [PtCl<sub>6</sub>]<sup>2-</sup> of the solutions described above, i.e. to determine if isotope shifts may be used to investigate preferential solvation indicated by <sup>195</sup>Pt NMR chemical shift measurements. Accurate determination of these isotope shifts requires that NMR spectra be recorded under conditions of optimal spectral resolution (see Section 2.2.2), while not affecting the phenomenon under study (preferential solvation). Sadler *et al.*<sup>42</sup> originally recorded the <sup>195</sup>Pt NMR spectrum of the [Pt<sup>35</sup>Cl<sub>*n*</sub><sup>37</sup>Cl<sub>6-*n*</sub>]<sup>2-</sup> (*n* = 0–6) in aqueous solution at 294 K; similarly, the preliminary study of the effect of temperature on spectral resolution in the <sup>195</sup>Pt NMR spectra of similar solutions by Gerber *et al.*<sup>37</sup> identified a temperature close (within *ca.* 1–2 degrees) to 293 K as providing essentially optimal signal resolution.

The physical properties of mixed solvents are known to be temperature dependent. Corsaro *et al.*<sup>68</sup> showed, using <sup>1</sup>H spin relaxation time measurements, that the microscopic structure of water–methanol solutions change with temperature, from stable water–methanol clusters at low temperatures (205 K) to clusters of single species at higher temperatures (295 K). If, as suggested by Hawlicka and Swiatla-Wojcik,<sup>66,67</sup> the preferential solvation phenomenon observed for chloride ions in water–methanol mixtures has its origin in the properties of the solvent mixture, i.e. strong interactions among water molecules and a “collective

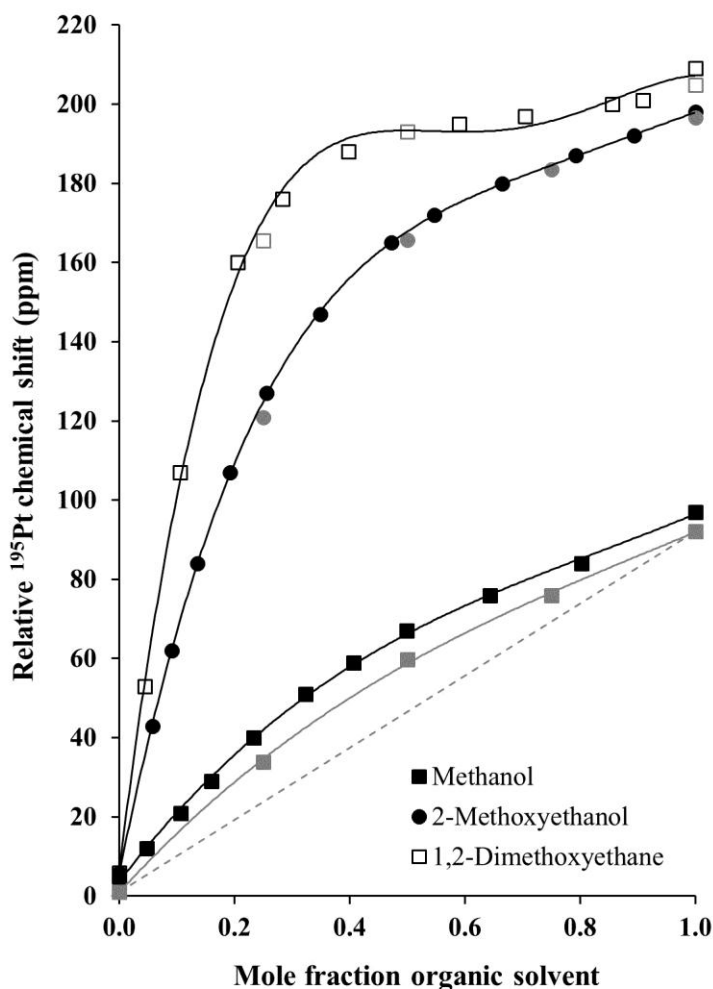


**Figure 2.11** <sup>195</sup>Pt NMR chemical shifts of  $[\text{PtCl}_6]^{2-}$  in solutions of hexachloroplatinic acid (ca. 0.1 M) in binary mixtures of water ( $\text{D}_2\text{O}$ ) and selected water-miscible organic solvents at 303 K (black data symbols); selected measurements repeated (0.2 M) in normal solvent mixtures at 293 K (grey symbols). Polynomial trends fitted to data, with dashed grey line connecting limiting values measured in the water–methanol mixture, indicating curved data trend. Data (black symbols) reproduced from Westra.<sup>30</sup>

exclusion” effect, it is reasonable to expect that this phenomenon, too, should be temperature dependent.

Fig. 2.11 shows the overall <sup>195</sup>Pt NMR chemical shift trends reported by Westra *et al.* for  $[\text{PtCl}_6]^{2-}$  dissolved (as hexachloroplatinic acid hexahydrate, “ $\text{H}_2\text{PtCl}_6 \cdot 6\text{H}_2\text{O}$ ”) in binary mixtures of  $\text{D}_2\text{O}$  with methanol, 2-methoxyethanol and 1,2-dimethoxyethane (a subset of the data in Fig. 2.2) at 303 K;<sup>30</sup> as described in Section 2.1.2, the curved chemical shift trends were suggested by Westra to indicate preferential solvation of the platinum complex by the organic solvent component over water. Also plotted on this graph are measurements repeated

at selected solvent compositions (but with *normal* water instead of D<sub>2</sub>O) at 293 K. The near coincidence of the data acquired at the two temperatures for solutions containing 2-methoxyethanol and 1,2-dimethoxyethane suggests that similar preferential solvation phenomena are likely at the lower temperature (293 K), at which <sup>195</sup>Pt NMR isotope shifts may be resolved. In the case of water–methanol mixtures, these two data sets are offset by *ca.* 5 ppm, with consistently lower chemical shifts measured at the lower temperature (this is not unexpected in view of the estimated temperature dependence of the <sup>195</sup>Pt chemical shift in this molecule in aqueous solution of ~+1 ppm/K),<sup>16,37</sup> however, the limited data collected at 293 K indicates a similar curved trend as a function of solvent composition to that obtained at 303 K.

Several factors may contribute to differences between the <sup>195</sup>Pt chemical shift data of Westra and that reported here. Temperature, isotopic composition of solvent and salt concentration (original measurements at 303 K were made using samples with a platinum salt concentration approximately 100 mM) are expected to contribute to some extent,<sup>16,17</sup> but the chemical shift trends clearly are qualitatively similar, i.e. in the water–methanol solution a moderate degree/extent of preferential solvation of the platinum complex by the organic component may be inferred, while in the water–1,2-dimethoxyethane mixture there is apparently a much more pronounced preferential solvation effect (the curved trend essentially reaches a plateau); the water–2-methoxyethanol mixture represents perhaps an intermediate case (while maintaining similar functional groups in the organic component).<sup>30</sup> It follows from these observations that the preferential solvation phenomenon detected originally at 303 K may be studied also at the lower temperature of 293 K, where resolution of <sup>195</sup>Pt NMR signals of the isotopologues [Pt<sup>35</sup>Cl<sub>*n*</sub><sup>37</sup>Cl<sub>6-*n*</sub>]<sup>2-</sup> (*n* = 0–6) is expected to be optimal.

### 2.3.4 The effect of solvent on <sup>195</sup>Pt NMR isotope shifts

The <sup>195</sup>Pt NMR spectra of the [PtCl<sub>6</sub>]<sup>2-</sup> anion in solutions of hexachloroplatinic acid in the pure solvents water, methanol, 2-methoxyethanol and 1,2-dimethoxyethane at 293 K are shown in Fig. 2.12. Accurate determination of the  $^1\Delta^{195}\text{Pt}(^{37/35}\text{Cl})$  isotope shift in these solvents involves fitting a model function to the experimental data by a nonlinear least-squares method described in detail in Section 2.2.2. The model function used here is a sum of uniformly dispositioned Lorentzian peaks with a common line width at half-height, representing the signals of the isotopologues [Pt<sup>35</sup>Cl<sub>*n*</sub><sup>37</sup>Cl<sub>6-*n*</sub>]<sup>2-</sup>, *n* = 0–6. The signals of [Pt<sup>35</sup>Cl<sup>37</sup>Cl<sub>4</sub>]<sup>2-</sup> and [Pt<sup>37</sup>Cl<sub>6</sub>]<sup>2-</sup> were not detected due to the low natural abundances of these isotopologues (0.34 and 0.02 %), and only five Lorentzian peaks were included in the model function fitted to the experimental data. A detailed description of the fitting procedure is given in Section 2.2.2, and the numerical results are collected in Table 2.2. Here, the contributions of individual peaks to the total area of the fitted model function are compared to the natural abundances of the corresponding isotopologues and in most cases good agreement is found. Inspection of the residual functions included in Fig. 2.12 (“raw” residuals produced by fitting program) reveals that, technically, a notably poorer fit to the experimental spectrum was obtained in the case of 2-methoxyethanol as solvent (Fig. 2.12 (c)), where signal widths at half-height (commonly simply referred to as “line widths”) are smallest (*ca.* 4 Hz), possibly due to deviations from ideal peak shape and the lower digital resolution in this spectrum. The visual differences in the spectra reported in Figure 2.12 are due mainly to differences in line width, reflecting the different spin relaxation times in these solvents (this is considered in detail in the next chapter).

The  $^1\Delta^{195}\text{Pt}(^{37/35}\text{Cl})$  isotope shifts reported in Table 2.2 differ on the order of a few thousandths of parts per million, or parts per billion (0.001 ppm = 1 ppb). Such small differences are not uncommon in the few studies of the variation of NMR isotope shifts with molecular structure, temperature and physical state of the sample (e.g. comparison of isotope shifts in solid state and solution by Wasylishen and co-workers<sup>43</sup>). Pertinent in this context is the work of Risley *et al.*<sup>69</sup> on correlations of  $^1\Delta^{13}\text{C}(^{18/16}\text{O})$  shifts of carbonyl carbons with bond properties, and also that of Gombler.<sup>65</sup> When reporting such results, it is desirable to have at least an estimate of the errors associated with their measurement, so as to determine the significance the small variations. This turns out to be a nontrivial task, however, since the

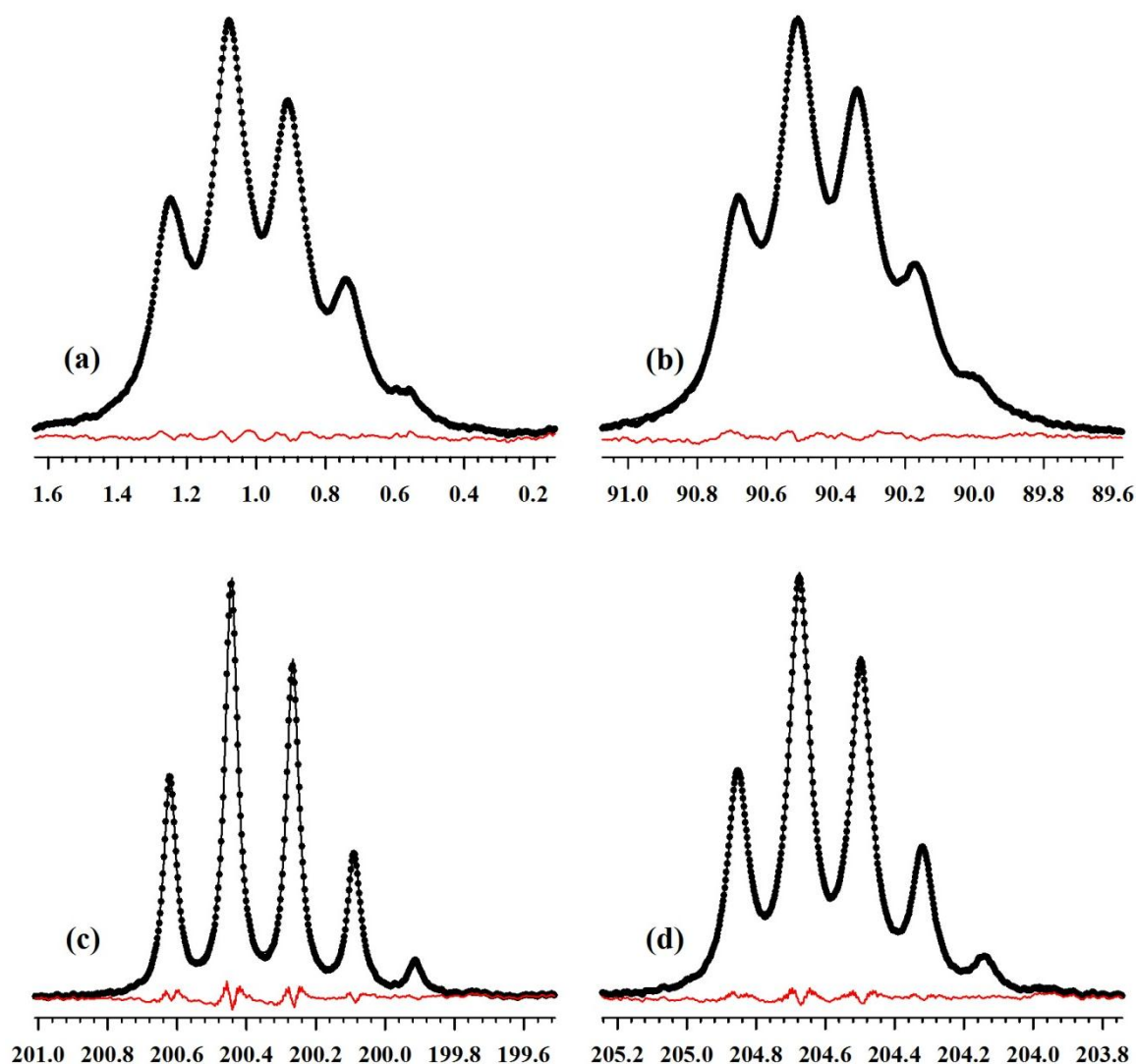


**Figure 2.12**  $^{195}\text{Pt}$  NMR spectra of  $[\text{Pt}^{35}\text{Cl}_n^{37}\text{Cl}_{6-n}]^{2-}$  in 0.2 M solutions of hexachloroplatinic acid in (a) water, (b) methanol, (c) 2-methoxyethanol and (d) 1,2-dimethoxyethane (d) at 293 K (black circles). Least-squares fit of model function (black line) and raw residuals (red line) from nonlinear regression procedure (SigmaPlot 13).

relative importance of the various factors expected to affect accuracy of the isotope shift measurement are not known, e.g. the effect of temperature variations and intermolecular interactions (ion-pairing). Technically, the determination of the isotope shift from the experimental spectrum is expected to yield values that are conservatively estimated to be variable within 1 ppb, i.e. assuming isotope shifts to be additive, the  $^1\Delta^{195}\text{Pt}(^{37/35}\text{Cl})$  isotope shift in water may be reported as  $-0.171\pm 0.001$  ppm. A recent estimate of this isotope shift in aqueous solution under similar physical conditions by Gerber *et al.*,<sup>37</sup> using an essentially



**Table 2.2** Relative peak intensities of <sup>195</sup>Pt NMR signals of isotopologues [Pt<sup>35</sup>Cl<sub>n</sub><sup>37</sup>Cl<sub>6-n</sub>]<sup>2-</sup> in various solvents at 293 K, determined by a signal deconvolution procedure (see Fig. 2.12 and text for details).

Isotopologue	Relative peak intensities (%)				Natural abundance (%)
	Water	Methanol	2-ME <sup>a</sup>	1,2-DME <sup>b</sup>	
[Pt <sup>35</sup> Cl <sub>6</sub> ] <sup>2-</sup>	19.7	18.6	19.0	19.0	18.92
[Pt <sup>35</sup> Cl <sub>5</sub> <sup>37</sup> Cl] <sup>2-</sup>	37.5	36.8	36.5	36.8	36.31
[Pt <sup>35</sup> Cl <sub>4</sub> <sup>37</sup> Cl <sub>2</sub> ] <sup>2-</sup>	29.1	29.2	29.1	29.1	29.03
[Pt <sup>35</sup> Cl <sub>3</sub> <sup>37</sup> Cl <sub>3</sub> ] <sup>2-</sup>	11.7	12.5	12.4	12.3	12.38
[Pt <sup>35</sup> Cl <sub>2</sub> <sup>37</sup> Cl <sub>4</sub> ] <sup>2-</sup>	2.0	2.9	3.0	2.8	2.97
[Pt <sup>35</sup> Cl <sup>37</sup> Cl <sub>5</sub> ] <sup>2-</sup>	—	—	—	—	0.38
[Pt <sup>37</sup> Cl <sub>6</sub> ] <sup>2-</sup>	—	—	—	—	0.02
<sup>1</sup> Δ <sup>195</sup> Pt( <sup>37/35</sup> Cl)	-0.171	-0.174	-0.177	-0.178	—

<sup>a</sup> 2-Methoxyethanol. <sup>b</sup> 1,2-Dimethoxyethane.

similar line fitting procedure, yielded a value of -0.171 ppm (the original 1980 report by Sadler and co-workers at 294 K was -0.169 ppm;<sup>42</sup> note that the isotope shift is expected to be temperature dependent, decreasing in magnitude with increasing temperature<sup>65</sup>).

The <sup>1</sup>Δ<sup>195</sup>Pt(<sup>37/35</sup>Cl) isotope shifts in Table 2.2 then can be reported as varying only slightly in magnitude in the order 1,2-dimethoxyethane ≥ 2-methoxyethanol > methanol > water, with an overall range of ~7 ppb. No other studies of solvent effects on NMR isotope shifts have been reported, and the reason for this trend is not clear at present. In a review of isotope effects on nuclear shielding, Jameson and Osten<sup>51</sup> mention solvent effects on isotope shifts, but merely note that such effects are expected to be small in polyatomic molecules dissolved in liquids (at least in the absence of specific interactions e.g. strong hydrogen bonding). Gombler<sup>65</sup> studied the relationship between <sup>1</sup>Δ<sup>19</sup>F(<sup>34/32</sup>S) isotope shifts and S-F bond lengths in a series of chalcogen compounds, as well as the temperature dependence in selected members. It was demonstrated that the magnitude of the isotope shift *decreases* with increasing bond length; possible explanations for this inverse relationship were presented (Section 2.3.2). Risley, Defrees and van Etten<sup>69</sup> reported correlations between <sup>1</sup>Δ<sup>13</sup>C(<sup>18/16</sup>O) shifts of carbonyl carbons and carbonyl bond properties in acetophenones and showed, for example, that a direct correlation exists between the magnitude of the isotope shift and the carbonyl stretching frequency in this series of compounds. Indeed, solvent effects on vibrational frequencies of small anionic probes, e.g. thiocyanate, have been reported and

identified with differences in the hydrogen bonding interactions in these environments.<sup>53</sup> It follows that the variation in  ${}^1\Delta^{195}\text{Pt}$  NMR isotope shifts with solvent observed in the current study may be due to differences in dynamic and structural properties of the platinum complex in the different solvents, resulting from the nature of interaction with surrounding solvent molecules.

Jameson *et al.*<sup>48</sup>, in a study of isotope and temperature effects on transition metal shielding in octahedral complexes reported that the  ${}^1\Delta^{51}\text{V}({}^{13/12}\text{C})$  isotope shift of certain vanadium carbonyl complexes show a direct correlation with the  ${}^{51}\text{V}$  chemical shifts of these compounds. This observation was shown to be consistent with theory from which it follows that the sensitivity of nuclear shielding to changes in bond displacements, e.g. as brought about by isotopic substitution or a change in temperature, should correlate directly with the magnitude of paramagnetic shielding of the nucleus in a series of structurally similar compounds. A similar observation was reported by Risley *et al.* in their study of factors affecting the size of the  ${}^1\Delta^{13}\text{C}({}^{18/16}\text{O})$  isotope shift in acetophenones mentioned above.<sup>69</sup> The relationship described by Jameson *et al.*<sup>48</sup> also appears to describe the solvent dependence of the  ${}^1\Delta^{195}\text{Pt}({}^{37/35}\text{Cl})$  isotope shifts reported here: the magnitude of the isotope shift clearly scales with the  ${}^{195}\text{Pt}$  chemical shift in the various solvent environments (see Table 2.2 and Section 2.1.2).

The  ${}^{195}\text{Pt}$  NMR spectra of  $[\text{PtCl}_6]^{2-}$  in equimolar mixtures of water with methanol and 1,2-dimethoxyethane are presented in Figure 2.13, and have been processed and analysed by a line fitting procedure similar to that described for the spectra obtained in pure solvents discussed above. The  ${}^1\Delta^{195}\text{Pt}({}^{37/35}\text{Cl})$  isotope shifts determined by this method are  $-0.173$  and  $-0.179$  ppm, respectively, and are essentially identical with the shifts obtained in the respective pure *organic* solvents (Table 2.2 and 2.3). This observation is consistent with a preferential solvation of the platinum complex by the organic component in these binary solvent mixtures, since the magnitude of the isotope shift is expected to reflect the composition of its primary solvation shell. Interestingly, the isotope shifts do not seem to reflect accurately the different *extent* of preferential solvation in these two mixtures: moderate preference for methanol is expected in the water–methanol mixture based on the  ${}^{195}\text{Pt}$  NMR chemical shift measurements of Westra and co-workers,<sup>30</sup> yet the isotope shift in this mixture is equal to the limiting value measured in pure methanol, which is intuitively

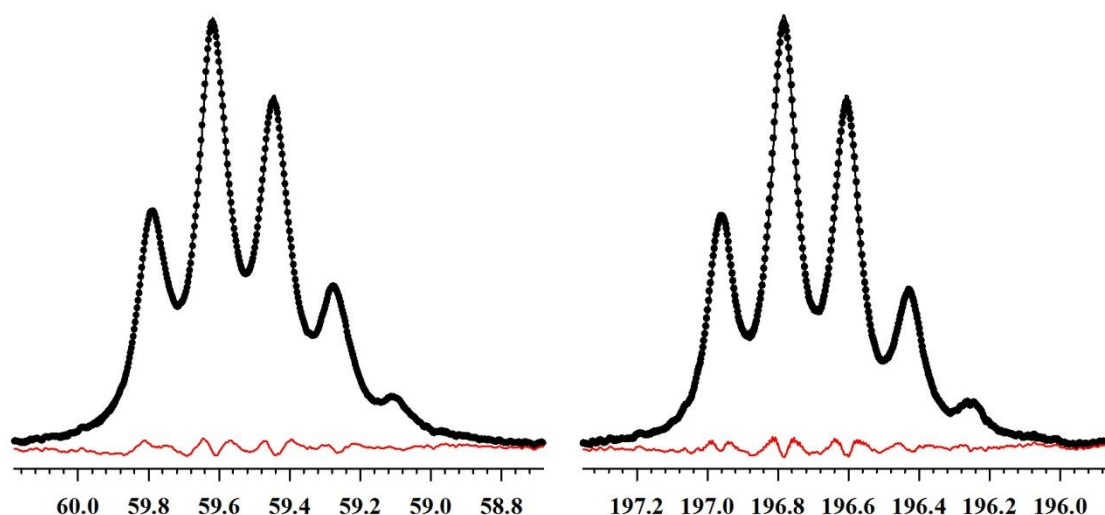


**Figure 2.13**  $^{195}\text{Pt}$  NMR spectra of  $[\text{Pt}^{35}\text{Cl}_n^{37}\text{Cl}_{6-n}]^{2-}$  in 0.2 M solutions of hexachloroplatinic acid in equimolar binary mixtures of water and methanol (**left**) and 1,2-dimethoxyethane (**right**) at 293 K (black circles). Least-squares fit of model function (black line) and raw residuals (red line) from nonlinear regression procedure (SigmaPlot 13).

**Table 2.3** Relative peak intensities of  $^{195}\text{Pt}$  NMR signals of isotopologues  $[\text{Pt}^{35}\text{Cl}_n^{37}\text{Cl}_{6-n}]^{2-}$  in equimolar mixtures of water with methanol and 1,2-dimethoxyethane (1,2-DME) at 293 K (see Fig. 2.13 and text for details).  $^1\Delta^{195}\text{Pt}(^{37/35}\text{Cl})$  NMR isotope shifts reported in bottom row.

Isotopologue	Relative peak intensities (%)		Natural abundance (%)
	Water + Methanol	Water + 1,2-DME	
$[\text{Pt}^{35}\text{Cl}_6]^{2-}$	18.8	18.9	18.92
$[\text{Pt}^{35}\text{Cl}_5^{37}\text{Cl}]^{2-}$	36.8	36.7	36.31
$[\text{Pt}^{35}\text{Cl}_4^{37}\text{Cl}_2]^{2-}$	29.3	29.2	29.03
$[\text{Pt}^{35}\text{Cl}_3^{37}\text{Cl}_3]^{2-}$	12.2	12.2	12.38
$[\text{Pt}^{35}\text{Cl}_2^{37}\text{Cl}_4]^{2-}$	2.9	2.9	2.97
$[\text{Pt}^{35}\text{Cl}^{37}\text{Cl}_5]^{2-}$	—	—	0.38
$[\text{Pt}^{37}\text{Cl}_6]^{2-}$	—	—	0.02
$^1\Delta^{195}\text{Pt}(^{37/35}\text{Cl})$	-0.173	-0.179	—

expected to indicate *complete* solvation by methanol. In the case of the water–1,2-dimethoxyethane mixture, however, this equality is fully consistent with a stronger preference for the organic component inferred from chemical shift measurements.<sup>30</sup>

Unfortunately, the use of  $^1\Delta^{195}\text{Pt}(^{37/35}\text{Cl})$  NMR isotope shifts for the study of preferential solvation in the present case is limited by the relatively small differences between these intrinsic isotope shifts in the pure solvents (limiting values). A further limitation is that the <sup>195</sup>Pt NMR isotope shifts and the overall paramagnetic shielding (i.e. chemical shifts) are probably intimately connected (at least for similar compounds, and of course also in the present case), as suggested by Jameson, and so are *not* independent measures of the solution environment of the platinum complex.<sup>48</sup>

### 2.3.5 Effect of partial solvent deuteration on <sup>195</sup>Pt NMR chemical shifts

Several NMR chemical shift studies of preferential solvation of monoatomic ions (particularly cations) in mixed solvents were reported in the 1970s, notably by Covington and co-workers.<sup>25</sup> Here nonlinear variation of the solute chemical shift with changing solvent composition is typically interpreted as indicative of preferential solvation by one component of the solvent mixture. An alternative approach, proposed by Gustavsson, Ericsson and Lindman,<sup>74</sup> for studying preferential solvation in aqueous solutions, makes use of the effect of isotopic substitution in the *solvent* molecules (specifically that of substitution of D<sub>2</sub>O for water, referred to by the authors as the “water isotope effect” on shielding) on the solute chemical shift. Here, as with the interpretation of NMR chemical shift data collected as a function of solvent composition, it is assumed that only solvent molecules in direct contact (i.e. in the primary solvation shell) with the solute affect the NMR chemical shift of its nuclei and that the solvation number remains constant at all solvent compositions. The magnitude of the “water isotope effect” on solute chemical shifts in mixed solvent systems was taken to be a direct measure of the extent of contact, or interaction, between water and the solute, thus providing information on preferential solvation. This effect was used to study preferential solvation of Cs<sup>+</sup> in mixtures of water and *N,N*-dimethylformamide.

For <sup>113</sup>Cs NMR in the above solutions, the water isotope effect (on going from normal water to D<sub>2</sub>O for the aqueous solution component) was found to be *negative* over the entire mixed solvent composition range, being largest in pure water (*ca.* -1.2 ppm).<sup>74</sup> Hansen,<sup>54</sup> in his review of NMR isotope effects, lists such “solvent isotope induced shifts”, or SIIS, in several systems. In the present work, a water isotope effect on the <sup>195</sup>Pt NMR chemical shift of -5 ppm was found for the [PtCl<sub>6</sub>]<sup>2-</sup> complex on going from pure normal water to D<sub>2</sub>O. Note that no magnetic susceptibility correction has been made to the water isotope effect, since this

effect is likely to be negligible.<sup>74</sup> The water isotope effect in binary solvent mixtures involving water is expected to range from zero (no water in primary solvation shell) up to the value obtained in pure water, with preferential solvation indicated by a shift which differs from that expected based on a linear change between these two extremes (i.e. does not fall on the straight line connecting the two extreme values), provided the overall solvation number remains constant. Water isotope effects on the <sup>195</sup>Pt NMR chemical shift of [PtCl<sub>6</sub>]<sup>2-</sup> were measured in an equimolar mixture of water with methanol, 2-methoxyethanol and 1,2-dimethoxyethane. Surprisingly, the water isotope effect in the <sup>195</sup>Pt NMR spectra of these solutions is *positive* in all cases, with the largest effect observed in 1,2-dimethoxyethane, where water–solute contact/interactions are expected to be weakest based on the solvent effect on the chemical shift.

The use of the water isotope effect for the study of preferential solvation in solvent mixtures requires essentially that deuterium nuclei reside in water only, i.e. no exchange or transfer of deuterium between water and the co-solvent occurs. In the case of the solvents methanol and 2-methoxyethanol H/D exchange is known to occur, i.e. hydroxyl protons exchange with protons of water in binary mixtures, and the technique is thus strictly not applicable.<sup>68</sup> Not surprisingly then, a similar partial deuteration effect is observed in these two solvent mixtures, a <sup>195</sup>Pt NMR shift of approximately +0.5–0.7 ppm. In mixtures of water and 1,2-dimethoxyethane (+2 ppm) no deuterium exchange is expected, but due to the differences in solute size it seems highly unlikely that the solvation number remains constant over the mixed solvent composition range, as required in a quantitative interpretation of the water isotope effect described by Gustavsson *et al.*<sup>74</sup> Nevertheless, it may be reasonable to expect that in this solvent mixture, where a stronger preferential solvation effect is indicated and the platinum complex expected to be solvated on average predominantly by 1,2-dimethoxyethane, the water isotope effect should be smaller than in the water–methanol mixture, in which a greater degree of water–platinum complex contact is expected. Interestingly, this is not the case, suggesting a more complex phenomenon, possibly related to differences in the effect of H/D isotopic substitution on the properties of the mixed solvents studied here.

### 2.3.6 Chemical speciation

The full  $^{195}\text{Pt}$  NMR spectra of solutions of hexachloroplatinic acid (0.2 M) in equimolar binary mixtures of water and methanol, 2-methoxyethanol and 1,2-dimethoxyethane used in this work are shown in Fig. 2.14. The major signals in these spectra correspond to  $[\text{PtCl}_6]^{2-}$  in the physically isolated sample and reference solutions, however several lower intensity signals are visible in the range  $\sim 490$  to  $650$  ppm. These additional signals are due to the products of chemical speciation reactions in which a solvent molecule displaces a chlorido-ligand in the primary coordination shell of the original platinum complex to form new solvate complexes.<sup>34,35</sup> The formation of such solvate complexes, e.g.  $[\text{PtCl}_5(\text{H}_2\text{O})]^-$ , is undesirable, for example in aqueous solutions in the platinum refining industry and also in the current study, and can typically be suppressed by addition of chloride ion to these solutions.<sup>34</sup> Fortunately, the extent of chemical speciation in the solutions studied here was found to be acceptable at chemical equilibrium, i.e. only a relatively small fraction of the precursor

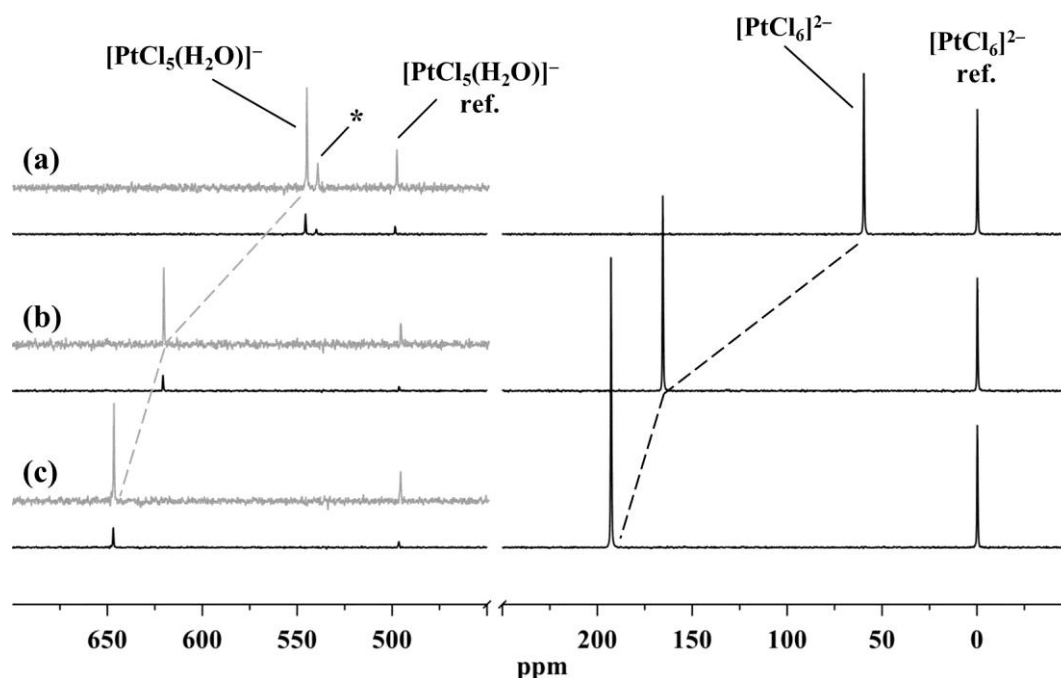


**Figure 2.14**  $^{195}\text{Pt}$  NMR spectra (*ca.* 128 MHz) of hexachloroplatinic acid (0.2 M) in equimolar mixtures of water and (a) methanol, (b) 2-methoxyethanol and (c) 1,2-dimethoxyethane at 293 K. The asterisk (\*) indicates a signal due possibly to a methanolato-complex. Grey traces are scaled to more clearly show the signals of solvolysis products. *Note the break in the  $^{195}\text{Pt}$  chemical shift axis between 250 and 450 ppm, a spectral region where no signals were found to occur.* Dashed lines connect signals of same chemical compound.

compound  $[\text{PtCl}_6]^{2-}$  was converted to solvolysis products (Fig. 2.14), and NMR measurement could be performed for the former without any additional preparative actions. It is desirable to perform NMR experiments under conditions of effectively constant analyte concentration, and this is particularly important when performing spin relaxation time measurements and PGSE experiments described in Chapter 3. While a detailed study of the reaction kinetics of the speciation reactions occurring in these solutions was beyond the scope of the current work, it may be noted that the relative <sup>195</sup>Pt NMR signal intensities were found to remain constant from within a few hours after dissolution of the platinum salt. Identical species distributions were obtained after sealed samples had been kept in a refrigerator at ~273 K for several days.

The speciation reactions of  $[\text{PtCl}_6]^{2-}$  in aqueous solutions (“aquation”) have previously been studied in detail using <sup>195</sup>Pt NMR spectroscopy (see Section 2.1.3).<sup>33–35</sup> Kramer and Koch demonstrated concentration dependence of species distribution in aqueous solutions of hexachloroplatinic acid: the solution concentrations of the aquo-complexes  $[\text{PtCl}_5(\text{H}_2\text{O})]^-$  and *cis*- $[\text{PtCl}_4(\text{H}_2\text{O})_2]$  were found to *increase* with decreasing total platinum salt concentration.<sup>34</sup> In experimental studies of solvation phenomena, it is typically necessary to repeat experiments under conditions of varying solute concentration, and to then extrapolate the value of the measured quantity to “infinite” dilution or, at least, to perform the measurements at reasonably low solute concentrations, so as to correct for, or minimise, the effects of additional interactions between solute particles e.g. ion-pairing interactions or other forms of aggregation. While this procedure is straightforward in studies of simple monoatomic ions, e.g. NaCl in water, the situation may be quite different for complex ions or molecules that can undergo chemical speciation reactions that are concentration dependent, as in the present case. Selected experiments were repeated at lower total concentration (50 mM) of platinum salt, specifically as a check for concentration dependencies of measured quantities (details in Chapter 3). In such solutions, the relative concentrations of the various chemical species at equilibrium were typically found to be different from that observed at higher concentrations.

The <sup>195</sup>Pt NMR spectrum of a *ca.* 100 mM solution of hexachloroplatinic acid in an equimolar mixture of water and methanol is shown in Fig. 2.15; the differences in relative signal intensities, reflecting approximately the concentrations of the various chemical species, compared to those in Fig. 2.14 are clearly visible. Based on previous studies<sup>33–35</sup> of <sup>195</sup>Pt NMR chemical shift trends in the series  $[\text{PtCl}_n(\text{H}_2\text{O})_{6-n}]^{4-n}$  and  $[\text{PtCl}_n(\text{OH})_{6-n}]^{2-}$ , where  $n = 0–6$ , the pairs of signals at 544–550 ppm and 1010–1030 ppm are assigned to solvate

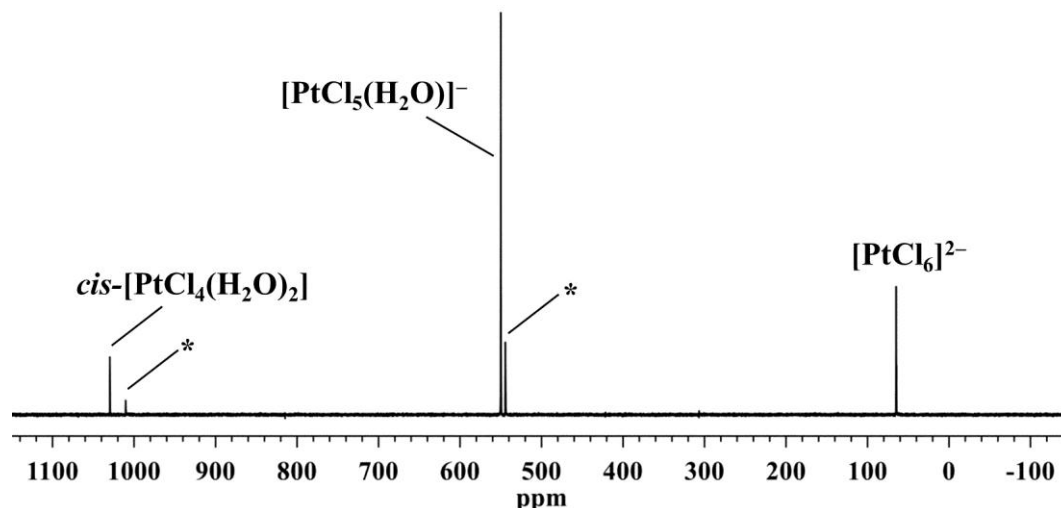


**Figure 2.15**  $^{195}\text{Pt}$  NMR spectrum (*ca.* 128 MHz) of 100 mM hexachloroplatinic acid in an equimolar mixture of water and methanol at 294 K.  $^{195}\text{Pt}$  chemical shift referencing by lock solvent (DMSO- $d_6$ ) contained in coaxial capillary tube. Asterisks (\*) indicate signals due possibly to methanolato-complexes (see text for details).

complexes in which respectively five and four chlorido-ligands are coordinated to platinum, i.e. where one and two chlorido-ligands have been displaced from the coordination sphere by solvent molecules. In these solutions, both water and methanol molecules can potentially coordinate to the platinum centre to form respectively aquo- and, conceivably, *methanolato*-complexes. An expansion of the sets of signals at  $\delta(^{195}\text{Pt}) \sim 544\text{--}550$  ppm is shown in Fig. 2.16 (a). The more *downfield* set of signals, centred about 550 ppm, is known from previous studies of  $^1\Delta^{195}\text{Pt}(^{37/35}\text{Cl})$  isotope shift profiles to correspond to isotopologues of the complex with general chemical formula  $[\text{PtCl}_5(\text{H}_2\text{O})]^-$ ; <sup>37</sup> the signals centred close to 544 ppm have a different overall profile, yet the fine structure appears to be due to <sup>37/35</sup>Cl isotope effects, since the signals are separated by *ca.* 0.17 ppm, a reasonable value for  $^1\Delta^{195}\text{Pt}(^{37/35}\text{Cl})$  isotope shifts in this context. <sup>37</sup> In a similar solution in a deuterated solvent mixture, i.e. D<sub>2</sub>O and methanol- $d_4$ , the more downfield of these two sets of signals, now due to complexes with formula  $[\text{Pt}^{37/35}\text{Cl}_5(\text{D}_2\text{O})]^-$ , shows a profile similar to that of their protonated isotopologues, while the other set is clearly different and shifted, relatively, downfield. In another experiment, a solution was prepared with <sup>18</sup>O-enriched water, so that approximately half of the *water* oxygen atoms was <sup>18</sup>O (natural abundance < 1%); due to a technical difficulty, the signal-to-noise ratio of the  $^{195}\text{Pt}$  NMR spectrum of this sample is rather poor, but signals of <sup>18</sup>O-containing complexes  $[\text{Pt}^{37/35}\text{Cl}(\text{H}_2^{18}\text{O})]^-$  can be seen between  $\sim 549.5\text{--}549.0$  ppm (these are present in a freshly prepared sample). <sup>50</sup> The signals at 544 ppm



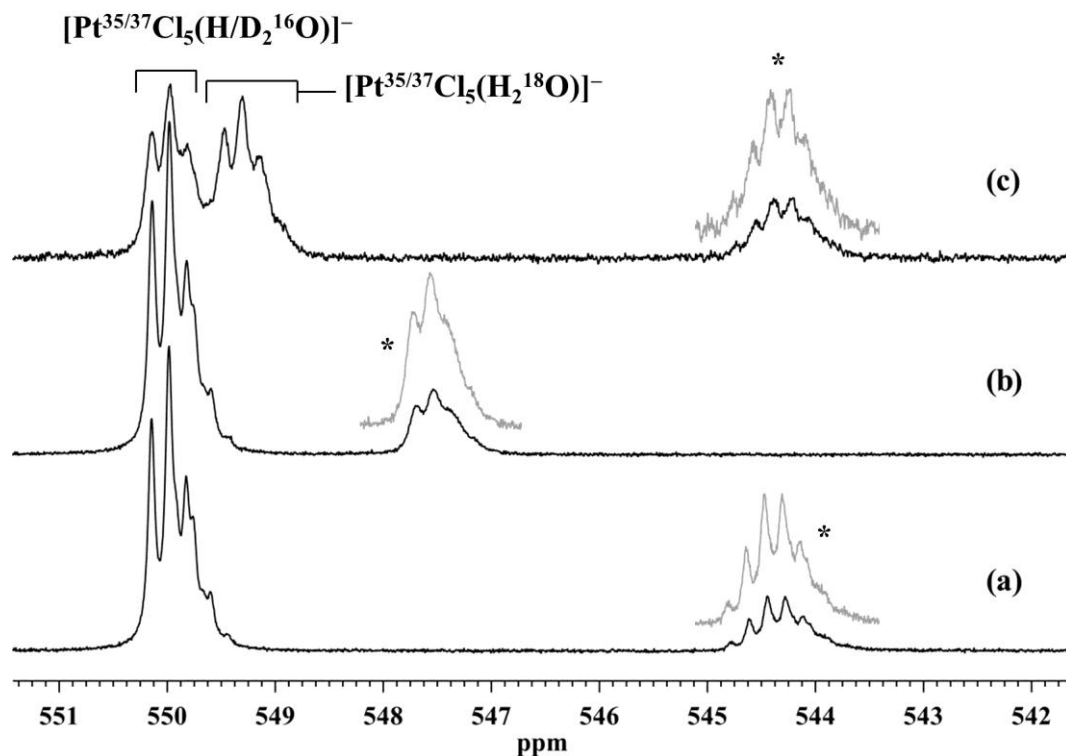


**Figure 2.16**  $^{195}\text{Pt}$  NMR spectra (*ca.* 128 MHz) of 100 mM hexachloroplatinic acid in an equimolar mixture of (a) normal water and methanol, (b)  $\text{D}_2\text{O}$  and methanol- $d_4$ , and (c) normal water/ $^{18}\text{O}$ -enriched water and normal methanol, at 294 K (grey traces show spectral regions with intensities adjusted to aid visual comparison).  $^{195}\text{Pt}$  chemical shift referencing by lock solvent ( $\text{DMSO-}d_6$ ) contained in coaxial capillary tube. Sets of signals marked with an asterisk (\*) due possibly to methanolato-complexes e.g.  $[\text{PtCl}_5(\text{MeOH})]^-$ . See note on  $^{195}\text{Pt}$  NMR chemical shifts in text.

clearly have a similar profile to that seen in the normal solvent mixture in Fig. 2.16 (a), suggesting that they are not due to complexes containing aquo-ligands, but are most likely a *methanolato*-complex or -complexes. Similar observations were made for the remaining solvation product signals (between  $\delta(^{195}\text{Pt}) \sim 1030\text{--}1010$  ppm), assigned to *cis*- $[\text{PtCl}_4(\text{H}_2\text{O})_2]$  and possibly a methanolato-complexes, e.g. *cis*- $[\text{PtCl}_4(\text{MeOH})_2]$ . A note on  $^{195}\text{Pt}$  chemical shifts in these spectra: the set of signals of the complexes  $[\text{Pt}^{35/37}\text{Cl}_5(\text{H}/\text{D}_2\text{O})]^-$  were overlaid in the three spectra in Fig. 2.16 so as to aid in their visual comparison; in reality the  $\delta(^{195}\text{Pt})$  of  $[\text{Pt}^{35/37}\text{Cl}_5(\text{H}_2\text{O})]^-$  and  $[\text{Pt}^{35/37}\text{Cl}_5(\text{D}_2\text{O})]^-$  differ by approximately 5 ppm, the latter having the smaller shift. The  $^{195}\text{Pt}$  chemical shift scale displayed is appropriate for spectrum (a) only (all spectra have the same overall range, though, and can thus be directly compared), which was determined by the spectrometer operating software based on the  $^2\text{H}$  lock signal of  $\text{DMSO-}d_6$  contained in a coaxial capillary tube (spectrum acquired at 294 K).

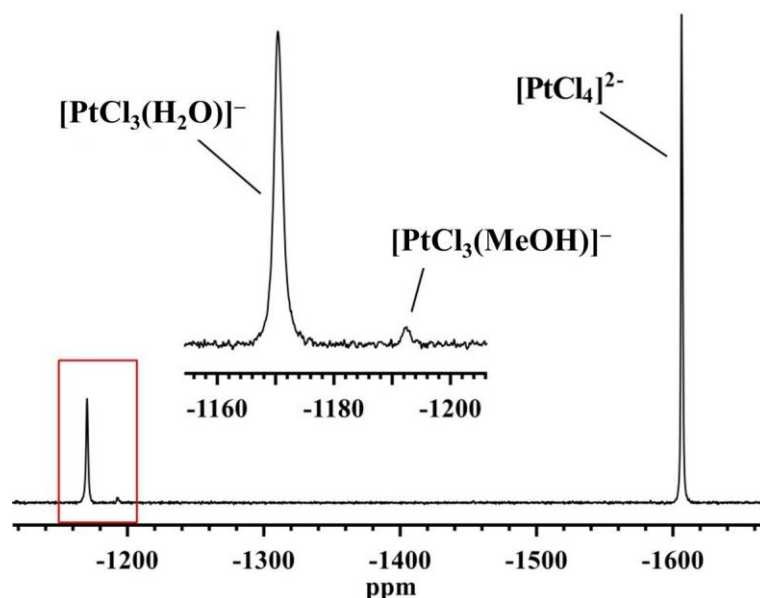


**Figure 2.17**  $^{195}\text{Pt}$  NMR spectrum (ca. 128 MHz) of a 100 mM  $\text{K}_2\text{PtCl}_4$  solution in a water–methanol mixture (10:3 v/v) at 293 K. The spectral region indicated by red box is enlarged in the centre of the figure to show more clearly the signals of  $[\text{PtCl}_3(\text{H}_2\text{O})]^-$  and the proposed methanolato-complex  $[\text{PtCl}_3(\text{MeOH})]^-$ . Figure adapted from ref. 75.

Similar speciation products have recently been reported in solutions of  $\text{K}_2\text{PtCl}_4$  in mixtures of water and methanol, in which a *methanolato*-complex,  $[\text{PtCl}_3(\text{MeOH})]^-$  where “Me” indicates the methyl group, was proposed to be a key precursor in the photo-induced reduction of  $[\text{PtCl}_4]^{2-}$  to metallic platinum (Fig. 2.17).<sup>75</sup> Photo-induced reduction of  $[\text{PtCl}_6]^{2-}$  in alcohols have also been reported, by Bocarsly and co-workers, and this is also found to occur in the water–methanol solutions studied here.<sup>55</sup> Irradiation of samples for 3–5 hours with intense white light from a commercial 5 W (4000 K) LED light source at room temperature resulted in reduction of  $[\text{PtCl}_6]^{2-}$  to  $[\text{PtCl}_4]^{2-}$ . While the reactions were not extensively studied, and not performed under carefully controlled and directly comparable conditions, the  $[\text{PtCl}_4]^{2-}$  species were found to form in all solutions containing methanol (no other  $^{195}\text{Pt}$  NMR signals attributed to Pt(II) complexes were detected). The  $^{195}\text{Pt}$  NMR chemical shift of  $[\text{PtCl}_4]^{2-}$  in the water–methanol mixtures follow a similar, curved trend as a function of solvent composition as that reported for  $[\text{PtCl}_6]^{2-}$ , suggesting that this complex, too, is preferentially solvated by methanol in such mixtures (Fig. 2.18).<sup>30</sup> The solvent shift on going from water to methanol is smaller (+69) than that observed for  $[\text{PtCl}_6]^{2-}$  (+91 ppm), however, which is consistent with the observations of Pesek and Mason<sup>17</sup> (reported as +137 and +222 ppm, respectively for the *n*-butylammonium salts of these anions).

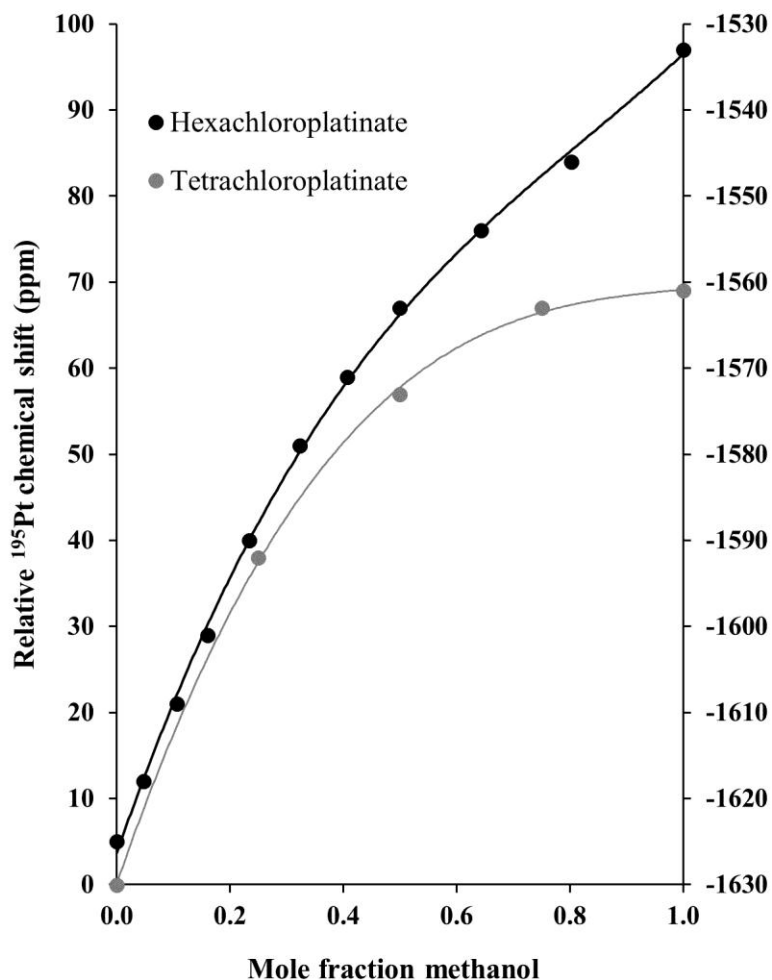


**Figure 2.18**  $^{195}\text{Pt}$  NMR chemical shifts of  $[\text{PtCl}_6]^{2-}$  (left axis) and  $[\text{PtCl}_4]^{2-}$  (right axis) in solutions of  $\text{H}_2\text{PtCl}_4$  in mixtures of water and methanol, plotted on the same scale (100 ppm range). Data for  $[\text{PtCl}_6]^{2-}$  reproduced from Westra<sup>30</sup> ( $\text{D}_2\text{O}$  and normal methanol, 303 K), that for  $[\text{PtCl}_4]^{2-}$  from photo-induced reduction of  $[\text{PtCl}_6]^{2-}$  in mixtures of normal water and methanol, at 293 K (see text for details).

## 2.4 Conclusions

In this component of the study, the  $^1\Delta^{195}\text{Pt}(^{37/35}\text{Cl})$  NMR isotope shifts in  $[\text{Pt}^{35}\text{Cl}_n^{37}\text{Cl}_{6-n}]^{2-}$  were shown to be solvent dependent, ranging from  $-0.171$  ppm in water to  $-0.178$  ppm in 1,2-dimethoxyethane at 293 K. The magnitude of the isotope shift in the solvents studied has the order water < methanol < 2-methoxyethanol < 1,2-dimethoxyethane. The reasons for this particular trend are not clear at present, but, as suggested by Jameson and co-workers<sup>48</sup> in their study of isotope effect in transition metal complexes, may be related to variations in paramagnetic shielding of the nucleus in these solution environments. The  $^1\Delta^{195}\text{Pt}(^{37/35}\text{Cl})$  isotope shift was also measured in selected solvent mixtures: in equimolar mixtures of water

with methanol and 1,2-dimethoxyethane the shift was found to be  $-0.173$  and  $-0.179$  ppm, respectively, close to those measured in the corresponding pure organic solvents. While these results do appear to be consistent with the notion of preferential solvation of the platinum complex by the organic solvent component in such binary mixtures, it does not necessarily provide additional and independent information on this phenomenon compared to <sup>195</sup>Pt NMR chemical shift trends. The additional fact that solvent dependence of the  $^1\Delta^{195}\text{Pt}(^{37/35}\text{Cl})$  isotope shift measured in these solutions is relatively small, suggests that the use of such isotope shift variations in the study of preferential solvation phenomena may be limited, at least in the present case.

An alternative approach to the study of these phenomena may involve investigations of translational and rotational diffusion, since these characteristics are expected to be dependent on the immediate environment of the platinum complex (as discussed in Chapter 3), and, conceivably, vibrational (Raman) spectroscopy could be employed.<sup>76</sup> Computational techniques, specifically Molecular Dynamics (MD) simulations and *ab initio* <sup>195</sup>Pt NMR chemical shift calculations based on Density Functional Theory (DTF), have been used to study the nature of hydration of  $[\text{PtCl}_6]^{2-}$  and other transition metal complexes.<sup>77-79</sup> These techniques may also provide detailed information on the preferential solvation phenomenon in the present case, and indeed MD simulations have previously been used extensively in this field of study.

The chemical speciation of  $[\text{PtCl}_6]^{2-}$  in equimolar binary mixtures of water with methanol, 2-methoxyethanol and 1,2-dimethoxyethane, as well as the pure organic solvents, was investigated. Under the conditions of the present study, where relatively high precursor ( $\text{Na}_2\text{PtCl}_6$  and hexachloroplatinic acid) concentrations were required, the extent of speciation was found to be small; however, when the precursor concentration is reduced, as is typically necessary in studies of ionic solvation, significant conversion to solvolysis products was found to occur in an equimolar mixture of water and methanol, where possible methanolato- or methoxy-platinum complexes were detected.

## References

1. Proctor, W. G.; Yu, F. C. *Phys. Rev.* **1951**, *81* (1), 20–30.
2. Harris, R. K.; Becker, E. D.; Cabral de Menezes, S. M.; Goodfellow, R.; Granger, P. *Pure Appl. Chem.* **2001**, *73* (11), 1795–1818.
3. Von Zelewsky, A. *Helv. Chim. Acta* **1968**, *51* (4), 803–807.
4. Pidcock, A.; Richards, R. E.; Venanzi, L. M. *J. Chem. Soc. A* **1968**, 1970–1973.
5. Dean, R. R.; Green, J. C. *J. Chem. Soc. A* **1968**, 3047–3050.
6. Ramsey, N. F. *Phys. Rev.* **1950**, *78* (6), 699–703.
7. Kaupp, M.; Malkina, O. L.; Malkin, V. G.; Pyykkö, P. *Chem. Eur. J.* **1998**, *4* (1), 118–126.
8. Gilbert, T. M.; Ziegler, T. *J. Phys. Chem. A* **1999**, *103*, 7535–7543.
9. Pregosin, P. S. *Coord. Chem. Rev.* **1982**, *44*, 247–291.
10. Priqueler, J. R. L.; Butler, I. S.; Rochon, F. D. *App. Spectrosc. Rev.* **2006**, *41*, 185–226.
11. Koch, K. R.; Burger, M. R.; Kramer, J.; Westra, A. N. *Dalton Trans.* **2006**, No. 27, 3277–3284.
12. Still, B. M.; Kumar, P. G. A.; Aldrich–Wright, J. R.; Price, W. S. *Chem. Soc. Rev.* **2007**, *36*, 665–686.
13. Maliarik, M.; Berg, K.; Glaser, J.; Sandström, M.; Tóth, I. *Inorg. Chem.* **1998**, *37*, 2910.
14. Pidcock, A.; Richards, R. E.; Venanzi, L. M. *J. Chem. Soc.* **1966**, 1707–1710.
15. Shelimov, B.; Lambert, J–F.; Che, M.; Didillon, B. *J. Am. Chem. Soc.* **1999**, *121*, 545–556.
16. Freeman, W.; Pregosin, P. S.; Sze, S. N.; Venanzi, L. M. *J. Magn. Reson.* **1976**, *22*, 473–478.
17. Pesek, J. J.; Mason, W. R. *J. Magn. Reson.* **1977**, *25*, 519–529.
18. Bloor, E. G.; Kidd, R. G. *Can. J. Chem.* **1968**, *46* (22), 3425–3430.
19. Popov, A. I. *Pure Appl. Chem.* **1975**, *41*, 275–289.
20. Frankel, L. S.; Langford, C. H.; Stengle, T. R. *J. Phys. Chem.* **1970**, *74*, 1376–1381.
21. Eaton, D. R.; Rogerson, C. V.; Sandercock, A. C. *J. Phys. Chem.* **1982**, *86*, 1365–1371.
22. Ben-Naim, A. *Pure Appl. Chem.* **1990**, *62*, 25–34.
23. Burgess, J. *Metal ions in solution*, Ellis Horwood, Chichester, 1978.
24. Marcus, Y. *Ion Solvation*, Wiley-Interscience, Chichester, 1985.
25. Covington, A. K.; Lilley, T. H.; Newman, K. E.; Porthouse, G. A. *J. Chem. Soc. Faraday Trans. I* **1973**, *69*, 963.

26. Langford, C. H.; Stengle, T. R. *J. Am. Chem. Soc.* **1969**, *91*, 4014–4016.
27. Stengle, T. R.; Pan, Y-C.; Langford, C. H. *J. Am. Chem. Soc.* **1972**, *94*, 9037–9041.
28. Tong, J. P. K.; Langford, C. H.; Stengle, T. R. *Can. J. Chem.* **1974**, *52*, 1721–1731.
29. Holz, M.; Weingärtner, H.; Hertz, H. G. *J. Chem. Soc. Faraday Trans. I* **1977**, *73*, 71–83.
30. Westra, A. N. *High Resolution NMR Studies Concerning the Solvation/Hydration and Coordination Chemistry of Pt(II/IV) Compounds*, PhD Dissertation, University, 2005.
31. Templeton, D. M.; Ariese, F.; Cornelis, R.; Danielsson, L. G.; Muntau, H.; Van Leewen, H. P.; Łobiński, R. *Pure App. Chem.* **2000**, *72*, 1453–1470.
32. Gröning, Ö.; Drakenberg, T.; Elding, L. I. *Inorg. Chem.* **1982**, *21*, 1820–1824.
33. Carr, C.; Goggin, P. L.; Goodfellow, R. J. *Inorg. Chim. Acta*, **1984**, *81*, L25–L26.
34. Kramer, J.; Koch, K. R. *Inorg. Chem.* **2006**, *45*, 7843–7855.
35. Kramer, J.; Koch, K. R. *Inorg. Chem.* **2007**, *46*, 7466–7476.
36. Cohen, S. M.; Brown, T. H. *J. Chem. Phys.* **1974**, *61* (7), 2985–2986.
37. Gerber, W. J.; Murray, P.; Koch, K. R. *Dalton Trans.* **2008**, 4113–4117.
38. Ramsey, N. F. *Phys. Rev.* **1952**, *87* (6), 1075–1079.
39. Batiz-Hernandez, H.; Bernheim, R. A. *Prog. Nucl. Magn. Reson. Spectrosc.* **1967**, *3*, 63–85.
40. Anet, F. A. L.; Dekmezian, A. H. *J. Am. Chem. Soc.* **1979**, *101* (18), 5449–5451.
41. Jameson, C. J.; Osten, H. J. *J. Am. Chem. Soc.* **1986**, *108* (10), 2497–2503.
42. Ismail, I. M.; Kerrison, S. J. J.; Sadler, P. J. *J. Chem. Soc. Chem. Commun.* **1980**, 1175–1176.
43. Stringfellow, T. C.; Wu, G.; Wasylishen, R. E. *J. Phys. Chem. B*, **1997**, *101*, 9651–9656.
44. Jokisaari, J.; Räisänen, K. *Mol. Phys.* **1978**, *36*, 113–123.
45. Jameson, C. J.; Jameson, A. K. *J. Chem. Phys.* **1986**, *85*, 5484–5492.
46. Jameson, C. J.; Osten, H. J. *J. Chem. Phys.* **1984**, *81* (10), 4293–4299.
47. Jameson, C. J.; Jameson, A. K.; Oppusunggu, D. *J. Chem. Phys.* **1986**, *85* (10), 5480–5483.
48. Jameson, C. J.; Rehder, D.; Hoch, M. *J. Am. Chem. Soc.* **1987**, *109*, 2589–2594.
49. Murray, P.; Gerber, W. J.; Koch, K. R. *Dalton Trans.* **2012**, *41*, 10533–10542.
50. Engelbrecht, L.; Murray, P.; Koch, K. R. *Inorg. Chem.* **2015**, *54* (6), 2752–2764.
51. Jameson, C. J.; Osten, H. J. *Annu. Rep. NMR Spectrosc.* **1986**, *17*, 1–78.
52. Li, M.; Owrutsky, J.; Sarisky, M.; Culver, J. P.; Yodh, A.; Hochstrasser, R. M. *J. Chem. Phys.* **1993**, *98* (7), 5499–5507.
53. Schultz, P. W.; Leroi, G. E.; Popov, A. I. *J. Am. Chem. Soc.* **1996**, *118*, 10617–10625.

54. Hansen, P. E. *Prog. NMR. Spectrosc.* **1988**, *20*, 207–255.
55. Cameron, R. E.; Bocarsly, A. B. *Inorg. Chem.* **1986**, *25*, 2910–2913.
56. Harris, R. K.; Becker, E. D.; Cabral de Menezes, S. M.; Granger, P.; Hoffman, R. E.; Zilm, K. W. *Pure Appl. Chem.* **2008**, *80* (1), 59–84.
57. Saito, T.; Nakaie, S.; Kinoshita, M.; Ihara, T.; Kinugasa, S.; Nomura, A.; Maeda, T. *Metrologia* **2004**, *41*, 213–218.
58. Farrar, T. C.; Becker, E. D. *Pulsed and Fourier Transform NMR*, Academic Press, New York, 1971.
59. *NMR Spectroscopy, User Guide*, Varian, Inc., 2007.
60. *MestReNova Manual*, MestReNova 7.1.1, Mestrelab Research S. L., 2012.
61. SigmaPlot for Windows Version 13.0, Systat Software, Inc., 2014.
62. Marquardt, D. W. *J. Soc. Indust. App. Math.* **1963**, *11*, 431–441. See SigmaPlot 13 User's Guide for related references.
63. Hoffman, R. E.; Becker, E. D. *J. Magn. Reson.* **2005**, *176*, 87–98.
64. Jameson, C. J. *Annu. Rev. Phys. Chem.* **1996**, *47*, 135–169.
65. Gombler, W. *Zeitschrift Naturforsch. Teil B* **1985**, *40*, 782–786.
66. Hawlicka, E.; Swiatla-Wojcik, D. *J. Mol. Liq.* **1998**, *78*, 7–18.
67. Hawlicka, E.; Swiatla-Wojcik, D. *J. Phys. Chem. A* **2002**, *106*, 1336–1345.
68. Corsaro, C.; Spooren, J.; Branca, C.; Leone, N.; Broccio, M.; Kim, C.; Chen, S. H.; Stanley, E.; Mallamace, F. *J. Phys. Chem. B* **2008**, *112*, 10449–10454.
69. Risley, J. M.; DeFrees, S. A.; Van Etten, R. L.; *Org. Magn. Reson.* **1983**, *21* (1) 28–35.
70. Appleton, T. G.; Hall, J. R.; Ralph, S. F. *Inorg. Chem.* **1985**, *24*, 4685–4693.
71. Bondar, V. I.; Potekhin, K. A.; Rau, T. F.; Rozman, S. P.; Rau, V. G.; Struchkov, Y. T. *Sov. Phys. Dokl.* **1988**, *33*, 395–396.
72. Steinborn, D.; Gravenhorst, O.; Hartung, H.; Baumeister, U. *Inorg. Chem.* **1997**, *36*, 2195–2199.
73. Gröning, Ö.; Elding, L. I. *Inorg. Chem.* **1989**, *28*, 3366–3372.
74. Gustavsson, H.; Ericsson, T.; Lindman, B. *Inorg. Nucl. Chem. Letters* **1978**, *14*, 37–43.
75. Xian, L.; Engelbrecht, L.; Barkhuysen, S.; Koch, K. R. *RSC Adv.* **2016**, *6*, 34014–34018.
76. Preetz, W.; Peters, G.; Bublitz, D. *Chem. Rev.* **1996**, *96*, 977–1025.
77. (a) Lienke, A.; Klatt, G.; Robinson, D. J.; Koch, K. R.; Naidoo, K. J. *Inorg. Chem.* **2001**, *40*, 2352–2357. (b) Naidoo, K. J.; Klatt, G.; Koch, K. R.; Robinson, D. J. *Inorg. Chem.* **2002**, *41*, 1845–1849.
78. Truflandier, L. A.; Autschbach, J. *J. Am. Chem. Soc.* **2010**, *132*, 3472–3483.
79. Matthews, R. P.; Venter, G. A.; Naidoo, K. J. *J. Phys. Chem. B* **2011**, *115*, 1045–1055.

3. A Study of Dynamic Properties of Hexachloroplatinate (IV) in Binary Mixtures of Water and Selected Organic Solvents using  $^{195}\text{Pt}$  NMR Spectroscopy



## Abstract

The rotational and translational diffusion characteristics of molecules in solution reflect the nature of their interactions with solvent molecules, i.e. solvation, and with other solution components. In this chapter, measurements of  $^{195}\text{Pt}$  NMR spin relaxation times and pulsed gradient spin-echo (PGSE) translational diffusion coefficients of hexachloroplatinate (IV),  $[\text{PtCl}_6]^{2-}$ , in water, selected organic solvents (methanol, 2-methoxyethanol and 1,2-dimethoxyethane) and their equimolar mixtures are presented. The measurements are interpreted and discussed in the context of the proposed preferential solvation of the platinum complex by the organic solvent component in such mixtures, using well-known hydrodynamic models of molecular diffusion. These models, however, are not ideally suited for studying complex samples, and do not provide direct information on the composition and structure of the solvation environment of the platinum complex. The use of an alternative, computational approach to the interpretation of these results is proposed, specifically, Molecular Dynamics computer simulations.

## 3.1 Introduction

### 3.1.1 Molecular motion in solution: some background

Translational diffusion refers to the random thermal motion of molecules or ions, where on average no net displacement of an individual molecule is found and where motions of molecules are generally not correlated, which is generally known also as Brownian motion.<sup>1</sup> The term “self-diffusion” refers to the diffusive motions of molecules in a pure liquid at thermal equilibrium and is described by a diffusion coefficient  $D$ , with units  $\text{m}^2/\text{s}$ , e.g. the self-diffusion coefficient of water<sup>2</sup> at 298 K is  $2.3 \times 10^{-9} \text{ m}^2/\text{s}$ . In solvent mixtures or solutions, the translational diffusion of each component is described by its own diffusion coefficient, and these typically range on the order  $10^{-9} \text{ m}^2/\text{s}$  for mobile liquids to  $10^{-12} \text{ m}^2/\text{s}$  for large polymers in solution (diffusion coefficients of gasses can be much higher, and those in e.g. glasses much lower).<sup>1,3</sup> These phenomena are depicted in Figure 3.1 (a, b), which is a reproduction of a scheme by Price.<sup>1</sup>

The rotational motion, or rotational relaxation, of a molecule in solution often also is diffusive, proceeding in small steps *via* a sequence of collisions with neighbouring molecules (Figure 3.1 c).<sup>4,5</sup> Rotational diffusion is characterised by correlation times for molecular re-

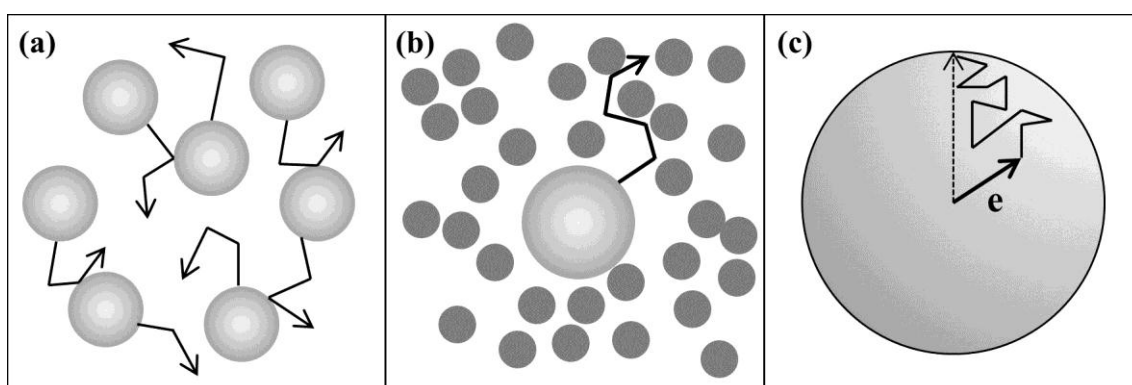


**Figure 3.1** Molecular motions in solution: (a) translational self-diffusion of similar particles characterised by a single diffusion coefficient; (b) translational diffusion (Brownian motion) of a large particle in a liquid consisting of much smaller particles, where the diffusion coefficients of these two particle types are different; (c) rotational diffusion of a vector  $e$  on the surface of a sphere (e.g. a bond vector in a molecule) proceeding through a series of collisions (small steps), and characterised by a reorientational correlation time, the average time required to rotate through one radian. Panels (a) and (b) based on a scheme by Price.<sup>1</sup>

orientation,  $\tau_l$ , and angular momentum,  $\tau_J$ .<sup>4,6</sup> Reorientational correlation times  $\tau_1$  and  $\tau_2$  are given by

$$\tau_l = \int_0^\infty \langle P_l(\mathbf{e}(t) \cdot \mathbf{e}(0)) \rangle dt \quad (3.1)$$

where  $P_l$  is the  $l$ th order Legendre polynomial and  $\mathbf{e}$  is the time-dependent unit vector that points along a particular molecular axis (e.g. a chemical bond or bisector); the angular brackets indicate an average over all molecules. For rotational diffusion, the reorientational correlation function  $\langle P_l(\mathbf{e}(t) \cdot \mathbf{e}(0)) \rangle$  decays exponentially. The following relationship between the reorientational and angular momentum correlation times generally holds, where  $I$  is the molecular moment of inertia and other symbols have their usual meaning.<sup>6</sup>

$$\tau_l = \frac{I}{l(l+1)kT\tau_J} \quad (3.2)$$

Most experimental techniques for studying molecular rotation provide only one characteristic time, e.g. NMR experiments measure  $\tau_2$ , usually referred to in related literature simply as the *reorientational correlation time*,  $\tau_c$ .<sup>7</sup> As explained by Martin *et al.*,<sup>8</sup> the correlation time  $\tau_c$  represents the time required for an average molecule to rotate through one radian, while the angular momentum correlation time  $\tau_J$  may be identified approximately with the time between molecular collisions, and in the case of diffusive molecular rotation  $\tau_c \gg \tau_J$ .

Measurements of dynamic properties of molecules in solution can provide valuable information on their effective solution dimensions and the nature of their interactions with other solution components.<sup>1,9,10</sup> NMR spectroscopic techniques can be used to study both translational and rotational diffusion characteristics of molecules: measurements of nuclear spin relaxation times have long been used to study molecular reorientations, but their interpretation usually requires making certain assumptions regarding the spin relaxation process and the nature of molecular motion. Pulsed gradient spin-echo experiments, however, provide direct information on translational diffusion, which can then be further interpreted in the context of hydrodynamic models of molecular diffusion.<sup>3</sup>

### 3.1.2 Relaxation in NMR spectroscopy

The fundamental concepts of NMR spectroscopy were introduced in Chapter 1, and the theory of nuclear magnetic shielding expanded on in Chapter 2. Following the perturbation of the populations of nuclear spin energy levels (Zeeman levels) in an applied magnetic field after application of radiofrequency energy to an ensemble of magnetically active (non-zero spin) nuclei, a slow thermal equilibration period follows during which nuclei exchange energy with their surroundings to recover the thermal equilibrium distribution. This process is known as nuclear spin relaxation, or NMR relaxation, and is central to the NMR spectroscopy technique and it is during this period that data are collected in an NMR experiment.<sup>9,11</sup>

Macroscopically, the NMR relaxation process is described by two characteristic quantities: the longitudinal, or spin–lattice, relaxation time,  $T_1$ , that describes the return of net sample magnetisation parallel to the applied magnetic field, while the transverse, or spin–spin, relaxation time,  $T_2$ , characterises the rate of change of magnetisation in the plane perpendicular to the applied field.<sup>9</sup> The two quantities may be expected to be equal, but this is often not the case, and the following relationship is found:

$$T_1 \geq T_2 \quad (3.3)$$

Relaxation in NMR may be considered as resulting from Larmor-frequency magnetic field fluctuations occurring at the nucleus. These magnetic field fluctuations are produced by modulation of interactions between the nucleus and its environment by molecular motion, such as rotational and translational diffusion, resulting in spin–lattice relaxation. Several types of interactions, usually referred to as “relaxation mechanisms”, may contribute to the overall observed spin relaxation of a nucleus, but often one such mechanism is found to be dominant under certain physical conditions. Theoretical descriptions of common relaxation mechanisms may be found in most NMR textbooks.<sup>9,11</sup> These include the dipole–dipole (DD) and so-called quadrupolar relaxation mechanisms, as well as those resulting from the modulation of chemical shift anisotropy (CSA) and scalar spin coupling (SC), of which there are two types.<sup>9</sup>

Longitudinal ( $T_1$ ) spin relaxation times, which are often found to be informative in the context of molecular structure, are typically measured using the simple inversion–recovery pulse sequence.<sup>11</sup>

### 3.1.3 Pulsed gradient spin-echo (PGSE) experiments

The history and fundamental principles of translational diffusion measurements by nuclear spin-echo (SE) techniques are described in review articles and textbooks.<sup>1,3</sup> Modern experiments use variations of the basic pulsed gradient spin-echo (PGSE) pulse sequence elements shown in Figure 3.2 (a), practically introduced by Stejskal and Tanner<sup>12</sup> in the mid-1960s, or a three-pulse stimulated-echo (b) pulse sequence.

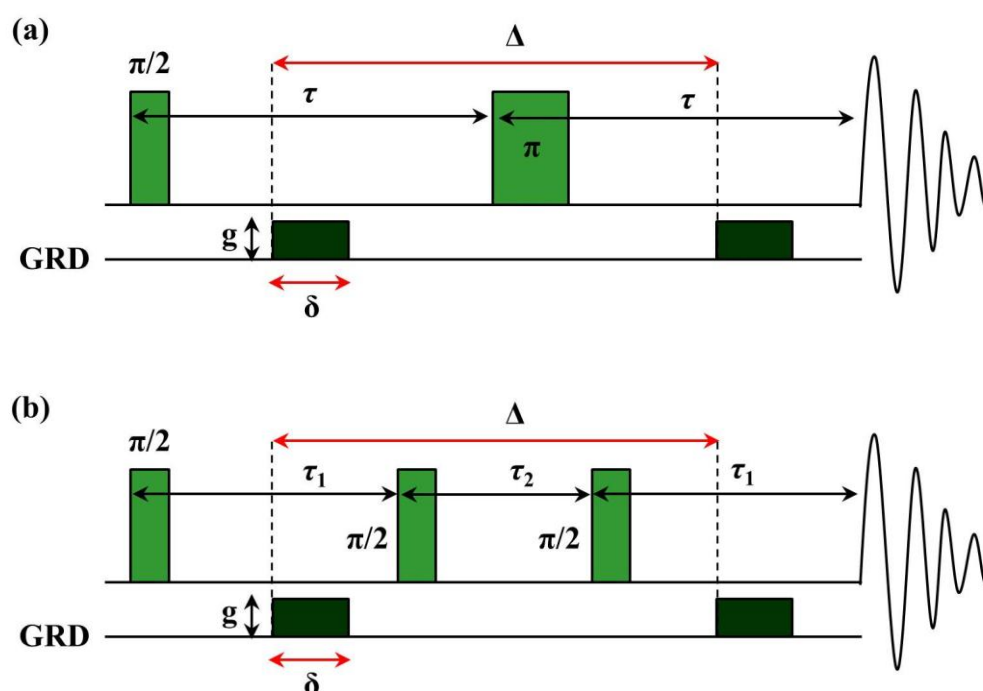


**Figure 3.2** (a) Basic spin-echo (SE) and (b) stimulated-echo (STE) PGSE pulse sequences. The field gradient pulses are indicated by label “GRD”, and the meanings of various symbols are given in the text. The wave pattern indicates the second half of the spin echo that is acquired as FID data. Diagrams adapted from Price.<sup>1</sup>

Essentially, application of such pulse sequences result in the attenuation of the NMR signal intensity ( $I$ ) of a nucleus with translational diffusion coefficient  $D$  compared to that observed in the absence of magnetic field gradients ( $I_0$ ), the nature of which is related to the pulse sequence parameters by Eq. 3.4, where  $g$  is the strength of the magnetic field gradient,  $\delta$  its duration, and  $\Delta$  the diffusion delay (the period during which diffusion is monitored).

$$\ln(I/I_0) = -D(g\delta\gamma)^2[\Delta - (\delta/3)] \quad (3.4)$$

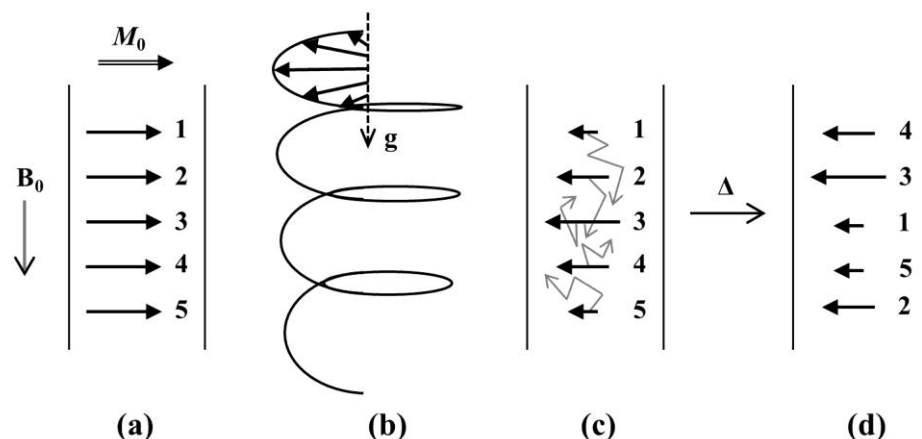


**Figure 3.3** Schematic representation of fundamental aspects of gradient spin-echo experiment: following a  $\pi/2$  r.f. pulse, (a) nuclear spins (arrows 1–5) experiencing the same applied magnetic field  $\mathbf{B}_0$  are aligned as shown (coherent transverse magnetisation); when a magnetic field gradient pulse,  $\mathbf{g}$ , is applied parallel to  $\mathbf{B}_0$ , (b) nuclei spatially separated along this direction experience different effective magnetic fields and dephasing occurs, creating a “magnetisation helix” as indicated by the solid curve. (c) View of spin component in plane perpendicular to helix, with possible diffusion (occurring during time  $\Delta$ ) indicated by grey lines. If no diffusion of spins occurs along  $\mathbf{B}_0$ , application of an identical, but reversed gradient pulse  $-\mathbf{g}$  will result in complete recovery of transverse coherence as in (a), however, translational diffusion of spins along  $\mathbf{B}_0$  results in an *irreversible* change in the magnetisation helix (d), and coherence is not completely recovered after the second gradient pulse, resulting in an attenuated NMR signal being detected. Scheme adapted from Price.<sup>1</sup>

Note that these diagrams are not intended to convey accurately the relationship (duration) between the various periods of the sequences, i.e. the r.f. pulses  $\pi/2$  and  $\pi$  are essentially instantaneous (microseconds) compared to  $\delta$  (milliseconds), which itself is typically much shorter than  $\Delta$  (tens to hundreds of milliseconds).

The accompanying Figure 3.3, based on a scheme by Price,<sup>1</sup> illustrates the basic concept on which gradient spin-echo experiments are based. Here, a  $\pi/2$  ( $90^\circ$ ) r.f. pulse creates coherent transverse magnetisation,  $M_0$ : spatially separated nuclear spins 1–5 experience the same (homogeneous) applied magnetic field,  $\mathbf{B}_0$ , and precess at the same frequency (a). When a magnetic field gradient,  $\mathbf{g}$ , is applied parallel to  $\mathbf{B}_0$  as indicated (b), the effective field experienced by these spins is different, resulting in different precession frequencies (“dephasing”), as indicated by the “magnetisation helix”. The gradient pulse is now switched off (c), and nuclear spins are allowed to undergo translational diffusion (during diffusion delay  $\Delta$ , a period much longer than the short gradient duration  $\delta$ ) in the homogeneous applied

field  $\mathbf{B}_0$  only. When an identical gradient pulse, but of opposite sign,  $-\mathbf{g}$ , is applied, spins are refocussed, as in (a), and the nett transverse magnetisation detected (second half of echo); complete refocussing does not occur, however, when individual spins have on average a non-zero net displacement parallel to  $\mathbf{B}_0$  since the magnetisation helix is irreversibly altered (d) and the spins do not experience the exact opposite effect from application of  $-\mathbf{g}$ . Since the signal amplitude is proportional to the vector sum of spins, the signal is attenuated compared to that obtained in the case of complete refocussing (i.e. no field gradients or no translation parallel to  $\mathbf{B}_0$ ). Note that the pulse sequences in Fig 3.2 use gradient pulses of the *same* sign, since a  $\pi$  pulse (or two  $\pi/2$  pulses) are inserted between them. In practice, the pulse sequence is repeated many times for different values of the gradient strength  $g$ , resulting in a set of NMR spectra where the signal is progressively attenuated as  $g$  is increased. The diffusion coefficient  $D$  is then obtained by least-squares fitting of Eq. 3.4 to the signal attenuation data (Section 3.2.3).

### 3.1.4 Rationale and aims

The dynamic properties of transition metal complexes in solution have been extensively studied using NMR spectroscopic techniques, e.g. spin relaxation time measurements and PGSE experiments to study rotational and translational motion respectively.<sup>9,10</sup> In the majority of such studies, however, it is not the transition metal nucleus itself that is detected, but instead lighter nuclei, e.g.  $^1\text{H}$ ,  $^{13}\text{C}$ ,  $^{19}\text{F}$ , residing in the ligands coordinated to the metal ion. Even when the metal nucleus can be directly detected, these lighter nuclei usually possess magnetic properties that are more suitable for high-resolution NMR spectroscopy, e.g. high receptivity and longer spin relaxation times, and are preferred for the experiments mentioned above.<sup>13</sup> In some cases, however, the transition metal complex of interest does not contain such convenient nuclei, as is case for the platinum complexes studied here. These simple complexes contain only platinum and chlorine (or bromine) nuclei. Chlorine has two naturally occurring isotopes,  $^{35}\text{Cl}$  (natural abundance 75.53 %) and  $^{37}\text{Cl}$  (24.47 %), both of which are quadrupolar nuclei with spin  $3/2$ .<sup>14</sup> While many NMR studies of these nuclei have been reported, including nuclear spin relaxation time measurements<sup>15</sup> as well as PGSE experiments,<sup>16,17</sup> also with the aim of studying preferential solvation phenomena,<sup>18</sup> these invariably involve the chloride ion, or highly symmetrical molecules in which the chlorine nucleus is situated at the symmetry centre, e.g. the perchlorate anion. The reason for this is that the quadrupole spin relaxation mechanism by which such  $I > 1/2$  nuclei relax becomes

highly efficient when the nucleus is located in a low-symmetry molecular environment in which it experiences a strong *electric field gradient*, resulting in extremely broad NMR signals. More information on this spin relaxation mechanism may be found in excellent NMR textbooks<sup>9,10</sup> and research articles.<sup>14,15</sup> This is also the case for the chlorine nuclei in the octahedral  $[\text{PtCl}_6]^{2-}$  in aqueous solution.

As described earlier,  $^{195}\text{Pt}$  is one of the more commonly studied transition metal nuclei (using NMR, of course) due to its relatively high receptivity and other favourable magnetic properties.<sup>19</sup> Moreover,  $^{195}\text{Pt}$  NMR spin relaxation times have also been measured for many platinum complexes, more recently, the first  $^{195}\text{Pt}$  PGSE experiments were reported.<sup>20</sup> The aim of the work presented in this section was to explore the use of these  $^{195}\text{Pt}$  NMR techniques to study the dynamic properties specifically of  $[\text{PtCl}_6]^{2-}$  in the solvents water, methanol, 2-methoxyethanol and 1,2-dimethoxyethane, and also in binary mixtures of the organic compounds with water. Attempts to interpret the measurements in terms of the solvation environment of the platinum complex are described, specifically in the context of preferential solvation phenomena thought to be prevalent in these solvent mixtures.<sup>21</sup>



## 3.2 Materials and methods

### 3.2.1 Sample preparation and instrumentation

The samples used in this component of the work were similar, and in some cases identical, to those described in Chapter 2. Two series of samples were prepared in water–methanol solutions, one with hexachloroplatinic acid concentration 0.2 M, as used previously, and one in which the concentration was reduced to 50 mM. The latter series was prepared to evaluate the effect of analyte concentration (conceivably due to ion-pairing interactions) on the measured dynamic properties. Selected samples were degassed by the freeze-pump-thaw technique: samples were frozen in a mixture of dry ice and acetone, placed under high vacuum and then allowed to thaw under these conditions; this process was repeated three times. In studies of NMR relaxation times it is frequently necessary to remove dissolved paramagnetic molecular oxygen from the sample solution.<sup>9,11</sup> This procedure was found to have no detectable effect on the  $T_1$  relaxation times measured here, possibly due to the fact that the resonant  $^{195}\text{Pt}$  nucleus is located at the centre of an octahedral complex, surrounded by chlorido-ligands, not allowing for close approach of oxygen molecules (the relaxation mechanism is dependent on the distance between unpaired electrons and the resonant nucleus).

NMR instrumentation was described in Chapter 2. Pulsed gradient spin-echo experiments were performed on a Varian <sup>Unity</sup>*Inova* 400 NMR spectrometer equipped with a 5 mm  $^1\text{H}$   $\{^{15}\text{N} - ^{31}\text{P}\}$  dual broadband PFG probe with a Performa II gradient system.

### 3.2.2 Measurement of $^{195}\text{Pt}$ NMR relaxation times

Two methods are available for the measurement of  $T_1$  relaxation times: the inversion recovery and saturation recovery techniques (a third, the progressive saturation technique, also exists).<sup>9</sup> The former is the most common and preferred for reasons of simplicity and robustness, and was also used exclusively in this work. Technical details of these experiments are described in NMR textbooks.<sup>9,11</sup>  $^{195}\text{Pt}$  NMR pulse widths (or durations) were calibrated for each sample by the usual experiment in which the pulse width is varied and signal intensity monitored visually.

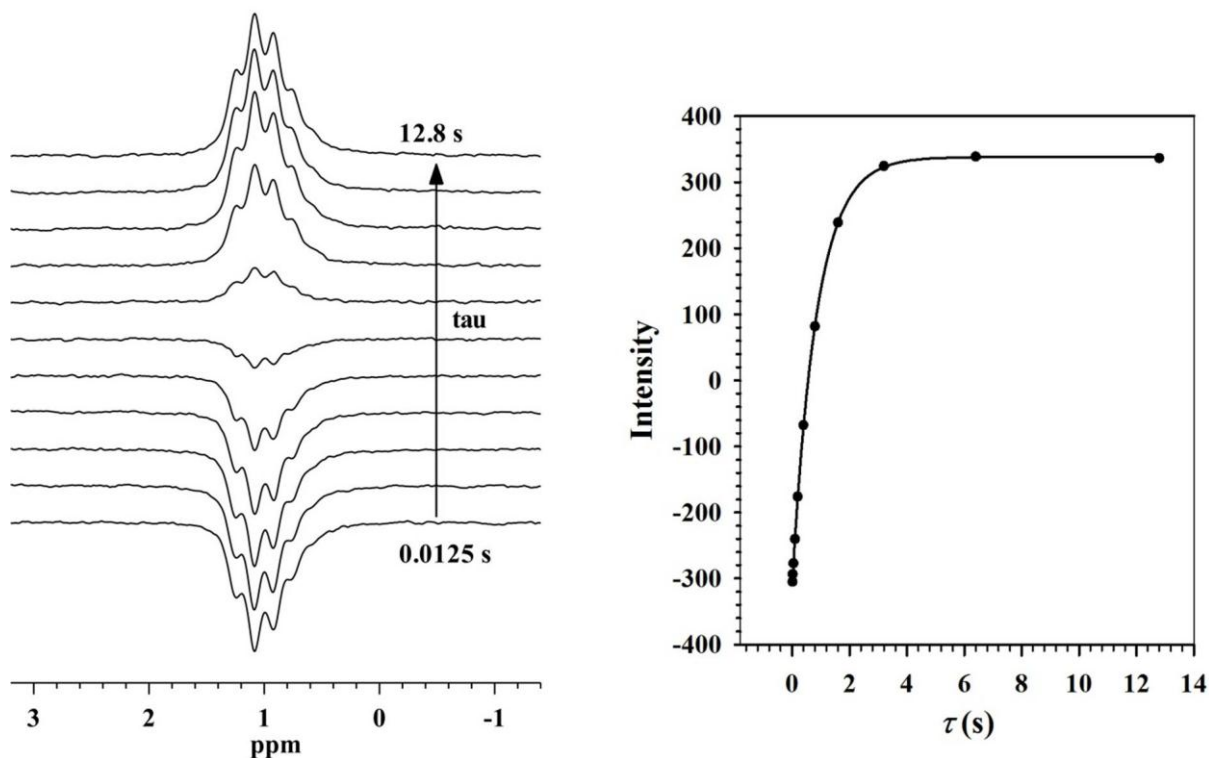


**Figure 3.4**  $^{195}\text{Pt}$  NMR spectra (left) from an inversion recovery experiment for  $[\text{PtCl}_6]^{2-}$  in  $\text{D}_2\text{O}$  at 298 K. Spectra were processed with 5 Hz exponential line broadening to improve signal-to-noise ratio. Right: Signal intensities plotted and fitted with a three-parameter exponential function (“Exponential Rise to Maximum, Single, 3 Parameter” function in SigmaPlot 13).

Inversion recovery experiments were set up and processed using the standard procedure of the VnmrJ 2.1B operating software: the number of FIDs collected per relaxation delay increment typically ranged between *ca.* 500 and 1000, depending on time constraints, with a fixed relaxation delay between successive pulse/acquisition periods of five times the maximum  $T_1$  estimate; total experiment times were about 12 hours. FID data were typically processed with a 20 Hz exponential weighting and phase and baseline correction, where necessary, performed by inspection of the final (positive amplitude) spectrum. Relaxation times were determined from peak intensity data by least-squares fitting a three-parameter exponential function, the standard technique in both VnmrJ and MestReNova. The results of a typical  $^{195}\text{Pt}$  inversion recovery experiment are shown in Fig. 3.4.

It is desirable to determine at least an estimate of the typical error associated with the  $^{195}\text{Pt}$   $T_1$  values reported here. Bakhmutov, for example, lists several possible sources of error in the measurement of NMR relaxation times in his textbook.<sup>9</sup> These include contributions from

instrumental imperfections and limitations, experiment setup (i.e. incorrect acquisition parameters), sample preparation and effects inherent to the nature of the sample. Some of these effects were estimated in the present study by performing repeated measurements with different samples for selected solutions; the measurements were found to be highly reproducible in general, with a typical variation of less than 10 %. Other possible sources of systematic error are more difficult to evaluate e.g. homogeneity of radiofrequency pulses and temperature control in different solvents.

### 3.2.3 Measurement of translational diffusion coefficients

Translational diffusion coefficients were measured using the Pulsed Gradient Spin-Echo (PGSE) technique. The DOSY Bipolar Pulse Pair Stimulated Echo (Dbppste) pulse sequence available in VnmrJ 2.1B was used exclusively (Figure 3.5).<sup>22</sup> Alternative sequences intended for suppression of convective current in the sample due to thermal gradients (“convection compensated” sequences) were not used, since the longer sequence duration results in an unacceptable loss in signal sensitivity (see note below on  $^{195}\text{Pt}$  NMR sensitivity).<sup>23</sup> Instead, samples were prepared with a lower total sample height, 400  $\mu\text{l}$  sample volume placed in a standard 5 mm outer diameter (o.d.) NMR tube by Wilmad (PP series) or NewEra (HL5), and allowed at least 15 minutes in the NMR probe to reach thermal equilibrium (298 K) before starting experiments.

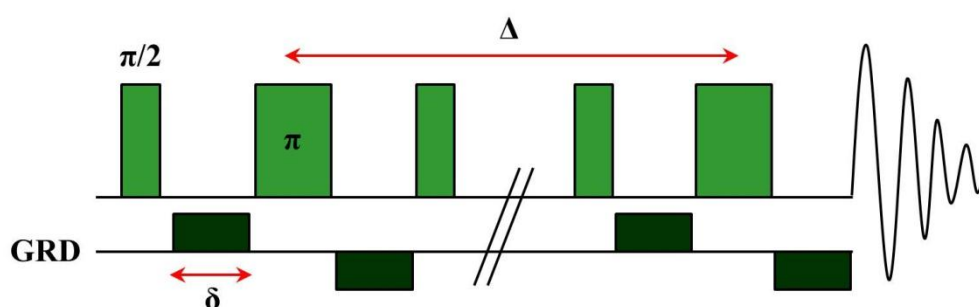


**Figure 3.5** DOSY Bipolar Pulse Pair Stimulated Echo (Dbppste) pulse sequence (scheme reproduced from VnmrJ 2.2 User Manual).<sup>22</sup> The line marked “GRD” indicates the magnetic field gradient pulses used for spatial encoding; the meaning of symbols  $\delta$  and  $\Delta$  are given in the text, and other symbols have their usual meaning.

Pulse sequence parameters were determined for each sample, monitoring the signal attenuation obtained with lowest and highest intended magnetic field gradients, which is the recommended method. In  $^{195}\text{Pt}$  PGSE experiments the gradient pulse duration,  $\delta$ , was set between 5 and 7 ms, and the diffusion delay,  $\Delta$ , ranged between 80 and 120 ms. Longer values of  $\delta$  and  $\Delta$ , required for diffusion measurements in samples slower diffusion rates, resulted in significant loss of sensitivity due to rapid spin relaxation processes operative during these periods. The gradient pulse strength,  $g$ , was varied between 0.001 and 0.5 T/m, with  $g^2$  values incremented uniformly. A standard gradient stabilisation delay of 0.3 ms followed all gradient pulses; this was also tested up to 1 ms (see below). Other NMR acquisition parameters were as described previously, and relaxation delays were set to 5 times the measured  $T_1$  values (Section 3.2.2). A typical  $^{195}\text{Pt}$  PGSE experiment required at least 1000 FIDs per gradient increment due to loss of sensitivity during the pulse sequence, resulting in total experiment times in excess of 12 hours for each experiment.<sup>14</sup>  $^{195}\text{Pt}$  FID data were processed as above with a 20 Hz exponential weighting function to improve the signal-to-noise ratio. For measurements in normal solvents, a coaxial capillary tube containing a deuterated solvent was placed in the standard 5 mm o.d. sample tube, resulting in reduction of active sample volume, poorer signal-to-noise ratio and even longer experiment times.

Measurement of accurate translational diffusion coefficients requires careful calibration of the magnetic field gradient strength.<sup>23</sup> Calibration was performed using a standard method based on the known diffusion coefficient ( $19.02 \times 10^{-10} \text{ m}^2/\text{s}$ ) of  $^1\text{H}$  in a “doped” water reference sample (1%  $\text{H}_2\text{O}$  in  $\text{D}_2\text{O}$ , 0.1% DSS, 0.1 mg/ml  $\text{GdCl}_3$ ; Varian, Inc., Palo Alto, CA) at 298 K (Figure 3.6). Translational diffusion coefficients,  $D$ , were calculated from signal attenuation data by the usual method of least-squares fitting of a straight line to a plot of  $\ln(E/E_0)$  (where  $E_0$  is the signal intensity/area at the lowest gradient strength) as a function of  $(g\delta\gamma)^2(\Delta-\delta/3)$ , the slope corresponding to the diffusion coefficient (see Section 3.1.3). Close inspection of the least-squares fit of a linear function to the  $^1\text{H}$  signal attenuation data of the calibration experiment reveals a slight deviation from linearity at higher gradient values.

Antalek<sup>23</sup> describes methods for characterising artefacts and obtaining optimum results in PGSE experiments. Non-ideal signal decay in PGSE experiments may result from at least three phenomena: 1) eddy currents that form in the NMR probe body during application of the gradient pulse; 2) gradient non-uniformity resulting from gradient coil design; 3)

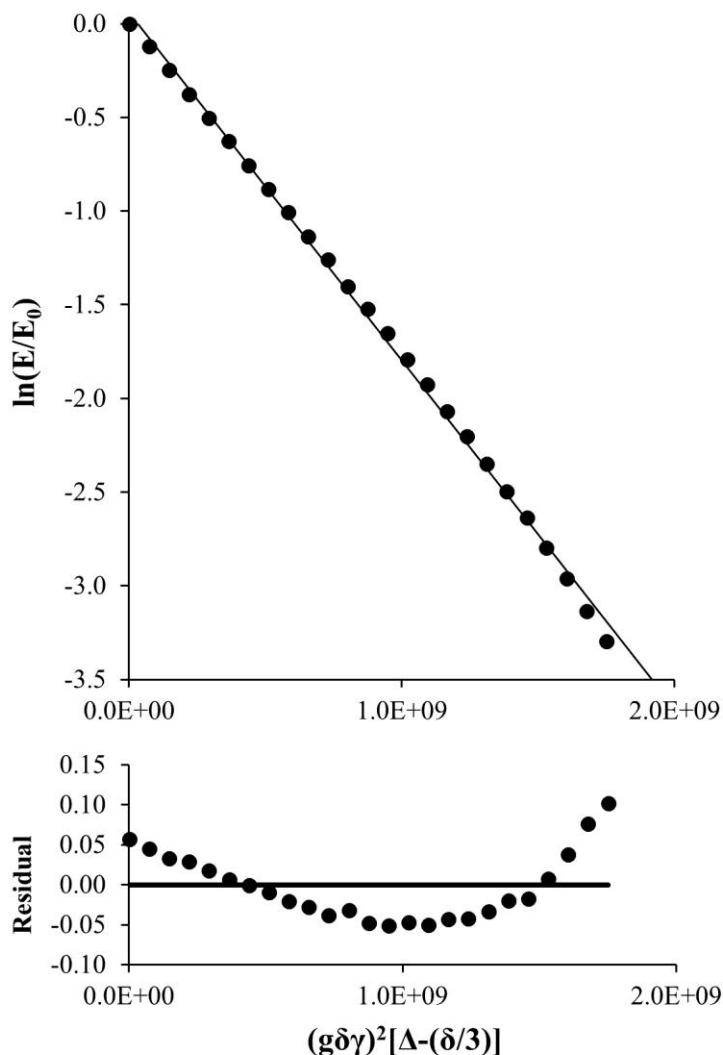


**Figure 3.6**  $^1\text{H}$  PGSE (DOSY) signal attenuation plot for doped water sample at 298 K, using standard Dbppste pulse sequence with  $\delta = 2$  ms,  $\Delta = 70$  ms, gradient stabilisation delay (gstab parameter) 0.3 ms and gradient strength (gzlv11 parameter, or  $g$ ) incremented from 500 to 15 000 DAC units (approximately 0.001 to 0.3 T/m) so that  $g^2$  uniformly spaced. Linear least-squares fit of data with raw residuals plotted below.<sup>23</sup>

convection currents set up in the sample by temperature gradients.<sup>23</sup> Convection currents are often problematic when performing PGSE experiments in low viscosity solvents at temperatures far removed from room temperature. In such cases, “convection compensated” PGSE pulse sequence variants are available that aim to reduce this artefact by introducing an additional pair of  $90^\circ$  and gradient pulses. Unfortunately, these sequences result in fairly significant sensitivity loss and were not suited for  $^{195}\text{Pt}$  experiments. Instead, the sample height was reduced (see above) in an attempt to avoid non-uniform heating, since temperature control (“VT”) gas/air is introduced from the bottom of sample compartment. Experiments

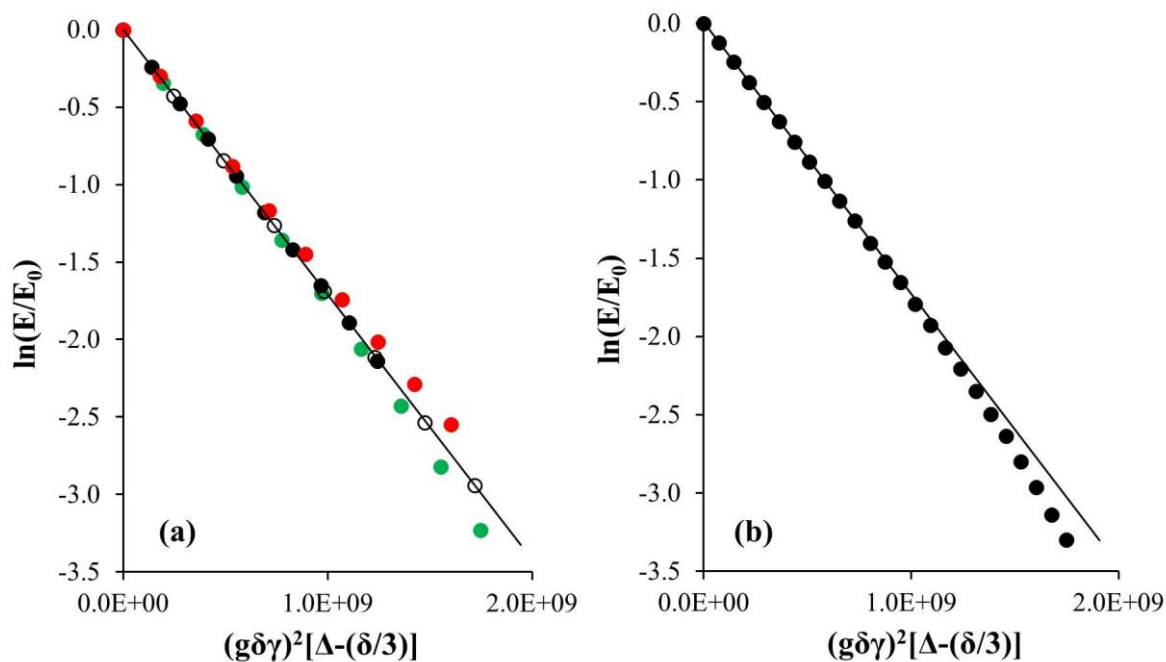


**Figure 3.7**  $^1\text{H}$  PGSE signal attenuation plots as in **Fig. 3.6**. **(a)** Experiments with different pulse sequence parameters. Solid black:  $\Delta = 50$  ms,  $g(\text{max}) \sim 0.3$  T/m; open black:  $\Delta = 50$  ms,  $g(\text{max}) \sim 0.35$  T/m; solid green:  $\Delta = 70$  ms; solid red:  $\Delta = 100$  ms. Linear least-squares fit to data indicated by solid black markers. **(b)** Data from **Fig. 3.6**, with linear least-squares fit through first 10 points only; used for gradient calibration (see text for details).

were also repeated with sample spinning (at 20 Hz; this did not improve data) and with different pulse sequence parameters (diffusion delay  $\Delta$ ); in the presence of convection currents, increasing the diffusion delay is expected to result in greater deviation ideal signal attenuation. While it was found that changing the diffusion delay did affect the results (Figure 3.7 (a)), the expected systematic change in the data trend was not observed. As a final check, experiments were performed with the VT unit switched off, i.e. at room temperature, but here too the deviation persisted. The effect of eddy currents was also investigated by increasing the gradient stabilisation delay following the gradient pulses from the standard 0.3 to 1 ms, which resulted in only minor improvement.

Antalek proposes the use of a “slice selection” technique for reducing the effect of gradient pulse non-uniformity in PGSE experiments.<sup>23</sup> In this method, a selective RF pulse is applied to excite only nuclei in a narrow, central region of the sample which then experience a more uniform gradient pulse and is subsequently detected. Unfortunately, introduction of slice selection elements in the pulse sequence also results in significant loss in sensitivity (up to 80 %), and the technique was deemed unsuitable for the  $^{195}\text{Pt}$  PGSE experiments described here.

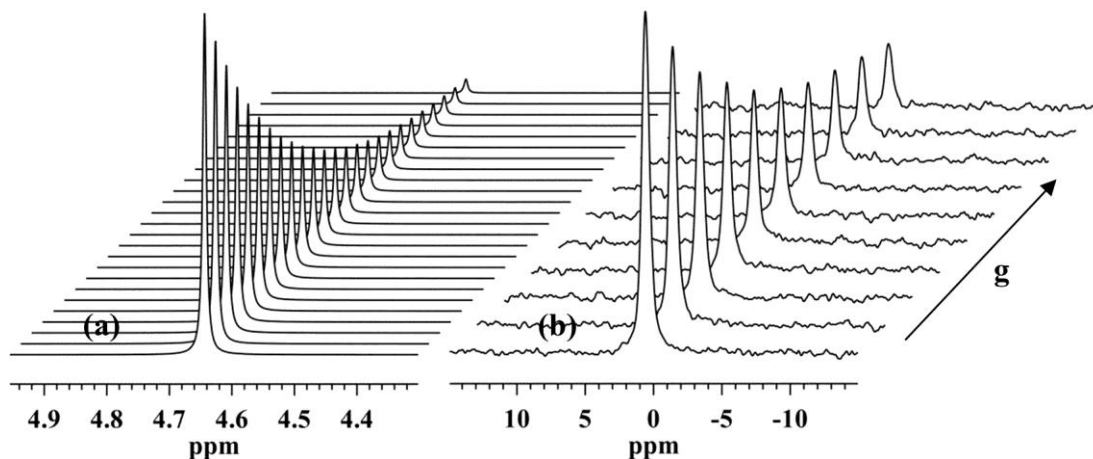


**Figure 3.8** Signal attenuation in PGSE (Dbppste sequence) experiments: (a)  $^1\text{H}$  NMR in doped water sample (Varian, Inc.); data plotted and processed in **Fig. 3.6** and **3.7**; (b)  $^{195}\text{Pt}$  NMR signals of  $[\text{PtCl}_6]^{2-}$  in 0.2 M hexachloroplatinic acid in  $\text{D}_2\text{O}$ ; plotted in **Fig. 3.9**. Both experiments were performed at 298 K.

The diffusion coefficient calculation for the  $^1\text{H}$  calibration data then involved least-squares fitting of a straight line through the first ten data points only (Figure 3.7 (b)); the difference in slope between the fitted lines in Figures 3.6 and 3.7 (b), calculated using the gradient calibration estimate available on the instrument (“DAC\_to\_G” value) is  $1.3 \times 10^{-10} \text{ m}^2/\text{s}$ .

Examples of typical  $^1\text{H}$  and  $^{195}\text{Pt}$  PGSE spectra are compared in Figure 3.8; the difference in signal-to-noise ratio and number of gradient increments used in the experiments is illustrated. Fewer gradient increments, typically only six, were used in  $^{195}\text{Pt}$  PGSE experiments for solutions in normal solvents, since it was necessary to acquire more FIDs (about 2000) per gradient increment in order to obtain an adequate signal-to-noise ratio (capillary insert replacing active sample volume; see above). The attenuation plot and least-squares fit used to calculate the diffusion coefficient of the platinum complex is shown in Figure 3.9. The typical error associated with the  $^{195}\text{Pt}$  PGSE diffusion coefficients reported here is estimated conservatively at  $\pm 0.3 \times 10^{-10} \text{ m}^2/\text{s}$  (on the basis of repeated experiments for selected samples); Pregosin and co-workers,<sup>20</sup> on the basis of their experience with diffusion measurements, reported an error of  $0.06 \times 10^{-10} \text{ m}^2/\text{s}$  for their  $^{195}\text{Pt}$  PGSE-derived diffusion coefficients with similar samples and experimental setup.

### 3.3 Results and discussion

#### 3.3.1 Relaxation times and molecular rotation

Spin-lattice, or  $T_1$ , NMR relaxation times of nuclei are determined by interactions between the nucleus and its environment, and so may provide structural information provided the relaxation mechanism is known.<sup>9</sup> Often, however, several relaxation mechanisms contribute to the observed relaxation rate and it is necessary to determine these contributions by performing appropriate experiments e.g. measurements as a function of temperature and magnetic field strength.<sup>9,11</sup> In the case of heavy dipolar nuclei e.g.  $^{13}\text{C}$ ,  $^{19}\text{F}$  or  $^{31}\text{P}$  in small, highly mobile molecules or fragments, the spin-rotation mechanism often makes an important contribution to the relaxation rate.<sup>4</sup> In this mechanism, the electron distribution in the molecule creates a magnetic moment at the resonant nucleus that fluctuates and results in spin relaxation when the molecule rotates rapidly.<sup>9</sup> The rate of spin-rotation relaxation for a nucleus situated at the centre of symmetry of a spherical molecule is given by the following equation:<sup>4</sup>

$$\frac{1}{T_1^{\text{SR}}} = \frac{8\pi^2 I k T}{\hbar^2} C^2 \tau_J \quad (3.5)$$

Here,  $I$  is the moment of inertia of the molecule,  $C$  the spin-rotation constant which reflects the strength of the interaction and  $\tau_J$  the angular momentum correlation time of the molecule (see Section 3.1.1). The spin-rotation constant  $C$  is related to the paramagnetic shielding experienced by a nucleus in a molecule.<sup>24,25</sup> Unlike other common relaxation mechanisms, the rate of spin-rotation relaxation increases with increasing temperature, i.e.  $T_1$  relaxation times *decrease* with increasing temperature.<sup>9,11,26</sup>

Pesek and Mason<sup>27</sup> first studied the  $^{195}\text{Pt}$  NMR relaxation times of  $[\text{PtCl}_6]^{2-}$  and square-planar  $[\text{PtCl}_4]^{2-}$  in aqueous solution and showed that spin-rotation relaxation is the only relaxation mechanism operative in these complexes in the temperature range 298 to 340 K. The temperature dependences of the  $^{195}\text{Pt}$   $T_1$  relaxation times in  $[\text{PtCl}_6]^{2-}$  (in  $\text{D}_2\text{O}$  and methanol- $d_4$ ) and  $[\text{PtBr}_6]^{2-}$  (in  $\text{D}_2\text{O}$ ) are shown in Figure 3.10. In this logarithmic plot it can be seen that the  $1/T_1$  values decrease linearly as a function of inverse temperature (i.e.  $T_1$  decreases with increasing temperature), suggesting a single dominant relaxation mechanism.<sup>11</sup>



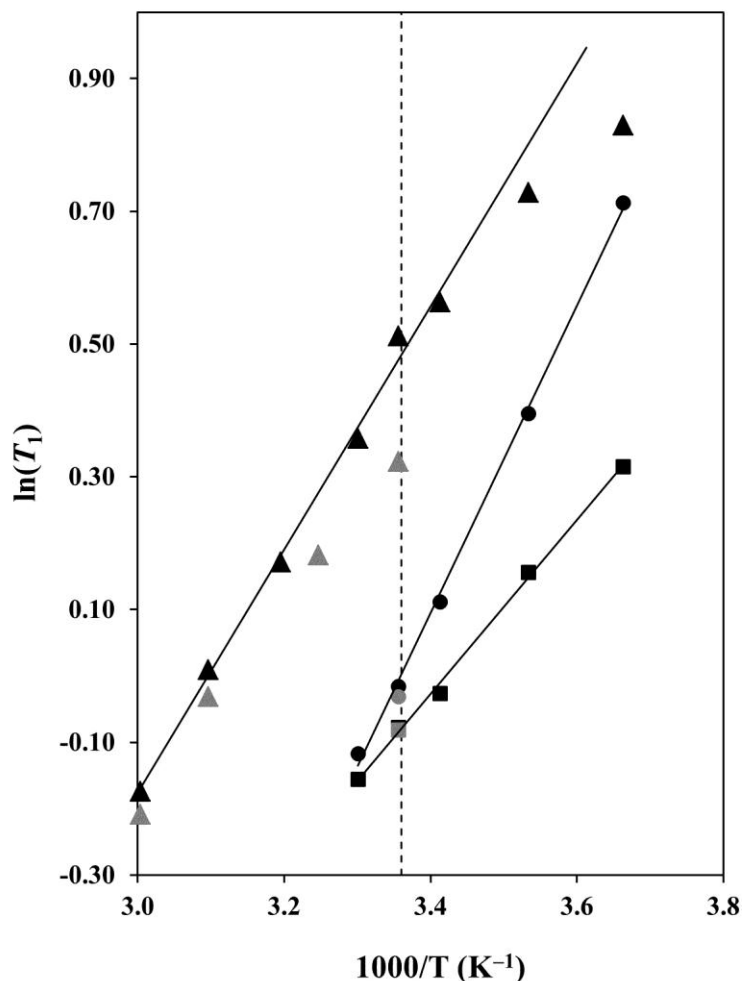


**Figure 3.10** Variable-temperature  $^{195}\text{Pt}$   $T_1$  relaxation times of  $[\text{PtCl}_6]^{2-}$  in 0.2 M solutions of hexachloroplatinic acid in  $\text{D}_2\text{O}$  (solid black circles) and methanol- $d_4$  (solid black squares), and of  $[\text{PtBr}_6]^{2-}$  in similar solution of hexabromoplatinic acid in  $\text{D}_2\text{O}$  (solid black triangles) at 14.1 T (128 MHz). Grey symbols with corresponding shapes indicate measurements at 9.4 T (85 MHz), and the dotted vertical line is drawn at 298 K to aid comparison. Solid black lines are linear least-squares fits to the data, except in the case of  $[\text{PtBr}_6]^{2-}$ , where only high-temperature ( $T > 298$  K) data are fitted. Note difference in data collected at different fields for  $[\text{PtBr}_6]^{2-}$  (identical for  $[\text{PtCl}_6]^{2-}$ ), expected to increasingly deviate at temperatures  $< 298$  K due to a scalar relaxation mechanism.<sup>11</sup>

Note, however, that for  $[\text{PtBr}_6]^{2-}$  a deviation from linearity occurs at lower temperatures, and the relaxation rate is greater than expected. This deviation is due to an additional relaxation mechanism, scalar (coupling) relaxation of the second kind (i.e. modulated by rapid spin relaxation of the  $J$ -coupled nucleus), contributing to the relaxation rate at lower temperatures, since the scalar coupling mechanism has the usual temperature dependence i.e. becomes more efficient as temperature decreases.<sup>11,27</sup> The  $T_1$  of this complex is also dependent on the magnetic field strength at the lower temperatures, since the scalar relaxation rate is dependent

on the frequency difference between the resonant/relaxing nucleus and that of another nuclide interacting with it *via* spin–spin ( $J$ , or *scalar*) coupling, in this case bromine isotopes. Note that this appears not to be the case for  $[\text{PtCl}_6]^{2-}$ , possibly due to the greater frequency difference between  $^{195}\text{Pt}$  and  $^{35/37}\text{Cl}$  under these conditions.<sup>27</sup>

$^{195}\text{Pt}$   $T_1$  measurements for  $[\text{PtCl}_6]^{2-}$  in water, methanol, 2-methoxyethanol and 1,2-dimethoxyethane at 298 K are given in Table 3.1. The spin–spin, or  $T_2$ , relaxation times of  $^{195}\text{Pt}$  measured in selected samples by the Carr–Purcell–Meiboom–Gill (CPMG) technique<sup>11</sup> were found to be consistently shorter than the  $T_1$  values, possibly due to a scalar relaxation mechanism (likely to be of the second kind) which is known to affect these times differently;<sup>27</sup> a similar observation was reported by Pesek and Mason.<sup>17</sup> We will be concerned here with analysis of the  $T_1$  relaxation time data, since these can be identified with a single relaxation mechanism, namely spin–rotation, which may be understood in the context of Eq. 3.1.<sup>4</sup>

With the exception of 1,2-dimethoxyethane, the  $T_1$  relaxation times in Table 3.1 can be seen to increase with increasing solvent viscosity, where molecular rotation is expected to slow down, consistent with the spin–rotation relaxation mechanism. The rotational diffusion of a spherical molecule in a solution with dynamic viscosity  $\eta$  is characterised by its *rotational correlation time*, which may be expressed by the Stokes–Einstein–Debye equation,<sup>29,30</sup>

$$\tau_c = \frac{V\eta}{kT} \quad (3.6)$$

where  $V$  is the volume of the molecule (or “probe” in related literature), with other symbols having their usual meaning. This simple equation has been shown to describe fairly accurately the rotational motion of large, spherical molecules in solution. A general expression for the rotational correlation time of a molecule in solution is given by Dote *et al.*<sup>7</sup>

$$\tau_c = \frac{V\eta}{kT} \phi C + \tau_0 \quad (3.7)$$

Here, the rotational correlation time has two components: the first is proportional to the solution viscosity (“hydrodynamic”), where the symbols have the same meaning as in Eq. 3.6,  $\phi$  is a shape parameter (with a value 1 for a spherical molecule) and  $C$  is a dimensionless parameter, the value of which ranges from 0 to 1, reflecting the nature of the interactions

**Table 3.1**  $^{195}\text{Pt}$   $T_1$  NMR relaxation times of  $[\text{PtCl}_6]^{2-}$  in different solvents at 298 K, with angular momentum ( $\tau_j$ ) and reorientational ( $\tau_c$ ) correlation times calculated by a method describe in the text. Also given are reorientational correlation times calculated using the Stokes–Einstein–Debye equation (viscosities,  $\eta$ ,<sup>39</sup> and ionic radius 3.13 Å),<sup>40</sup>  $\tau(\text{SED})$ .

Solvent	$\eta$ (mPa.s)	$^{195}\text{Pt}$ $T_1$ (s)	$\tau_j$ (fs)	$\tau_c$ (ps)	$\tau_c(\text{SED})$ (ps)
Water	0.89	0.854	34	15	28
Methanol	0.54	0.645	45	11	17
2-Methoxyethanol	1.54	1.796	16	33	48
1,2-Dimethoxyethane	0.46	1.143	25	21	14

of the molecule with its environment, and for which several theoretical interpretations have been presented; the second term,  $\tau_0$ , is related to the moment of inertia of the molecule.<sup>7,31</sup>

Rotational correlation times of molecules in solution can be determined by NMR relaxation time measurements provided the relaxation mechanism and other parameters affecting the relaxation process are known, e.g. internuclear distances for the dipole–dipole, and electric field gradients at the nucleus for the quadrupolar relaxation mechanisms.<sup>9</sup> In the case of relaxation by the spin–rotation mechanism, the angular momentum correlation time of a molecule may be determined from relaxation time data and a known spin–rotation constant. The spin–rotation constant was shown by Flygare and Goodisman to be related to the nuclear magnetic shielding  $\sigma$  by the following equation,<sup>6,32</sup>

$$\sigma = \sigma_{\text{FA}} + \frac{MC}{2mBg_k} \quad (3.8)$$

where  $\sigma_{\text{FA}}$  is the nuclear shielding in the isolated free atom, identified with the diamagnetic shielding ( $\sigma_d$ ) contribution,  $M$  and  $m$  the proton and electron mass respectively, and  $B$  the spectroscopic rotational constant equal to  $\hbar/4\pi I$  (where  $I$  is the moment of inertia), and  $g_k$  the nuclear  $g$ -factor, which is related to the magnetogyric ratio ( $\gamma_k$ ) of the nucleus.

$$\gamma_k = \frac{e}{2m_p} g_k \quad (3.9)$$

The angular momentum correlation time,  $\tau_j$ , of a spherical molecule undergoing small-step rotational diffusion is related to its reorientational correlation time,  $\tau_c$ , by the Hubbard relationship (where the symbols have their usual meaning).<sup>4</sup>

$$\tau_c = \frac{I}{6kT\tau_j} \quad (3.9)$$

The Hubbard relationship is a special case of Eq. 3.2, and its validity limited to effectively spherical molecules for which  $\tau_c \gg \tau_j$ ;<sup>6</sup> it is straightforward to calculate the moment of inertia,  $I$ , about molecular axes for simple regular molecular geometries e.g. tetrahedral and octahedral molecules.

The angular momentum correlation times of  $[\text{PtCl}_6]^{2-}$  in water, methanol, 2-methoxyethanol and 1,2-dimethoxyethane were estimated from the spin-rotation  $T_1$  data obtained in this work using Eq. 3.5 and 3.8.<sup>6</sup> The calculation requires knowledge of the paramagnetic shielding of the  $^{195}\text{Pt}$  nucleus in the various environments. While it is not possible to determine this quantity experimentally, it may be computed using *ab initio* electronic structure methods based on Density Functional Theory (DFT).<sup>33</sup> Several computational studies concerning the calculation of  $^{195}\text{Pt}$  NMR chemical shifts in platinum complexes in solution have appeared in the last decade, notably by Autschbach and co-workers.<sup>34</sup> The paramagnetic shielding of Pt in  $[\text{PtCl}_6]^{2-}$  reported by Burger *et al.*<sup>35</sup> was used in the present study to estimate the spin-rotation constant (Eq. 3.8) and ultimately the angular momentum correlation time of the complex in solution (Eq. 3.5). Burger *et al.*<sup>35</sup> used a DFT-based method with relativistic corrections (using the zeroth-order regular approximation, spin-orbit ZORA) to calculate  $^{195}\text{Pt}$  chemical shifts of complexes  $[\text{PtX}_{6-n}\text{Y}_n]^{2-}$ , where X,Y = Cl, Br, F and I, in aqueous solution using the COSMO continuum solvent model to account for electrostatic effects of the solvation environment on the electronic structure. The  $^{195}\text{Pt}$  paramagnetic shielding in  $[\text{PtCl}_6]^{2-}$  obtained by this procedure was  $-10\,899$  ppm.<sup>35</sup>

The angular momentum correlation times ( $\tau_j$ ) calculated by the method described above are presented in Table 3.1. These values are in the typical range for molecules of similar size and moment of inertia: Laaksonen and Wasylishen<sup>6</sup> reported an angular momentum correlation time of  $77.0 \pm 4.6$  fs for liquid  $\text{SnCl}_4$  at 298 K (from Molecular Dynamics simulation), while Nichols and Rodriguez<sup>36</sup> reported a value of 173 fs for  $\text{CCl}_4$  in chlorobenzene- $d_5$  at 303 K (from  $^{13}\text{C}$   $T_1$  data and Eq. 3.1; note the solution viscosity is low). Calculations of angular

momentum correlation times were initially performed using a single value for the paramagnetic shielding, calculated by Burger *et al.*<sup>35</sup> for the platinum complex in water. However, this is not entirely accurate, since the  $^{195}\text{Pt}$  NMR chemical shift of the complex is known to increase by about 200 ppm on going from water to 1,2-dimethoxyethane,<sup>21</sup> and these solvent shifts are expected to be due largely to a changes in the paramagnetic shielding contribution. Taking this into account, the value for the paramagnetic shielding was adjusted by the solvent shift and the angular momentum times recalculated. These corrections, however, were found to have a negligible effect on the calculated correlation times ( $\leq 1$  fs).

Finally, reorientational correlation times were calculated using the Hubbard relationship.<sup>4</sup> The validity of the Hubbard relationship in the present case was evaluated on the basis of known reorientational correlation times of similar complex anions in aqueous solution; e.g. a reorientational correlation time of 8.28 ps was reported for  $[\text{Pt}(\text{CN})_6]^{2-}$  in water at 322 K,<sup>37</sup> and 18 ps for  $[\text{Co}(\text{CN})_6]^{3-}$  at 298 K, also in water.<sup>38</sup> Assuming similar values for  $[\text{PtCl}_6]^{2-}$  in the solvents studied here, the Hubbard relationship can reasonably be taken to be appropriate also for the present system ( $\tau_c \gg \tau_J$ ).<sup>6</sup> Reorientational correlation times calculated by this procedure in Table 3.1 compare well with literature values for similar-size molecules in aqueous solution.<sup>37</sup>

Reorientational correlation times calculated by the Stokes–Einstein–Debye (SED) equation are also given in Table 3.1 for comparison.<sup>39</sup> The calculated hydrodynamic values,  $\tau_c(\text{SED})$ , are much larger than those determined experimentally, i.e. this theory predicts slower rotation than that based on relaxation time data. The overestimation of reorientational correlation times by the SED equation has, however, been reported by others: Rodriguez and co-workers determined the reorientational correlation time of buckminsterfullerene ( $\text{C}_{60}$ ) in chlorobenzene- $d_5$  to be 8.99 ps (at 303 K, using  $^{13}\text{C}$  NMR relaxation data), while the SED equation predicts a value of 31.2 ps;<sup>36</sup> this is a system for which the SED theory is expected to be reasonable (large, spherical and uncharged solute surrounded by smaller solvent molecules). The reorientational correlation times of  $[\text{PtCl}_6]^{2-}$  in the various solvents follow a similar trend to that predicted by the SED equation, with the exception of the 1,2-dimethoxyethane solution, for which the rotation of the platinum complex appears to be slower than expected (i.e. *longer* reorientational correlation time). To investigate the possible effect of solute–solute interactions, i.e. ion-pairing, in this solvent, the measurement was repeated using a different precursor salt,  $\text{Na}_2\text{PtCl}_6$ , at a lower concentration (due to solubility restrictions). The  $^{195}\text{Pt}$   $T_1$  relaxation time (at 298 K) measured in this sample was found to be

essentially identical to that reported in Table 3.1, strongly suggesting this effect to be due to the nature of solvation of the complex.

Clearly, the “stick” boundary condition ( $C = 1$  in Eq. 3.7) used in the SED equation overestimates the hydrodynamic friction experienced by the rotating platinum complex in the solvents studied here.<sup>7</sup> Several alternative hydrodynamics-based theoretical interpretations of the parameter  $C$  have been presented to account for microscopic details of the solvation environment of a probe molecule in solution. The Gierer–Wirtz (GW) microviscosity theory<sup>41</sup> introduces some molecular detail of the solvation shell (solvent size) in the friction, which has been shown to improve the accuracy of reorientational correlation time predictions in several systems.<sup>36</sup> In this approach the  $C$  parameter is written as the product

$$C = \sigma_{GW} C_0 \quad (3.10)$$

where  $C_0$  is a function of the volumes of the probe ( $V_P$ ) and solvent ( $V_S$ ) molecules

$$C_0 = \left[ \frac{6(V_S/V_P)^{1/3}}{(1 + 2(V_S/V_P)^{1/3})^4} + \frac{1}{(1 + 4(V_S/V_P)^{1/3})^3} \right]^{-1} \quad (3.11)$$

and  $\sigma_{GW}$  has values between 0 (“slip” boundary condition) and 1 (“stick”) and is given by

$$\sigma_{GW} = \frac{1}{1 + 6(V_S/V_P)^{1/3} C_0} \quad (3.12)$$

The Gierer–Wirtz theory was derived for a spherical solute surrounded by uniform spherical solvent molecules, and the above expressions for  $C_0$  and  $\sigma_{GW}$  are approximate provided  $V_P > V_S$ .<sup>7</sup> This condition is clearly not appropriate for all solvents studied here, and the effective sizes of the conformationally flexible 2-methoxyethanol and 1,2-dimethoxyethane in the vicinity of the platinum complex are not known in general. Application of the GW theory reduces the rotational friction and consequently the reorientational correlation time predicted by the SED equation by a factor  $\sigma_{GW} C_0$ . In the case of water, the SED prediction of 28 ps is reduced to 10 ps, which is closer to the 15 ps estimated from the <sup>195</sup>Pt  $T_1$  relaxation time. However, in methanol, as well as the other two solvents, the reorientational correlation times obtained by the GW theory are unreasonably short (4 ps in the case of methanol; the experimental estimate is 11 ps and the SED value 17 ps). Moreover, the GW theory is not

**Table 3.2**  $^{195}\text{Pt}$   $T_1$  NMR relaxation times of  $[\text{PtCl}_6]^{2-}$  in equimolar mixtures of water with methanol, 2-methoxyethanol (2-ME) and 1,2-dimethoxyethane (1,2-DME) at 298 K, with calculated angular momentum ( $\tau_J$ ) and reorientational ( $\tau_c$ ) correlation times. Also given are reorientational correlation times calculated using the Stokes–Einstein–Debye equation (using viscosities,  $\eta$ ,<sup>39</sup> and ionic radius 3.13 Å).<sup>40</sup>

Solvent	$\eta$ (mPa.s)	$^{195}\text{Pt}$ $T_1$ (s)	$\tau_J$ (fs)	$\tau_c$ (ps)	$\tau_c(\text{SED})$ (ps)
Water + Methanol	1.33	0.890	33	16	42
Water + 2-ME	2.75	1.446	20	26	86
Water + 1,2-DME	0.80	0.989	29	18	25

strictly applicable to solvent mixtures, for which the composition and molecular arrangements in solvation shells are not known; this is also the case for other hydrodynamics-based models intended to introduce microscopic structural detail.<sup>7</sup>

Measurements of  $^{195}\text{Pt}$   $T_1$  relaxation times of  $[\text{PtCl}_6]^{2-}$  were also made for solutions in equimolar mixtures of water with methanol, 2-methoxyethanol and 1,2-dimethoxyethane (Table 3.2). These binary solvent mixtures have interesting physical properties in general, and they all show the phenomenon of “excess viscosity” i.e. the bulk viscosities of the solvent mixtures are greater than those of the pure solvent components (Figure 1.5).<sup>39,42</sup> Reorientational correlation times were estimated using the  $T_1$  measurements as for the pure solvent solutions, and are listed in Table 3.2; the results obtained in the solvent mixtures are discussed individually below.

In the equimolar water–methanol mixture, the reorientational correlation time of  $[\text{PtCl}_6]^{2-}$  is estimated at 16 ps, which is slightly longer than that in pure water (15 ps) and methanol (11 ps). This result is qualitatively consistent with the greater viscosity of the solvent mixture; the SED value is much longer at 42 ps. While it is generally difficult to identify the reorientational correlation time measured in a binary solvent mixture with a specific average solvation environment, it may be reasonable to argue that the reorientational correlation time of a small, approximately spherical solute is determined largely by interactions with solvent molecules in the primary solvation shell,<sup>43</sup> i.e. in direct contact with the solute, since its rotation does not necessarily require displacement of solvent molecules.<sup>44</sup> Assuming then, as an approximation, that the contributions from individual solvent molecules in the first solvation shell to the rotational retardation of the platinum complex are somehow additive,

one expects the reorientational correlation time of the complex in the solvent mixture to be intermediate or equal to those in the pure solvents, depending on the solvation shell composition. In the current solvent mixture,  $^{195}\text{Pt}$  chemical shift measurements suggest a primary solvation shell containing both solvent species, but with a slight preference for methanol, i.e. an excess of methanol, provided a constant solvation number at all mixed solvent compositions.<sup>21</sup> The measured reorientational correlation time is closer to that in pure water, however, and appears to exceed this value (15 ps), which is not consistent with the results of  $^{195}\text{Pt}$  chemical shift trends in the context of the assumption presented above.

The reorientational correlation time measured in the water–2-methoxyethanol mixture is 26 ps. This solvent mixture has a significantly higher bulk viscosity (2.75 mPa.s) compared to pure 2-methoxyethanol (1.544 mPa.s),<sup>39</sup> yet the platinum complex appears to rotate slightly faster than in the pure organic solvent (31 ps). While this observation is certainly *not* consistent with a simple hydrodynamic prediction, it suggests a solvation environment in which the rotational retardation is intermediate with that in pure water and 2-methoxyethanol, yet more similar to the latter,<sup>43</sup> i.e. possibly indicating preferential solvation by this component, as inferred from  $^{195}\text{Pt}$  chemical shift trends determined by Westra.<sup>21</sup> Indeed, a similar behaviour is seen in the water–1,2-dimethoxyethane mixture, where a strong preferential solvation effect (by 1,2-dimethoxyethane) is expected.<sup>21</sup> Here, the mixed solvent viscosity is intermediate with those of the pure solvents, since the excess viscosity effect persists only up to a mole fraction organic component of about 0.4, after which it steadily approaches that of pure 1,2-dimethoxyethane (Figure 1.5). However, at 21 ps the reorientational correlation time in the latter (pure 1,2-dimethoxyethane) was found to be *longer* than that in the more viscous water, i.e. the correlation time measured in the equimolar mixture is between those determined in the pure solvents, but not between those predicted on the basis of a hydrodynamic argument; this result suggests a primary solvation shell in which, on average, both water and 1,2-dimethoxyethane participate.

### 3.3.2 Translational diffusion

Pregosin and co-workers reported the first  $^{195}\text{Pt}$  PGSE experiments in 2004.<sup>20</sup> These experiments were designed to study ion-pairing processes in solutions of  $\text{Na}_2\text{PtCl}_6$  and  $\text{H}_2\text{PtCl}_6$  in water ( $\text{D}_2\text{O}$ ) and methanol ( $-d_4$ ).<sup>45</sup> The translational diffusion coefficients of the  $[\text{PtCl}_6]^{2-}$  anion were measured and used to calculate hydrodynamic radii of the complex in solutions of the salts in the pure solvents, which were then identified with the nature of ion-



pairing. The calculations involved the Stokes–Einstein equation,<sup>29,46</sup> which describes the translational diffusion of a spherical solute, with effective (hydrodynamic) radius  $r_H$ , in a solvent of viscosity  $\eta$ , and with other symbols having their usual meaning:

$$D = \frac{kT}{c\pi\eta r_H} \quad (3.13)$$

The parameter  $c$  describes the nature of the interaction between solute and surrounding solvent environment; a value of 6 is appropriate for describing the diffusion of large solutes, or of solutes interacting strongly with their surrounds (“stick” boundary condition), while a value of 4 is more appropriate for smaller solutes which do not engage in strong interactions with the solvent (“slip” boundary).<sup>1,47,48</sup>

As a first step in the current work, selected measurements by Pregosin and co-workers<sup>20</sup> were repeated as a general check of the instrumental conditions and experiment setup (different stimulated echo pulse sequence variant was used). The <sup>195</sup>Pt diffusion coefficients ( $D$ ) measured here were found to be consistently *lower* than those reported by Pregosin *et al.*, e.g. for a 0.2 M solution of Na<sub>2</sub>PtCl<sub>6</sub> in D<sub>2</sub>O at 298 K,  $D = 4.9 \times 10^{-10}$  m<sup>2</sup>/s, compared with their value of  $7.13 \times 10^{-10}$  m<sup>2</sup>/s (299 K). Pregosin *et al.* used this diffusion coefficient to estimate a hydrodynamic radius of 3.4 Å, a value interpreted as indicating an ion-separated, solvated platinum complex, based on a ~2.3–2.4 Å Pt–Cl bond length and a solvation shell of thickness ~1 Å.<sup>20</sup> It is clear, however, that the solvent viscosity used in this calculation was that of *normal* (non-deuterated) water at 298 K. Repeating the calculation using the correct viscosity for D<sub>2</sub>O at 299 K (1.089 mPa.s),<sup>49</sup> a “stick” hydrodynamic radius of only ~2.8 Å is obtained (Marcus,<sup>40</sup> in his book, lists an ionic radius of 3.13 Å for [PtCl<sub>6</sub>]<sup>2-</sup>). It is not straightforward to assess the accuracy of the diffusion coefficient estimates reported here. The only other <sup>195</sup>Pt PGSE experiment reported is that by Miyoshi,<sup>50</sup> who determined the translational diffusion coefficient of square-planar [PtCl<sub>4</sub>]<sup>2-</sup> in a solution of K<sub>2</sub>PtCl<sub>4</sub> in D<sub>2</sub>O (10 mM) to be  $3.08 \pm 0.04 \times 10^{-10}$  m<sup>2</sup>/s.

<sup>195</sup>Pt PGSE attenuation data for [PtCl<sub>6</sub>]<sup>2-</sup> in solutions of hexachloroplatinic acid in water, methanol and their equimolar mixture (0.2 M), measured in this work, are plotted in Figure 3.11. Diffusion coefficients measured in water and methanol were higher than those in the corresponding deuterated solvents at the same temperature, as expected based on the higher viscosity of the latter.

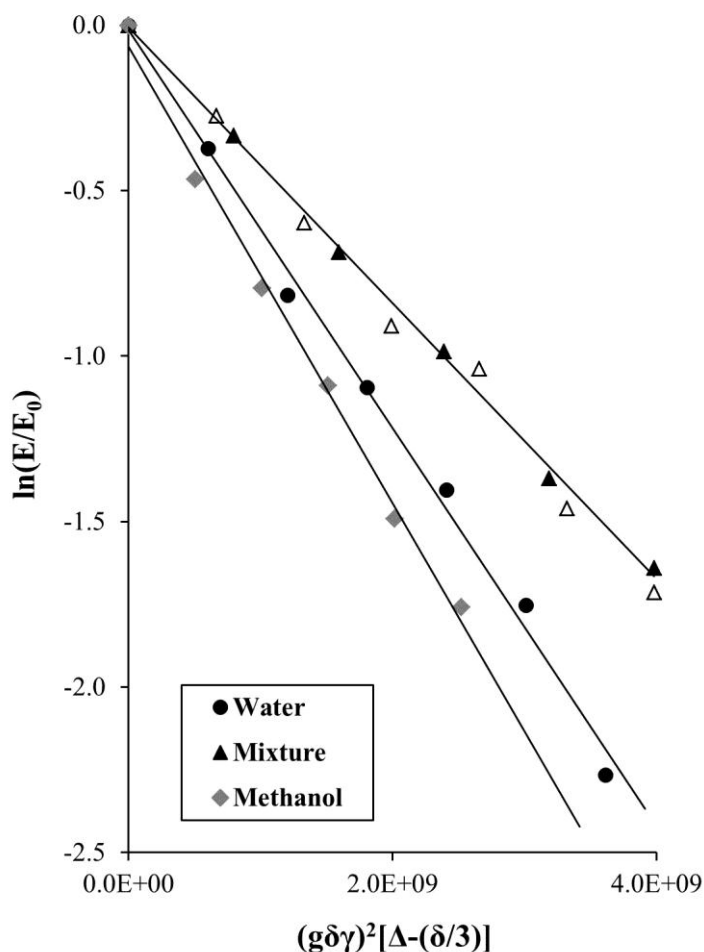


**Figure 3.11**  $^{195}\text{Pt}$  PGSE signal attenuation plot for 0.2 M hexachloroplatinic acid in water (black circles), methanol (grey diamonds) and equimolar water–methanol mixture (solid and open black triangles, from separate experiments) at 298 K. Linear least-squares fits (through solid black triangles for mixture) used to calculate translational diffusion coefficients. Dbppste pulse sequence:  $\delta = 5\text{--}7$  ms;  $\Delta = 80\text{--}120$  ms;  $g$  up to  $\sim 0.5$  T/m.

For the experiments in non-deuterated (“normal”, or “regular”) solvents, a coaxial capillary tube containing deuterated solvent was placed inside the normal 5 mm o.d. sample tube for field locking purposes (Section 3.2.3). This insert greatly reduced the active sample volume, resulting in generally poorer signal-to-noise and fewer gradient increments during a reasonable experiment time (up to *ca.* 20 hours per measurement). Measurements were, however, found to be typically reproducible despite the poorer data quality,<sup>23</sup> as shown in Fig. 3.11 for the sample in the water–methanol mixture.

Diffusion coefficients calculated using the attenuation data are reported in Table 3.3 with corresponding hydrodynamic radii calculated using the Stokes–Einstein equation with “stick” and “slip” boundary conditions. The hydrodynamic radius obtained in methanol is larger than

**Table 3.3**  $^{195}\text{Pt}$  PGSE translational diffusion coefficients of  $[\text{PtCl}_6]^{2-}$  in solutions (0.2 M) of hexachloroplatinic acid in water, methanol and their equimolar mixture at 298 K, with hydrodynamic radii calculated using the Stokes–Einstein equation.

Solvent	$\eta$ (mPa.s)	$D$ ( $10^{-10}$ m <sup>2</sup> /s)	$r_{\text{H}}$ (“stick”) (Å)	$r_{\text{H}}$ (“slip”) (Å)
Water	0.89	6.0	4.1	6.1
Methanol	0.54	6.9	5.9	8.8
Water + Methanol*	1.33	4.2	3.9	5.9

those in water and the equimolar solvent mixture; Pregosin *et al.* reported similar findings in  $\text{D}_2\text{O}$  and methanol- $d_4$  and have tentatively attributed this difference to ion-pairing or other aggregative processes in methanol.<sup>20</sup> Masuda *et al.*,<sup>44</sup> in a  $^{17}\text{O}$  NMR study of the rotational diffusion of tetrahedral oxo-anions in water and methanol, concluded that the rotational motion of perchlorate and sulphate ions in methanol is accompanied by the solvent to a greater extent than in water, despite expected weaker interactions of the ions with methanol molecules based on a lower average positive charge on methanol hydrogen sites. This phenomenon was rationalised as resulting from weaker intermolecular interactions (hydrogen bonding) between molecules of methanol compared to that in water in the pure solvents, i.e. differences in solvent–solvent interactions.<sup>44</sup> A similar reasoning may be appropriate in the present study, in which it is possible that methanol molecules are more closely associated with the diffusing platinum complex in pure methanol solvent, retarding its motion and increasing its effective hydrodynamic radius (calculated via the Stokes–Einstein equation).

However, as was the case for the study of rotational diffusion, it is not generally possible to directly link measured diffusion coefficients to a specific microscopic solvation shell structure or composition *via* a simple theory, especially in the case of mixed solvents. Translational diffusion additionally requires displacement of solvent molecules, and so the phenomenon is likely to be more closely linked to the bulk viscosity and properties of the solvent, and not simply the nature of the primary solvation shell of the solute, which is of interest in the present study.<sup>43</sup> This expectation, combined with the difficulties associated with diffusion measurements on especially samples in non-deuterated solvents, including time constraints, necessitated the suspension of further  $^{195}\text{Pt}$  PGSE measurements in the other solvent mixtures of interest. It is expected that better-quality diffusion data could be obtained using high-sensitivity modern cryoprobe hardware in the future.

### 3.4 Conclusions

$^{195}\text{Pt}$  longitudinal ( $T_1$ ) relaxation time measurements and PGSE translational diffusion experiments were performed for  $[\text{PtCl}_6]^{2-}$  in water, selected organic solvents, and their equimolar binary mixtures at 298 K. Reorientational correlation times of the platinum complex, estimated from the  $^{195}\text{Pt}$   $T_1$  measurements using an approach described by Laaksonen and Wasylishen,<sup>6,28</sup> were compared with those expected on the basis of hydrodynamic theories of rotational diffusion; while reasonable values were found for these correlation times, they do not agree well with hydrodynamic predictions. The Stokes–Einstein–Debye equation, in particular, is known to overestimate reorientational correlation times.<sup>36</sup> More importantly, since hydrodynamic theories are based on macroscopic (bulk) viscosity, comparison of their predictions with experimentally determined values does not provide direct structural information on the microscopic solvation environment of the solute (platinum complex), and are possibly not appropriate when mixed solvents (known for microscopic heterogeneity) are considered. An alternative, intuitive, interpretation of the measurements in the context of the primary solvation shell compositions, previously inferred from  $^{195}\text{Pt}$  chemical shift solvent dependent trends, was also presented.<sup>36</sup>

Translational diffusion measurements by  $^{195}\text{Pt}$  PGSE experiments proved to be more challenging than expected for these samples, and were restricted to normal water, methanol and their equimolar mixture. The platinum complex diffusion coefficients in the pure water and methanol were found to be significantly *lower* than those reported by Pregosin and co-workers<sup>20</sup> for the same salt in  $\text{D}_2\text{O}$  and methanol- $d_4$  under similar conditions. In the equimolar water–methanol mixture, the diffusion coefficient was found to be lower than in the pure solvents, qualitatively consistent with the higher viscosity of this mixture. Hydrodynamic radii calculated from the measured  $^{195}\text{Pt}$  diffusion coefficients using the Stokes–Einstein equation were found to be reasonable, with a notably larger radius “stick” boundary radius of  $\sim 6$  Å in methanol, compared with 4 Å in pure water and the equimolar mixture.

Measurements of the dynamic properties of simple platinum complexes in solution, specifically with the aim of studying solvation phenomena in mixed solvents, have, to the best of our knowledge, been rarely studied, certainly not by  $^{195}\text{Pt}$  NMR spectroscopic techniques.<sup>20,27</sup> Interpretation of the results in terms of microscopic differences in the primary solvation shell structures is challenging, since often-used hydrodynamic theories of molecular

diffusion are strictly not suited for this purpose. Molecular Dynamics (MD) computer simulations, on the other hand, are ideally suited for such studies, especially in combination with experimental results from NMR relaxation time and translational diffusion measurements.<sup>3,6,51</sup> Indeed, Naidoo and co-workers have developed the necessary potential functions and parameters (“force fields”) and performed classical MD simulations for  $[\text{PtCl}_6]^{2-}$  in both water and methanol with the aim of studying the hydration structure and ion-pairing interactions,<sup>52</sup> and recently also dynamic properties in water.<sup>53</sup> The results of similar classical MD simulations aimed at interpreting the measurements presented here are described in the following chapter of this work.

## References

1. Price, W. S. *NMR Studies of Translational Motion*, Cambridge University Press, Cambridge, 2009.
2. Price, W. S.; Ide, H.; Arata, Y. *J. Phys. Chem. A* **1999**, *103*, 448–450.
3. Stilbs, P. *Prog. NMR Spectrosc.* **1987**, *19*, 1–45.
4. Hubbard, P. S. *Phys. Rev.* **1963**, *131* (1), 1155–1165.
5. Steele, W. A. *J. Chem. Phys.* **1963**, *38*, 2404–2418. Moniz, W. B.; Steele, W. A.; Dixon, J. A. *J. Chem. Phys.* **1963**, *38*, 2418–2426.
6. Laaksonen, A.; Wasylshen, R. E. *J. Am. Chem. Soc.* **1995**, *117*, 392–400.
7. Dote, J. L.; Kivelson, D.; Schwartz, R. N. *J. Phys. Chem.* **1981**, *85*, 2169–2180.
8. Martin, N. H.; Issa, M. H.; McIntyre, R. H.; Rodriguez, A. A. *J. Phys. Chem.* **2000**, *104*, 11278–11281.
9. Bakhmutov, V. I. *Practical NMR Relaxation for Chemists*, John Wiley & Sons, Ltd., Chichester, 2004.
10. Pregosin, P. S. *Prog. NMR Spectrosc.* **2006**, *49*, 261–288.
11. Farrar, T. C.; Becker, E. D. *Pulse and Fourier Transform NMR*, Academic Press, New York, 1971.
12. Stejskal, E. O.; Tanner, J. E. *J. Chem. Phys.* **1965**, *42*, 288–292.
13. Harris, R. K.; Becker, E. D.; Cabral de Menezes, S. M.; Goodfellow, R.; Granger, P. *Pure Appl. Chem.* **2001**, *73* (11), 1795–1818.
14. Gee, M.; Wasylshen, R. E.; Laaksonen, A. *J. Phys. Chem. A* **1999**, *103*, 10805–10812.
15. Engström, S.; Jönsson, B.; Jönsson, B. *J. Magn. Reson.* **1982**, *50*, 1–20.
16. Heil, S. R.; Holz, M.; Kastner, T. M.; Weingärtner, H. *J. Chem. Soc. Faraday Trans.* **1995**, *91* (12), 1877–1880.
17. Martinez-Viviente, E.; Ruegger, H.; Pregosin, P. S.; Lopez-Serrano, J. *Organometallics* **2002**, *21*, 5841.
18. Holz, M.; Weingärtner, H.; Hertz, H. G. *J. Chem. Soc. Faraday Trans. I* **1977**, *73*, 71–83.
19. Still, B. M.; Kumar, P. G. A.; Aldrich-Wright, J. R.; Price, W. S. *Chem. Soc. Rev.* **2007**, *36*, 665–686.
20. Nama, D.; Kumar, P. G. A.; Pregosin, P. S. *Magn. Reson. Chem.* **2005**, *43*, 246–250.

21. Westra, A. N., *High Resolution NMR Studies Concerning the Solvation/Hydration and Coordination Chemistry of Pt(II/IV) Compounds*, PhD Dissertation, University of Stellenbosch, 2005.
22. Wu, D.; Chen, A.; Johnson, C. S., Jr., *J. Magn. Reson.* **1995**, *115*, Series (A), 260–264.
23. Antalek, B. *Concepts Magn. Reson.* **2002**, *14* (4), 225–258.
24. Ramsey, N. F. *Phys. Rev.* **1950**, *78*, 699–703.
25. Flygare, W. H.; *Chem. Rev.* **1974**, *74*, 653–687.
26. Farrar, T. C.; Druck, S. J.; Shoup, R. R.; Becker, E. D. *J. Am. Chem. Soc.* **1972**, *94* (3), 699–703.
27. Pesek, J. J.; Mason, W. R. *J. Magn. Reson.* **1977**, *25*, 519–529.
28. Lassigne, C. R.; Wells, E. J. *Can. J. Chem.* **1977**, *55* (6), 927–931.
29. Einstein, A. *Investigations on the Theory of Brownian Movement*, Dover, New York, 1956.
30. Debye, P. *Polar Molecules*, Dover, New York, 1929.
31. Alms, G. R.; Bauer, D. R.; Brauman, J. I.; Pecora, R. *J. Chem. Phys.* **1973**, *59*, 5310–5328.
32. Flygare, W. H.; Goodisman, J. *J. Chem. Phys.* **1968**, *49*, 3122–3125.
33. Foresman, J. B.; Frisch, A. E. *Exploring Chemistry with Electronic Structure Methods*, Gaussian, Inc., Pittsburgh, 1996.
34. See, for example: (a) Sterzel, M.; Autschbach, J. *Inorg. Chem.* **2006**, *45*, 3316–3324. (b) Truflandier, L. A.; Autschbach, J. *J. Am. Chem. Soc.* **2010**, *132*, 3472–3483.
35. Burger, M. R.; Kramer, J.; Chermette, H.; Koch, K. R. *Magn. Reson. Chem.* **2010**, *48*, S38–S47.
36. Nichols, K. B.; Rodriguez, A. A. *J. Phys. Chem. A* **2005**, *109*, 3009–3014.
37. Wasylishen, R. E.; Britten, J. F. *Magn. Reson. Chem.* **1988**, *26*, 1075–1078.
38. Gillies, D. G.; Sutcliffe, L. H.; Williams, A. J. *Magn. Reson. Chem.* **2002**, *40*, 57–64.
39. (a) Mikhail, S. Z.; Kimel, W. R. *J. Chem. Eng. Data* **1961**, *6* (4), 533–537. (b) Corsaro, C.; Spooren, J.; Branca, C.; Leone, N.; Broccio, M.; Kim, C.; Chen, S. H.; Stanley, E.; Mallamace, F. *J. Phys. Chem. B* **2008**, *112*, 10449–10454. (c) Pal, A.; Singh, Y. P. *J. Chem. Eng. Data* **1996**, *41*, 1008–1011. (d) Zheng, P.; Meng, X.; Wu, J.; Liu, Z. *Int. J. Thermophys.* **2008**, *29*, 1244–1256.
40. Marcus, Y. *Ion Properties*, Marcel Dekker, Inc., New York, 1997.
41. Gierer, A.; Wirtz, K. *Z. Naturforsch. A*, **1953**, *8*, 532.

42. Wensink, E. J. W.; Hoffmann, A. C.; Van Maaren, P. J.; Van der Spoel, D. *J. Chem. Phys.* **2003**, *119* (14), 7308–7317.
43. Kovacs, H.; Kowalewski, J.; Maliniak, A.; Stilbs, P. *J. Phys. Chem.* **1989**, *93*, 962–969.
44. Masuda, Y.; Sano, M.; Yamatera, H. *J. Phys. Chem.* **1985**, *89*, 3086–3091.
45. Naidoo, K. J.; Lopis, A. S.; Westra, A. N.; Robinson, D. J.; Koch, K. R. *J. Am. Chem. Soc.* **2003**, *125*, 13330–13331.
46. Sutherland, W. *Philos. Mag. Ser. 6* **1902**, *3*, 161–177.
47. Macchioni, A.; Ciancaleoni, G.; Zuccaccia, C.; Zuccaccia, D. *Chem. Soc. Rev.* **2008**, *37*, 479–489.
48. Virk, A. S.; Torres, A. M.; Willis, S. A.; Price, W. S. *J. Mol. Liq.* **2016**, *214*, 157–161.
49. Marcus, Y. *Ion Solvation*, Wiley-Interscience, Chichester, 1985.
50. Miyoshi, E., M.Sc. Thesis, University of Western Sydney, 2008.
51. Dahlberg, M.; Laaksonen, A. *J. Phys. Chem. A* **2006**, *110*, 2253–2258.
52. Lienke, A.; Klatt, G.; Robinson, D. J.; Koch, K. R.; Naidoo, K. J. *Inorg. Chem.* **2001**, *40*, 2352–2357.
53. Matthews, R. P.; Venter, G. A.; Naidoo, K. J. *J. Phys. Chem. B* **2011**, *115*, 1045–1055.



## 4. Molecular Dynamics Simulation Study of the Solvation of $[\text{PtCl}_6]^{2-}$ and $[\text{PtCl}_4]^{2-}$ in Binary Solvent Mixtures

## Abstract

Molecular Dynamics (MD) simulations can provide detailed information regarding the microscopic structure and dynamics of liquids and solutions, and can predict and assist in the interpretation of experimental results. Naidoo and co-workers recently presented mechanical force fields for the description of simple platinum group metal (PGM) complex anions in classical MD simulations, specifically in aqueous solution, but was also found to describe ion-association processes involving the octahedral  $[\text{PtCl}_6]^{2-}$  in methanol to good effect. The force field of Naidoo and co-workers is extended here for the simulation of  $[\text{PtCl}_6]^{2-}$  and, to some extent, the square-planar  $[\text{PtCl}_4]^{2-}$  in binary mixtures of water and the water-miscible solvents methanol, 2-methoxyethanol and 1,2-dimethoxyethane, with the specific aim of studying proposed preferential solvation phenomena. In all simulations with the standard force field, the platinum complexes are found to be solvated predominantly by water, i.e. appear to be preferentially hydrated, in contrast with the proposed preferential solvation by the organic component in these mixtures as inferred from  $^{195}\text{Pt}$  NMR chemical shift trends by Westra. In a similar series of simulations with ionic charges scaled according to the Molecular Dynamics in Electronic Continuum (MDEC) theory of Leontyev and Struchebukhov, proposed to account for the effect of dielectric screening of charged particles in condensed phases, the preferential hydration of the platinum complexes is attenuated to some extent, allowing the organic components to enter the solvation shell. While the MDEC model does not account for all aspects of electronic polarizability, which has been shown to be important in simulation studies of ion solvation, the results do appear to lend support for the proposed preferential solvation of  $[\text{PtCl}_6]^{2-}$  by the organic component in the binary solvent mixtures, despite technical difficulties in determining accurate solvation shell compositions, possibly related to nature of the organic solvent models. Finally, the rotational and translational dynamics of  $[\text{PtCl}_6]^{2-}$  were studied; while these characteristics were found to follow trends similar to those measured experimentally, they do not compare quantitatively, which is similarly expected to result from the dynamic properties of the solvent models, particularly the TIP3P (Transferable Intermolecular Potential, 3 Point) water component. Consequently, the results of the dynamics study do not support specifically the structural results of either the simulations with standard full or MDEC-scaled ionic charges.

## 4.1 Introduction

### 4.1.1 Molecular Dynamics simulations: some background

Molecular Dynamics (MD) simulation is a computational technique used for generating the evolution over time of a collection of particles, usually a model representing a molecular system, with the aim of studying the macroscopic (average over a large number of particles) physical properties of the system, e.g. solution structure or molecular diffusion processes.<sup>1</sup> MD computer simulations are based on Newton's equations of motion, specifically the time integrals providing the particle trajectories, which ultimately requires that the simulations proceed via finite time steps, the size of which is arbitrary and depends on the system under investigation. Of the different numerical integration methods, referred to as integration schemes or integrators, used in MD simulations, the leap-frog scheme, which calculates positions ( $r$ ) at full ( $\Delta t$ ), and velocities ( $v$ ) interleaved at half time steps, is preferred for its numerical stability and computational efficiency.<sup>2,3</sup> The particle positions at time  $t$  give the force  $F(t)$  acting on them, which is then used to update positions and velocities according to the following scheme ( $m$  is the particle mass):<sup>1</sup>

$$v\left(t + \frac{1}{2}\Delta t\right) = v\left(t - \frac{1}{2}\Delta t\right) + \frac{\Delta t}{m}F(t) \quad (4.1)$$

$$r(t + \Delta t) = r(t) + \Delta t v\left(t + \frac{1}{2}\Delta t\right) \quad (4.2)$$

Classical MD simulations make use of simple molecular models and classical mechanics, or Molecular Mechanics (MM), to compute the interactions between particles at each simulation time step. The computational simplicity of this method allows for simulations of large systems and it is widely used, especially for simulations of biological macromolecules, including lipid membranes, proteins and nucleic acids, but also for studies of liquids and solutions consisting of smaller molecules e.g. structure and dynamics of pure liquids. On the other hand, phenomena studied by classical MD simulation are limited also by this computational simplicity: fast motions of hydrogen atoms cannot be adequately described by classical mechanics, nor can chemical reactions be studied by this technique.<sup>1</sup>

### 4.1.2 Molecular Mechanics

Molecular Mechanics (MM) force fields used in MD simulations consist of a potential energy expression and appropriate parameters for all particles in the simulated system. The potential energy of the system is typically divided into two components:<sup>1</sup> an “intramolecular”, or bonded, and “intermolecular”, or non-bonded, component. Non-bonded interactions can also occur between atoms in the same molecules, but, computationally, this is typically not the case when atoms are in close proximity and their interactions are described by the bonded term.

$$U_{\text{total}} = U_{\text{bonded}} + U_{\text{non-bonded}} \quad (4.3)$$

The former contains terms describing bond stretching and bending (and where applicable torsional) vibrations and are based on harmonic oscillators, while the latter accounts for electrostatic and van der Waals interactions using Coulomb and Lennard-Jones potential functions respectively. Such force fields are empirical, and the necessary force field parameters are typically determined (parameterised) using a combination of experimental data and the results of *ab initio* electronic structure computations. Some examples of force fields currently available for MD simulations include the AMBER,<sup>4</sup> CHARMM,<sup>5</sup> GROMOS<sup>6</sup> and OPLS force fields.<sup>7</sup> These force fields have been parameterised using different parameterisation strategies and may differ in the potential form and particle types present, and also in the treatment of non-bonded interactions between different types of particles or atoms.<sup>1</sup>

Typically, such force fields contain parameters for many different types of particles, often atoms, and bonds or molecular fragments (e.g. parameters describing angle bending) which may be combined for the modelling of a large variety of molecules.<sup>1</sup> This transferability of force field parameters among different molecules is an important feature of the force fields mentioned above and is highly desirable since it allows for the modelling of large biomolecules by combining parameters determined for small model compounds, e.g. alkanes or simple alcohols (parameterised by comparing with experimental properties). While transferability of parameters is often approximate, many molecules may be modelled to good effect using this approach, especially in aqueous solution.<sup>1</sup>

Finally, force fields for classical MD are pair-additive, meaning that the non-bonded interactions of particles are calculated as a sum of pairwise interactions with other particles.

This treatment of non-bonded interactions, however, is not adequate for the description of non-pair additive interactions, most importantly atomic polarizability. While classical force fields do not treat electrons explicitly, polarizable force fields have been developed which aim to include some of the effects of electronic polarizability by introducing additional charged particles representing the electronic degrees of freedom. As will be described later, an important effect of electronic polarizability that is typically not fully accounted for by classical simulations is the dielectric constant of the medium, which reduces the strength of long range electrostatic interactions.<sup>1</sup>

### 4.1.3 More technical aspects of MD simulations

#### 4.1.3.1 Periodic Boundary Conditions and non-bonded interactions

While classical MD simulations allow for the simulation of systems consisting of many thousands of particles, these are still small with a large number of particles on the surface, essentially exposed to vacuum.<sup>1</sup> This situation is highly undesirable when simulating macroscopic systems and is avoided in practice by the application of Periodic Boundary Conditions (PBC), illustrated in Fig. 4.1. This technique essentially involves producing translated replicas of the simulation cell (or “box”), typically surrounding the primary cell in three dimensions, such that a particle, when reaching the boundary of the cell, effectively exits, maintaining its momentum, and enters the cell from the opposite side. However, application of PBC introduces artefacts in simulations of liquids, where long range spatial correlations may be present, but these effects are small for large systems (the effect can, of course, be evaluated by simulating systems of increasing size).<sup>1</sup>

Another important feature of MD simulations in this context is the treatment of non-bonded interactions, which are long-range interactions. The calculation of these pair interactions represents a major computational cost, and since the interaction strength decreases with increasing separation of particles, they are usually truncated, or cut off, at some defined distance. This is true especially of van der Waals interactions, represented by the Lennard-Jones potential (i.e. decreases with increasing distance,  $r$ , as a function of  $r^{-6}$ ), and these are invariably truncated in MD simulations, often gradually, or smoothly, by application of a switching function in the cut-off region. The minimum image convention, requiring that a particle should not interact with its replica image in neighbouring cells, sets limits for these cut-offs given certain cell dimensions, i.e. the cut-off may not exceed half the box length.<sup>1</sup>

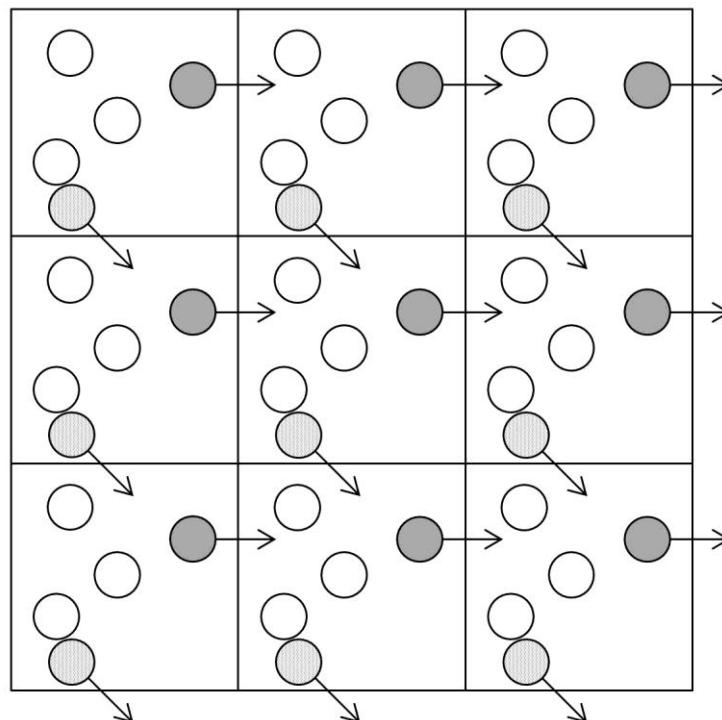


**Figure 4.1** Scheme illustrating periodic boundary conditions (PBC) in two dimensions: a particle encountering the simulation cell boundary enters it from the opposite side.

Electrostatic interactions, however, persist over larger distances and their truncation may result in serious artefacts in simulations; these interactions, then, are usually not truncated, but computed by special long-range electrostatics algorithms such as the Ewald summation or Particle Mesh Ewald (PME) methods.<sup>8,9</sup>

### 4.1.3.2 Temperature and pressure coupling

MD simulations technically produce systems in which the total number of particles,  $N$ , the system volume,  $V$ , and total energy,  $E$ , are conserved, a situation referred to as the micro-canonical, or  $NVE$ , ensemble.<sup>1</sup> However, it is often desirable to perform simulations under conditions of specific constant average temperature,  $T$ , and pressure,  $P$ . Simulations with such fixed macroscopic states can indeed be performed and make use of a variety of temperature and pressure coupling algorithms, giving rise to  $NVT$ , or canonical, and  $NPT$  ensembles.

The Berendsen weak-coupling algorithm<sup>10</sup> couples the system with a heat bath set at the desired, or reference, temperature and corrects for deviations from this reference temperature by coupling with a certain frequency. The temperature deviation of the system decays

exponentially over time, and the algorithm has the advantage that it rapidly relaxes the system to the target temperature (also, the strength of coupling may be set by the user). It does not generate a proper canonical ensemble, however, and while the errors introduced are typically small, it does affect fluctuation properties of the system e.g. heat capacity. The Nosé–Hoover thermostat<sup>11,12</sup> is among the algorithms that do produce a canonical ensemble, and involves a modification of the particles' equation of motion. However, an important difference is that the relaxation is oscillatory, and can induce oscillations in the particle dynamics.<sup>1</sup>

Pressure coupling of the system, i.e. simulations at constant applied pressure, is similarly realised and various barostats are available. The Berendsen algorithm<sup>13</sup> operates by rescaling of cell vectors and coordinates at a specified frequency, and again is highly efficient at reaching the target pressure and maintaining the correct average pressure, but does not generate a proper *NPT* ensemble. The Parrinello–Rahman barostat,<sup>14</sup> on the other hand, is similar to the Nosé–Hoover thermostat and, while it similarly generates a correct ensemble, it may introduce oscillations in the cell dimensions when the system is far removed from the target pressure. It is advisable to first use the Berendsen weak-coupling algorithm and allow the system to reach equilibrium at the target pressure, and then to switch to the Parrinello–Rahman barostat and resume the simulation in the correct *NPT* ensemble.<sup>1</sup>

#### 4.1.4 Aims

The previous two chapters described the results of experimental efforts to study the solvation environment of simple platinum complexes, octahedral  $[\text{PtCl}_6]^{2-}$  and square-planar  $[\text{PtCl}_4]^{2-}$ , specifically dissolved in mixtures of water and selected water-miscible organic solvents. In these solvent mixtures, the complexes are thought to be preferentially solvated by the organic solvent component,<sup>15</sup> yet the interpretation of experimental data is challenging and available theory does not provide direct information on the detailed structure of their primary solvation shells under these conditions.

Molecular Dynamics simulations, on the other hand, are ideally suited for the study of microscopic solution structure, and have been shown to provide important information in this context, notably also in studies of preferential solvation phenomena.<sup>16</sup> Moreover, MD simulations can provide dynamic properties of molecules in solution which may be directly compared with experimental observables, e.g. translational diffusion coefficients, and serve as a means of evaluating the relationship between the results obtained by these techniques. The dynamic properties of solutes are also expected to be influenced by the nature of their surrounding solvation environment, and thus the specific study of these properties may also provide important information in systems where preferential solvation of solutes is thought to occur.<sup>17</sup>

MD force fields for the description of the platinum complexes of interest in pure water have been reported recently;<sup>18-21</sup> these have also been used for simulations in methanol,<sup>20</sup> and it seems reasonable to expect that they should also perform well in simulations in the mixed solvent systems considered in the current study. In this component of the study, classical MD simulations of  $[\text{PtCl}_6]^{2-}$  and  $[\text{PtCl}_4]^{2-}$  in binary mixtures of water with methanol, 2-methoxyethanol and 1,2-dimethoxyethane were performed with the specific aim of studying the detailed solvation structure of these platinum complexes in the context of their proposed preferential solvation by the organic solution component in such mixtures.<sup>15</sup> Dynamic properties of the former complex are also computed from the MD trajectories with the aim of interpreting experimental measurements of these quantities presented in the previous section of this thesis, and it was the intention that this procedure should serve as a means of evaluating the structural simulation results.



## 4.2 Technical details

### 4.2.1 Simulation details

The GROMACS 5.0.5 software package was used for all system preparation, simulation and trajectory analyses reported here.<sup>22</sup> The metal solution force field (MSFF) of Naidoo and co-workers was used to model platinum complexes and ammonium cations.<sup>21</sup> This force field was developed specifically for use with the CHARMM computer program.<sup>5</sup> The potential energy expression for this force field has the following form, where the symbols have their usual meaning; the interested reader is referred to appropriate literature for more information.<sup>1,21</sup>

$$\begin{aligned}
 V = & \sum_{\text{bonds}} \frac{1}{2} k_{ij}^b (r_{ij} - b_{ij})^2 + \sum_{\text{improper dihed.}} \frac{1}{2} k_{\xi} (\xi_{ijkl} - \xi_0)^2 \\
 & + \sum_{\text{atoms}} \frac{q_i q_j}{4\pi\epsilon_0\epsilon_r r_{ij}} + \sum_{\text{atoms}} 4\epsilon_{ij} \left( \left( \frac{\sigma_{ij}}{r_{ij}} \right)^{12} - \left( \frac{\sigma_{ij}}{r_{ij}} \right)^6 \right)
 \end{aligned} \quad (4.4)$$

No angle bending potential terms are included in this function; instead, non-bonded interactions (electrostatic and van der Waals interactions, represented by the Coulomb and Lennard-Jones terms; note that Lorentz–Berthelot combining rules are used in determining the latter) were included for 1,3-bonded neighbouring particles (the chlorine atoms, Fig. 4.2 (a)).<sup>1</sup> As described by Naidoo and co-workers,<sup>18</sup> this procedure maintains the correct molecular geometry and vibrational characteristics. For metal complexes with a square-planar geometry (e.g.  $[\text{PtCl}_4]^{2-}$ ), however, it is necessary to include an additional improper dihedral potential to maintain planarity (Fig. 4.2 (b)); note that this term is included *only* for the square-planar complexes.

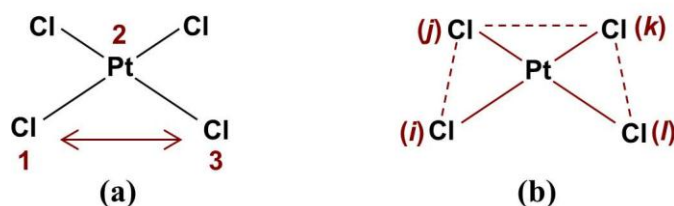


**Figure 4.2** Schemes showing (a) 1,3-nonbonded interaction, and (b) improper dihedral angle, defining offset of molecular planes (i, j, k) and (j, k, l), used to maintain planarity.

Force field parameters were derived by these workers in a manner generally consistent with the usual CHARMM force field parameterisation strategy.<sup>21</sup> The CHARMM36 force field (ported for use with GROMACS<sup>23</sup>) was used for all other molecules, except 2-methoxyethanol for which the special CHARMM ether force field parameters were adapted (note these are “all-atom” force fields).<sup>24,25</sup> The CHARMM variant of the TIP3P water model (“TIP3P” in the GROMACS version) was used to model water.

Systems for simulation were prepared using standard GROMACS programs for generating topologies and coordinates, and consisted of five platinum complexes and ten counter-ions (two types: sodium or ammonium) placed in cubic simulation cells with 2000 solvent molecules to reproduce approximately experimental conditions. Systems were relaxed by the steepest descent energy minimization algorithm, and the potential energy monitored.<sup>1</sup> For simulations the general scheme described by Naidoo and co-workers was followed, using a leap-frog integrator with a 1 fs time step.<sup>21</sup> Simulation settings (neighbour searching and non-bonded interaction cut-offs) were as recommended for use of CHARMM36 in GROMACS 5.0 versions, but with modifications as described by Naidoo and co-workers:<sup>21</sup> bonds involving hydrogen atoms were constrained using the LINCS algorithm<sup>26</sup> (default settings in GROMACS; SETTLE<sup>27</sup> for water); the Verlet cut-off scheme for neighbour searching, with neighbour lists updated every 10 steps; van der Waals interactions were truncated by smoothly switching forces to zero between 1.4 and 1.6 nm (“force-switch” cut-off modifier setting), and electrostatic interactions treated by Particle-Mesh Ewald (PME) summation (default grid spacing, 0.12 nm, and cubic interpolation).<sup>9</sup> Cubic periodic boundary conditions (pbc) were applied in all simulations. Typically, three equilibration simulations, or steps, were performed to stabilise system temperature and density (Fig. 4.3): an initial *NPT* simulation (usually 500 ps) using the Berendsen<sup>10</sup> thermostat (reference temperature 298 K, time constant 0.1 ps) and barostat (reference pressure 1 atm, time constant 1 ps), was followed by a second 2 ns *NPT* step, using the Nosé–Hoover thermostat<sup>11,12</sup> (coupling time 0.5 ps) and Parrinello–Rahman barostat<sup>13</sup> (coupling time 5 ps), in turn followed by a 5 ns *NVT* equilibration step. Production simulations were 40 ns in the *NVT* ensemble with trajectories saved every 0.5 ps. Simulations were performed with mixed precision (previously “single precision”) compilations of the program, which is recommended for most simulations, and trajectory files were converted to a portable format (.xtc file format) for analysis.<sup>1</sup>

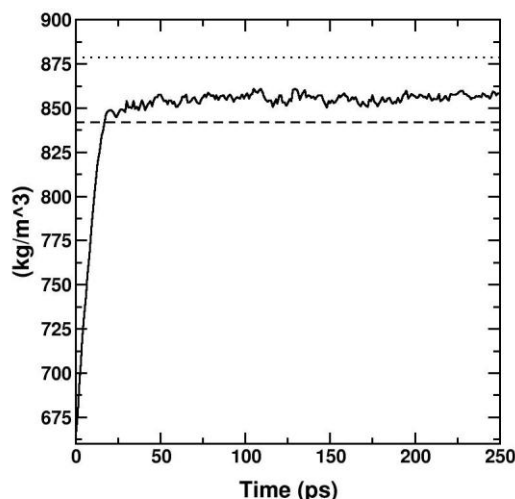


**Figure 4.3** System density in an *NPT* simulation of equimolar water–mixture at 298K, 1 atm. Dashed line indicates density reported by Lin *et al.*<sup>41</sup> for same model combination at 300 K, and the dotted line the experimental density at 298 K. Note the underestimation of about 20 kg/m<sup>3</sup>; similar observations have been reported for other additive force fields.<sup>35</sup>

### 4.2.2 Trajectory analysis

All trajectory analyses were performed using programs provided as part of the GROMACS package.<sup>1</sup> Of particular interest in the present study is the average solution structure around solutes, and the translational and rotational dynamics of these molecules. As described earlier, the structures of liquids and solutions can be described by radial distribution functions (RDFs);<sup>28</sup> RDFs were prepared essentially by partitioning the space around a solute in volume elements, or bins, of width 0.002 nm and accumulating occupancies/particle counts and averaging over the trajectory (GROMACS program “gmx rdf”). Such RDFs, of course, report the radially averaged pair correlation/probability. The three-dimensional structure, or ordering, of e.g. solvent molecules around a solute can be investigated by *spatial* distribution functions, or SDFs, which can be produced by a similar binning procedure, but that involves removal of the rotational and translational motion of the solute (or structure around which the SDF is to be computed) and fitting it to a reference structure.<sup>29</sup> This is done for each frame in the trajectory and the results averaged. The results are usually represented in the form of an iso-density surface, or isosurface, which is simply a collection of points centred on bins having the same (selectable) average occupancy or density.

SDFs are particularly useful in systems where strong and localised interactions between solution components are present, e.g. hydrogen bonding in liquid water, or between water and methanol molecules in mixtures.<sup>29,30</sup> Naidoo and co-workers have produced SDFs for atoms

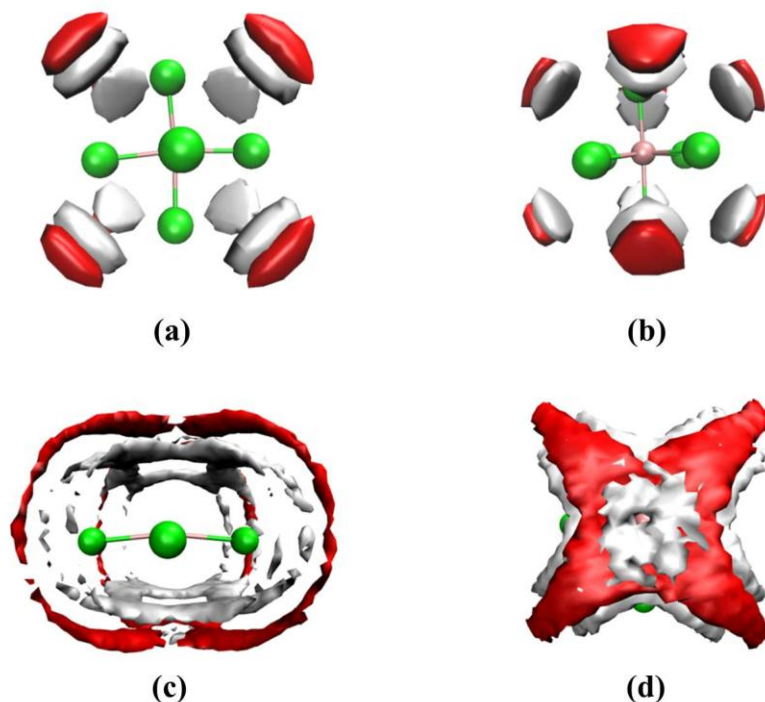


**Figure 4.4** Spatial distribution functions of water atoms surrounding platinum complexes in pure water, with red surfaces corresponding to O, and white surfaces H: [PtCl<sub>6</sub>]<sup>2-</sup> viewed approximately along Pt–Cl bond (a) and angle bisector (b); [PtCl<sub>4</sub>]<sup>2-</sup> along Pt–Cl bond (c) and perpendicular to molecular plane (“top view”) (d). Iso-density thresholds have been chosen so as to best represent the data.<sup>21</sup> Ball-and-stick models are simply representative complex geometries.

of water around platinum group metal chlorido-complexes, and, for the octahedral complexes in particular, have indicated a certain degree of localisation of water molecules on the faces of the octahedron formed by the six chlorine atoms.<sup>19,21</sup> Similar SDFs could be produced from simulations reported here using the GROMACS tool “gmx spatial”.<sup>1</sup> In solvent mixtures in particular, however, these functions were not found to be particularly informative or well-defined due to the diffuse nature of solvation shells. Examples of SDFs of hydrogen and oxygen atoms of water around [PtCl<sub>6</sub>]<sup>2-</sup> and [PtCl<sub>4</sub>]<sup>2-</sup> are shown in Fig. 4.4. Note that in some simulations of platinum complexes, however, SDFs can be highly informative, as shown by the simulation study of differences in the nature of hydration of *cis*- and *trans*-platin complexes by Fu and Tian.<sup>31</sup>

Reorientational correlation times were determined by integration of the corresponding rotational correlation functions (prepared using the program “gmx rotacf”).<sup>1</sup> Different integration schemes are proposed in literature.

$$\tau_l = \int_0^{\infty} \langle P_l[\mathbf{e}(t) \cdot \mathbf{e}(0)] \rangle dt \quad (4.5)$$

Van der Spoel *et al.*,<sup>32</sup> when determining reorientational correlation times of different water models, integrated the first 5 ps of the correlation function explicitly, and determined the integral of the tail by fitting with an exponential function between 5 and 500 ps. Since the platinum complexes considered here rotate much more slowly than water, their rotational correlation functions persist much longer, yet appear completely attenuated by about 200 ps; the integrals were determined explicitly using the trapezium rule. Reorientational correlation times of a number of platinum group metal chlorido-complexes in water were reported by Naidoo and co-workers,<sup>21</sup> presumably by exponential fitting of the rotational correlation function from their simulations; rather short correlation times were reported (even when scaled to account for the high mobility of the TIP3P water model, see subsequent sections), specifically  $\tau_2 < 5$  ps for most complexes. The second-order ( $l = 2$ ) Legendre polynomial representation of the rotational correlation function of  $[\text{PtCl}_6]^{2-}$  in water is shown in Fig. 4.5 (a). Integration of this function by the method described above yields a more reasonable reorientational correlation time  $\tau_2 \sim 5$  ps (298 K), to be compared with the reorientational correlation time derived from NMR spin relaxation time measurements (15 ps).

Translational diffusion coefficients of molecules may be obtained from MD simulations by monitoring the mean square displacement (MSD) or by integration of the velocity autocorrelation function of the molecule.<sup>1</sup> The latter, in particular, requires that trajectories be recorded with high frequency, and was not applicable in the present case. The translational diffusion coefficient is calculated from the mean square displacement using the Einstein relation,<sup>33</sup>

$$6D = \lim_{t \rightarrow \infty} \frac{d}{dt} \langle |\mathbf{R}(t) - \mathbf{R}(0)|^2 \rangle \quad (4.6)$$

Linear regression of the linear region of the MSD yields the translational diffusion coefficient (the slope); as explained by Impey, Madden and McDonald,<sup>34</sup> this procedure is complicated for simulations of ions in solution at low concentrations by poor statistics. The “gmx msd” program of GROMACS computes the translational diffusion coefficient by this procedure and reports an error estimate, which is simply the difference in the diffusion coefficient obtained by fitting two halves of the specified MSD fit interval.<sup>1</sup>

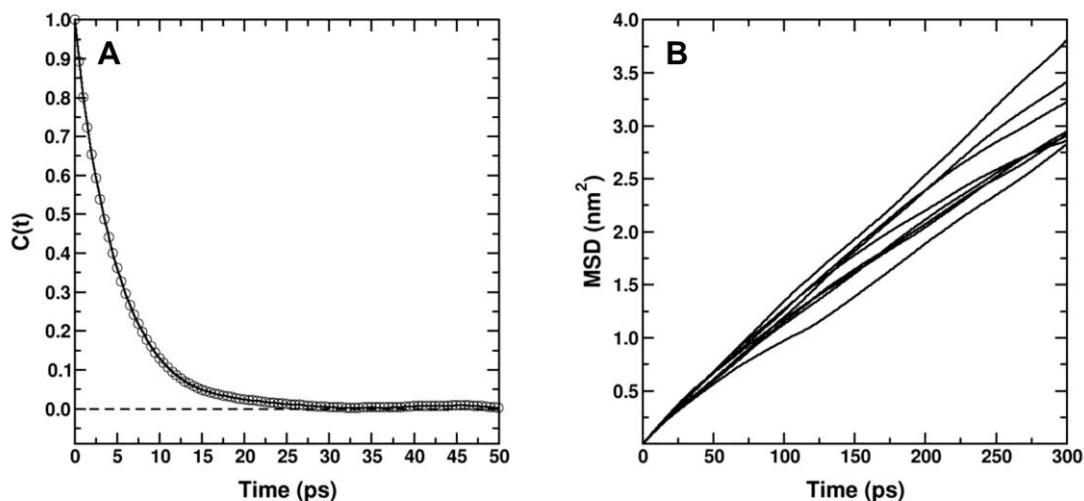


**Figure 4.5** (a) Rotational autocorrelation function of  $[\text{PtCl}_6]^{2-}$  from simulation in pure water at 298 K, and (b) mean square displacement plots for 5 ns simulation blocks used to estimate translational diffusion coefficient, as described in text.

An alternative approach involves plotting the MSD for blocks of the trajectory and calculating an average diffusion coefficient with associated uncertainty (block averaging procedure).<sup>35</sup> Naidoo and co-workers estimated translational diffusion coefficients for the single metal complexes in their 40 ns simulations using this approach: the trajectory was subdivided in blocks of 5 ns, the MSD plotted for each block up to 300 ps, and the diffusion coefficient calculated by linear regression between 50 and 100 ps.<sup>21</sup> The translational diffusion coefficients reported by these workers were very large, owing to the too high diffusion coefficient of the water model, but when appropriately scaled were reported to be in good agreement with experimental estimates; errors in the simulation results were large (~20–30%).<sup>36</sup> The diffusion coefficients reported here were determined by a similar procedure. An example of MSD(t) plots are shown in Fig. 4.5 (b) (note, the MSD is highly non-linear over 5 ns); the average translational diffusion coefficient of  $[\text{PtCl}_6]^{2-}$  in water (298 K) calculated from linear regression of the regions indicated (50–100 ps) is  $1.85 \pm 0.26 \times 10^{-9} \text{ m}^2/\text{s}$ , which is close to that reported by Naidoo and co-workers ( $2.15 \pm 0.55 \times 10^{-9} \text{ m}^2/\text{s}$ ) and, of course, about three times the experimental estimate.<sup>21</sup>

## 4.3 Results and discussion

In this section the different aspects of the simulation results are presented and discussed separately. In the first subsection the structure of the solvation environment of the platinum complexes was investigated using radial distribution functions (RDFs). In the second section the rotational and translational dynamics were investigated and compared with experimental estimates reported in the previous chapter of this work. Considering the nature of the solvent, and in particular water model used in this work, this comparison is only qualitative and involves comparing trends in dynamic properties.

### 4.3.1 Solvation structure

The nature of hydration of simple octahedral and square-planar platinum group metal complexes has been studied extensively in the last decade using MD computer simulations. Naidoo and co-workers,<sup>18–21</sup> in particular, have contributed force fields for classical simulation of several chlorido-complexes, while *ab initio* MD (“aiMD”) simulations have also been reported, notably by Marcos and co-workers<sup>37</sup> and by the group of Autschbach.<sup>38</sup> In such aiMD simulations the interactions between particles are calculated at each time step by *ab initio* electronic structure methods, based on Density Functional Theory (DFT); more information on these methods will be given later. In the present study, however, classical MD simulations were performed using the revised metal solution force field (MSFF) of Naidoo and co-workers.<sup>21</sup>

The Pt–O/H RDFs computed from simulations of octahedral  $[\text{PtCl}_6]^{2-}$  and square-planar  $[\text{PtCl}_4]^{2-}$  in water are given in Fig. 4.6. These functions were reported by Naidoo and co-workers and integrated to obtain hydration numbers of the platinum complexes.<sup>21</sup> The first minima in such solute–solvent RDFs are usually taken to indicate the average boundary of the first solvation shell of the solute (concerning that particular particle pair, of course); these minima are then also the integration limits, or ranges, for determining the solvation, or coordination, number. Note that often RDFs are computed for the centre of mass of a solute/solvent instead.<sup>16</sup> Specifically, the average number of A particles within a radius  $r'$  of a solute S (where  $r'$  may be the first minimum in the S–A RDF) can be computed by the following integral, where  $\rho_A$  is the bulk number density of particle A.<sup>28</sup>

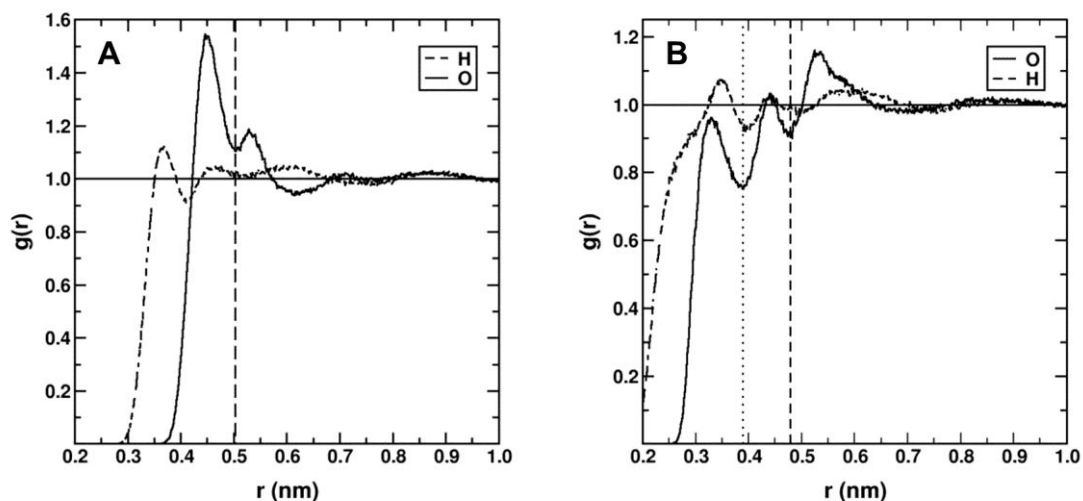


**Figure 4.6** Partial Pt–O/H radial distribution functions from simulations of (a)  $[\text{PtCl}_6]^{2-}$  and (b)  $[\text{PtCl}_4]^{2-}$  in water at 298 K; vertical dashed lines indicate Pt–O integration radii, and dotted line indicates approximate boundary of “meso-shell” region.

$$n_{SA}(r') = \rho_A \int_0^{r'} g_{SA}(r) 4\pi r^2 dr \quad (4.7)$$

The numerical information, positions of minima and corresponding solvation numbers, related to the RDFs in Fig. 4.6 are given in Table 4.1, where the results of Naidoo and co-workers<sup>21</sup> and those from the *ab initio* simulations of Truflandier and Autschbach<sup>38</sup> are also included for comparison. While most values are in generally good agreement, it is interesting to note that the Cl–H coordination numbers computed from the classical simulations (which are in good agreement) are significantly larger than the *ab initio* values for both platinum complexes. The first maxima in the RDFs from the simulation of  $[\text{PtCl}_4]^{2-}$  are important features: these occur at smaller distances than those of  $[\text{PtCl}_6]^{2-}$  and are, of course, due to water molecules occupying the axial regions (either side of the plane formed by the four chlorine atoms) of the square-planar complex. The nature of hydration in these regions, also referred to as the “meso-shell”, has been the subject on a number of recent simulation studies (also experimental), and controversy.<sup>39,40</sup> The hydration number of this complex is estimated by integrating to the *second* minima in the RDFs, i.e. to include both the axial water molecules as well as those in contact with the chlorine atoms.<sup>21,38</sup> The appearance of the meso-shell region of the Pt–O RDF differs markedly from that reported in the previous *ab initio* MD simulation study.<sup>38</sup>



**Table 4.1** Radial distribution function ( $g$ ) maxima positions,  $r_{\max}$ , and integration ranges,  $r_{\text{int}}$ , used in the determination of coordination numbers,  $n$ , for simulations of  $[\text{PtCl}_6]^{2-}$  and  $[\text{PtCl}_4]^{2-}$  in water, with corresponding values from Ref. 21 and 38.

	$[\text{PtCl}_4]^{2-}$			$[\text{PtCl}_6]^{2-}$		
	Current	Ref. 21	Ref. 38	Current	Ref. 21	Ref. 38
$g_{\text{ClH}}(r)$						
$r_{\max}$ (Å)	2.22	2.19	2.29	2.26	2.24	2.28
$r_{\text{int}}$ (Å)	2.84	2.7	2.9	2.80	2.7	2.8
$n_{\text{ClH}}$	4.2	4.1	2.5	2.8	2.6	1.4
$g_{\text{PtO}}(r)$						
$r_{\max}$ (Å)	3.29/4.40	4.38	4.79/4.49	4.49	4.4	4.95/4.64
$r_{\text{int}}$ (Å)	4.83	4.79	5.3	5.03	4.96	5.4 (6.0)
$n_{\text{PtO}}$	10.9	10.9	12.0	10.8	10.1	10.2 (13.8)

A similar set of simulations were performed for the platinum complexes in an equimolar mixture of water and methanol, but with five complexes (and ten sodium counter-ions) and 2000 solvent molecules (1000 each water and methanol). The pair correlation results of these simulations are shown in panels (a) and (b) of Fig. 4.7 and 4.8, with selected numerical data in Table 4.2. While no previous MD simulations of these complexes have been performed in solvent mixtures (or, to the best of our knowledge, for any other transition metal complexes), the solvent model combination used here has been studied in detail by MacKerell and co-workers;<sup>41</sup> these workers show in a comparative study of CHARMM additive and polarizable force fields (see below) that both reproduced several experimental properties of these mixtures reasonably well. No further testing of solvent model combinations was performed in the present study.

The RDFs of different atom pairs (Pt–X) are overlaid for each solvent type in Figs. 4.7/8. Since some atom types have different bulk number densities, their RDFs cannot be directly compared (without considering this stoichiometry), but the relative positions of the various maxima and minima are important, especially in the case of methanol. The expected orientation of both water and methanol in the primary solvation shells of the platinum

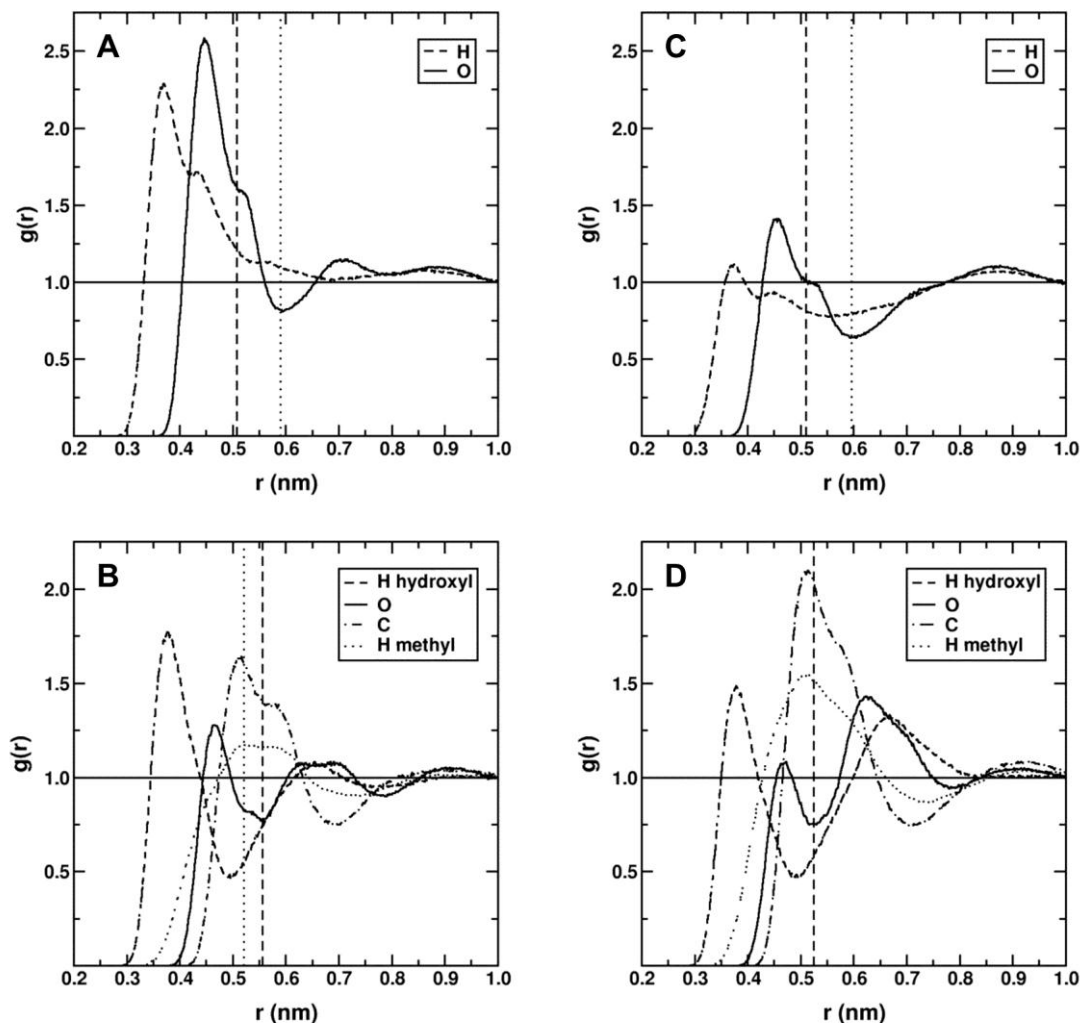


**Figure 4.7** Pt–X radial distribution functions, with X sites in water and methanol indicated in legend, for  $[\text{PtCl}_6]^{2-}$  in equimolar water–methanol mixture at 298 K: RDFs for water (**a**) and methanol (**b**) from simulation with full ionic charges; and, corresponding RDFs, (**c**) and (**d**), from identical simulation with MDEC scaled ionic charges. Vertical dashed lines indicate integration radii for Pt–O RDFs; dotted lines are alternative radii as indicated in Table 4.2. **Note the different  $g(r)$  ranges for the water and methanol plots.**

complexes may be noted, i.e. hydroxyl hydrogen atoms directed inward to the anionic complex, with the methyl group directed outward to the surrounding bulk solvent mixture.<sup>16</sup>

Naidoo and co-workers have performed simulation of  $[\text{PtCl}_6]^{2-}$  in pure methanol, and while aimed specifically at studying ion-pairing interactions, a similar orientation of methanol molecules around the platinum complex is evident in the spatial distribution functions (SDFs) reported by these workers.<sup>20</sup> Further, the appearance of the Pt–H/O RDFs of water in the mixture is similar to those reported above for simulations in pure water. Note, in particular,

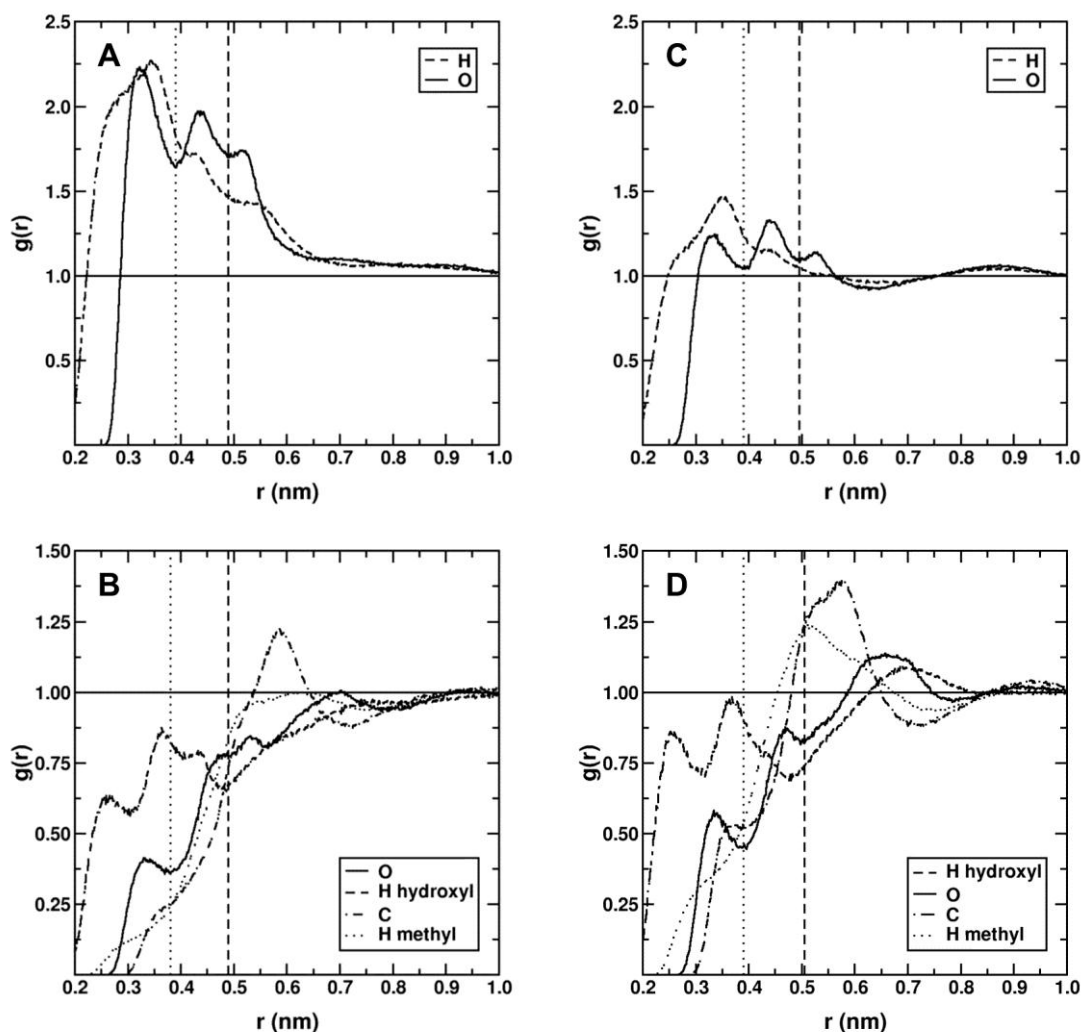


**Figure 4.8** Pt–X radial distribution functions, with X sites in water and methanol indicated in legend, for  $[\text{PtCl}_4]^{2-}$  in equimolar water–methanol mixture at 298 K: RDFs for water (a) and methanol (b) from simulation with full ionic charges; and, corresponding RDFs, (c) and (d), from identical simulation with MDEC scaled ionic charges. Vertical dashed lines indicate integration radii for Pt–O RDFs for calculation of total coordination numbers; dotted lines indicate boundary of “meso-shell” (Table 4.2).

the shoulders on the longer sides of the first maxima of the RDFs from the simulation of  $[\text{PtCl}_6]^{2-}$  that are present also for the complex in pure water; this feature was reported previously.<sup>21,38</sup>

It is clear from the RDFs in Fig. 4.7/8 (a) and (b) that water predominates in the solvation shells of both complexes in the water–methanol mixture; this is confirmed by the solvation numbers in Table 4.2, computed by the procedure described above (using the Pt–O RDFs). The preference of a solute S for a component in a mixture of solvents A and B may be evaluated by comparing the bulk mole fraction of solvent component A,  $x_A$ , which is the total

number of A divided by the total number of solvent molecules A + B, with its *local mole fraction* at a distance  $r$  from S (e.g. the boundary of the first solvation shell) defined similarly as:<sup>28</sup>

$$x_{SA}(r) = \frac{n_{SA}(r)}{n_{SA}(r) + n_{SB}(r)} \quad (4.8)$$

Here,  $n_{SA}(r)$  and  $n_{SB}(r)$  are the numbers of solvents A and B at a distance  $r$  from S, as determined by integration of the appropriate RDFs. The local mole fractions of water and methanol in the first solvation shells of the platinum complexes considered here are reported in Table 4.2.

**Table 4.2** Numerical data related to radial distribution functions in Figs. 4.7/8: RDF maxima,  $r_{\max}$ , and integration ranges,  $r_{\text{int}}$ , for computing coordination numbers,  $n$ . In the case of  $[\text{PtCl}_4]^{2-}$  two numbers are given: that relating to the meso-shell and the total primary coordination shell (indicated with asterisk). Numbers in parentheses refer to alternative integration ranges.

	$[\text{PtCl}_4]^{2-}$		$[\text{PtCl}_6]^{2-}$	
	Standard	MDEC	Standard	MDEC
<b>Water</b>				
$r_{\max}$ (Å)	3.21/4.36	3.32/4.42	4.47	4.53
$r_{\text{int}}$ (Å)	3.90/4.90*	3.90/4.95*	5.08 (5.90)	5.10 (5.96)
$n_{\text{PtO}}$	3.0/7.6*	1.7/4.8*	5.8 (9.7)	3.2 (6.0)
<b>Methanol</b>				
$r_{\max}$ (Å)	3.34/4.77	3.37/4.69	4.65	4.97
$r_{\text{int}}$ (Å)	3.89/4.90*	3.90/5.05*	(5.21) 5.56	5.24
$n_{\text{PtO}}$	0.5/2.1*	0.7/2.8*	(2.9) 4.0	2.6
$n_{\text{total}}$	9.7	7.6	9.8	5.8
$x_{\text{PtO(methanol)}}$	0.22	0.37	0.40	0.45

Westra,<sup>15</sup> in a  $^{195}\text{Pt}$  NMR study of the solvation of  $[\text{PtCl}_6]^{2-}$  in binary mixtures of water and water-miscible organic solvents, reported results indicating preferential solvation of the complex by the organic solvent in all mixtures studied; this was found to be the case also for water–methanol mixtures. The mole fraction methanol in the primary solvation shell, the solvation shell composition, of the platinum complex was estimated by these workers at several bulk solvent compositions based on the  $^{195}\text{Pt}$  NMR chemical shift in the mixture relative to that measured in the pure solvents, assuming also *constant overall solvation number* (eight solvent molecules) at all solvent compositions.<sup>15</sup> Specifically, for an equimolar water–methanol mixture (bulk methanol mole fraction 0.50), the mole fraction methanol in the primary solvation shell (local mole fraction) was reported to be 0.66, which is, of course, higher than the bulk mole fraction of this component, indicating preferential solvation of the platinum complex by methanol. The simulation results in Table 4.2, by contrast, indicate preferential solvation by water, with an average local methanol mole fraction of only 0.4 in the primary solvation shell of this platinum complex. Moreover, the average total solvation number from the simulation, 9.8, is found to be slightly less than that in pure water, 10.8; similar findings have been reported for simulations of monoatomic ions in water–methanol mixtures.<sup>16</sup> Preferential solvation by water and a reduction in the total average solvation number on going from pure water to the equimolar water–methanol mixture is also observed in the simulation of the square-planar  $[\text{PtCl}_4]^{2-}$ , while preliminary  $^{195}\text{Pt}$  NMR chemical shift measurements, presented in an earlier section of this work, suggest that this complex, too, is preferentially solvated by methanol in such mixtures.

A number of recent MD simulation studies indicate that accurate modelling of ion solvation requires the use of polarizable force fields.<sup>42,43</sup> Such force fields account for the electronic polarizability of molecules, and have been shown to be particularly important in reproducing many aspects of hydration of larger anions, specifically those of halides and small polyatomic anions e.g. sulphate and thiocyanate.<sup>44,45</sup> The surface preference of halide ions in water droplets<sup>43</sup> and preference of anions for a water–oil interface,<sup>46</sup> for example, are accurately reproduced only in simulations using polarizable force fields. Different types of polarizable models have been proposed, but these typically include additional interaction sites, intended to mimic the electronic response/degrees of freedom, also making them computationally more demanding compared to the common non-polarizable force fields.<sup>1</sup> The Drude oscillator model is a simple polarizable model in which additional Drude particles, having charge, but essentially no mass, are attached to atoms in the molecule via a harmonic potential (spring).

Recently this model has been implemented in GROMACS simulation package using the extended Lagrangian approach to treat Drude particle dynamics (separate thermostat for Drudes etc.; technical details are described in detail in the recent paper).<sup>47</sup> While these algorithmic developments have resulted in polarizable simulations becoming more practical, and polarizable models are now available in common force fields (e.g. CHARMM; and polarizable water models have been used for decades), models for ions currently available in GROMACS are limited to monoatomic ions, e.g. the chloride anion.<sup>47</sup>

Leontyev and Struchebukhov, in a recent series of articles,<sup>48–50</sup> introduced the Molecular Dynamics in Electronic Continuum (MDEC) theory, which accounts for electronic dielectric screening of ions in the condensed phase, an important consequence of electronic polarization of molecules, practically by scaling of ionic charges in non-polarizable MD simulations (also referred to as Electronic Continuum Correction, or ECC). The authors maintain that while the effects of electronic polarizability are included implicitly (to some extent) in the partial atomic charges in models of non-charged molecules and residues (e.g. TIP3P water model used here), this is not the case for charged species, resulting in their electrostatic interactions in condensed-phase simulations being greatly exaggerated. While molecular dipole enhancement, which increases the strength of electrostatic interactions, is also an important aspect of electronic polarizability for non-charged molecules, the electronic dielectric screening effect (which decreases the strength of such interactions) is the dominant effect for ions and charged groups. The authors show that scaling of formal ionic charges by a factor  $1/\sqrt{\epsilon_{\text{el}}}$ , where  $\epsilon_{\text{el}}$  is the high-frequency dielectric permittivity of the medium, which is related to the refractive index,  $n$ , with  $n^2 = \epsilon_{\text{el}} \sim 2$  for many liquids (1.78 for water), results in appropriate reduction in the strength of electrostatic interactions, consistent with the effect of electronic dielectric screening of the ionic charge by the medium. The interested reader is referred to the original articles by Leontyev and Struchebukhov for the derivation of the theory, as well as for some examples of its application.<sup>48–50</sup> The MDEC theory has been used in a number of recent simulation studies of ions in solution, notably by Jungwirth and co-workers, and was found to reproduce more accurately ion-pairing interactions,<sup>51</sup> and experimental surface and interfacial preferences of anions compared to simulations with full formal ionic charges (standard charges in most force fields).<sup>46</sup>

Accurate modelling of the phenomena mentioned above, e.g. surface preference of anions,<sup>43</sup> is dependent on a detailed balance between solvent–solvent and solvent–solute interactions, and, in the case of ions, electrostatic interactions are particularly important; similarly, it is

expected that preferential solvation in simulations of ions in mixtures of water and organic solvents would require an accurate description of such intermolecular interactions. Leontyev and Struchebrov suggest that the description of electrostatic interactions of ions in condensed phases can be improved by scaling of ion charges as described above.<sup>48–50</sup> In view of the fact that fully polarizable models of most complex ions, and certainly platinum complexes, are not yet readily available, the MDEC approach for the treatment of electronic polarization effects in the form of electronic dielectric screening was investigated in the present preferential solvation study. The charges of all ions were adjusted by multiplying a factor  $1/\sqrt{\epsilon_{el}}$ , using the high-frequency dielectric constant of water  $\epsilon_{el} = 1.78$ , resulting in a reduction of the overall negative charge of the platinum complexes from  $-2$  to  $\sim -1.5$  a.u.

The results of simulations of the platinum complexes with the MDEC scaled charges in equimolar water–methanol mixtures (note that simulated systems were identical, as was the simulation procedure and all settings) are given in panels (c) and (d) of Fig. 4.7/8 and Table 4.2. When comparing the RDFs in Fig. 4.7/8 (c) and (d) with those reported earlier for the standard simulations with full ionic charges (panels (a) and (b)), it is clear that the first, or closest, maxima (Pt–H, Pt–O) for both methanol and especially water are now lower; the positions of these first maxima are not noticeably affected by charge scaling. In the case of square-planar  $[\text{PtCl}_4]^{2-}$ , the first maxima correspond to the so-called meso-shell, and these, together with the second set of maxima are taken to constitute the primary solvation shell.<sup>38</sup> Interestingly, in this meso-shell region, the first maxima of methanol increase slightly in the simulation with MDEC scaled charges. The reduction in the total average solvation number following charge scaling is not unexpected for these platinum complexes; similar findings have been reported by Jungwirth and co-workers in their simulation studies of sulphate anion hydration.<sup>52</sup> The solvation numbers reported in Table 4.2, determined by integration of Pt–O RDFs, show that preferential solvation of the complexes by water persists in MDEC simulations, but is somewhat attenuated compared to that reported for the simulations with full ionic charges.

An interesting feature of the RDFs involving methanol (Fig. 4.7 and 4.8 (b) and (d)) is the enhanced methanol content in the second solvation shells of the complexes, the region  $\sim 0.55$ – $0.8$  nm, following charge scaling. Note also the shoulder on the first (closest) peak in the Pt–C RDFs, suggesting some degree of methyl group association between first and second solvation shells, conceivably with second-shell hydroxyl groups directed on average outward, to the bulk solvent mixture.

Similar sets of simulations, using full and MDEC scaled ionic charges, were performed for  $[\text{PtCl}_6]^{2-}$  in equimolar mixtures of water with 2-methoxyethanol and 1,2-dimethoxyethane (with ammonium instead of sodium counter-ions); the results are presented in Fig 4.9 and 4.10 in the form of Pt–X RDFs, with X selected atom types in the solvent molecule models. In these figures, the RDFs of water and those of the organic components are plotted separately, and the results of simulations with both full and MDEC scaled ionic charges are presented side-by-side. Here, in particular, the RDFs of the different atom types cannot be directly compared since they are normalised to different simulation bulk densities; nevertheless, the positions of maxima/minima and differences in relative intensities for different sets of ionic charges are important. Note that for the organic compounds, only the RDFs for hydrogen atom types are presented, since these sites are expected to interact with the anionic complex most strongly, i.e. occupy primary coordination shell region (note that the 2-methoxyethanol model consists of 6 different atom types).

Considering first the results for the simulation in the equimolar water–2-methoxyethanol mixture with full ionic charges in Fig. 4.9 (a) and (b), the intense first maxima of the water RDFs are striking. The intensities of these RDFs may be directly compared with those of the hydroxyl hydrogen and oxygen atoms of 2-methoxyethanol in Fig 4.9 (b); the water hydrogen and 2-methoxyethanol hydroxyl hydrogen atoms are expected to interact with the anionic platinum complex due to their higher positive charge (+0.42 a.u.), however, evidently the primary solvation shell of the complex consists on average mainly out of water molecules. This phenomenon may be due in part to the smaller size of water models considering the relatively more bulky methyl and methylene groups of 2-methoxyethanol. The hydrogen atoms of these groups have a smaller positive charge (+0.09 a.u.) and their RDFs are rather featureless, with low first maxima at distances greater than what is considered the boundary of the primary solvation shell of the platinum complex (possibly the shoulder on the water RDFs).

An identical simulation, but with MDEC-scaled ionic charges, yields relative RDF intensities which are notably different: a significant reduction of the first maxima of the Pt–water RDFs in the first solvation shell region is accompanied by an increase in the broad Pt–methyl and –methylene hydrogen RDF maxima in the region ~0.4–0.7 nm, with those of the hydroxyl group least affected, but increasing in the region 0.6–0.9 nm, which is well outside the primary solvation shell region. This second maximum is likely due to interactions of 2-methoxyethanol molecules in the primary shell with the bulk solution, i.e. at least two distinct



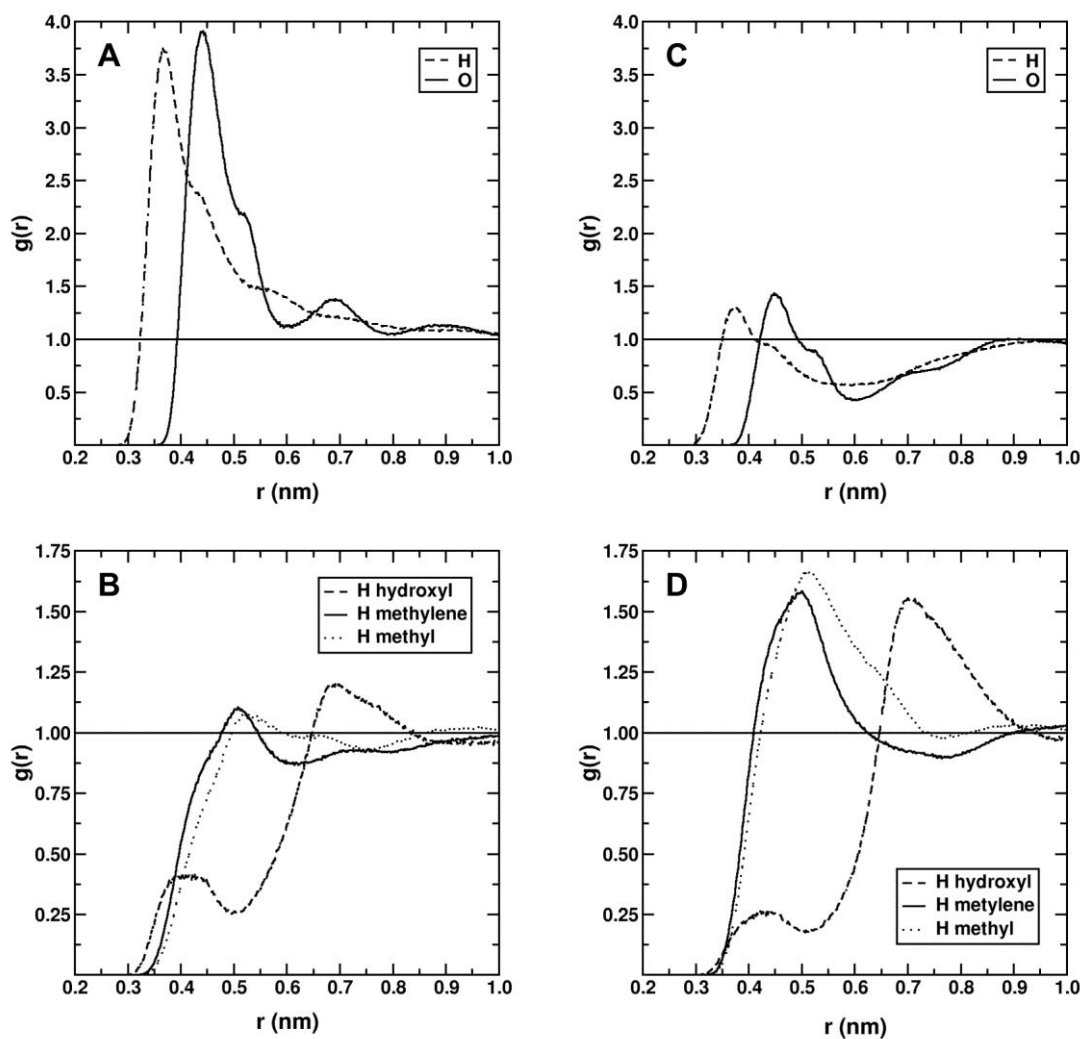


**Figure 4.9** Partial Pt–X radial distribution functions for different sites of (a) water and (b) 2-methoxyethanol (indicated in legend) from simulations of  $[\text{PtCl}_6]^{2-}$  in an equimolar mixture of these solvents at 298 K; panels (c) and (d) show corresponding sets of functions (water and 2-methoxyethanol, respectively) from an identical simulation with MDEC scaled ionic charges. **Note, specifically, differences in  $g(r)$  ranges.**

types of orientations of this molecule are possible when located in the primary solvation shell,<sup>16</sup> namely with hydroxyl group directed towards the platinum complex (first maximum) or outwards, to interact with the bulk solution (second maximum). While it is tempting to integrate the RDFs and determine the total solvation number and local mole fractions as before (water–methanol mixture), differences in the positions of RDF maxima/minima and their broad features, including shoulders, raise uncertainty in determining effective solvation shell boundaries. In particular, the question of whether to include the first RDF maxima of the aliphatic hydrogen atoms as part of the primary solvation shell, and the appropriate

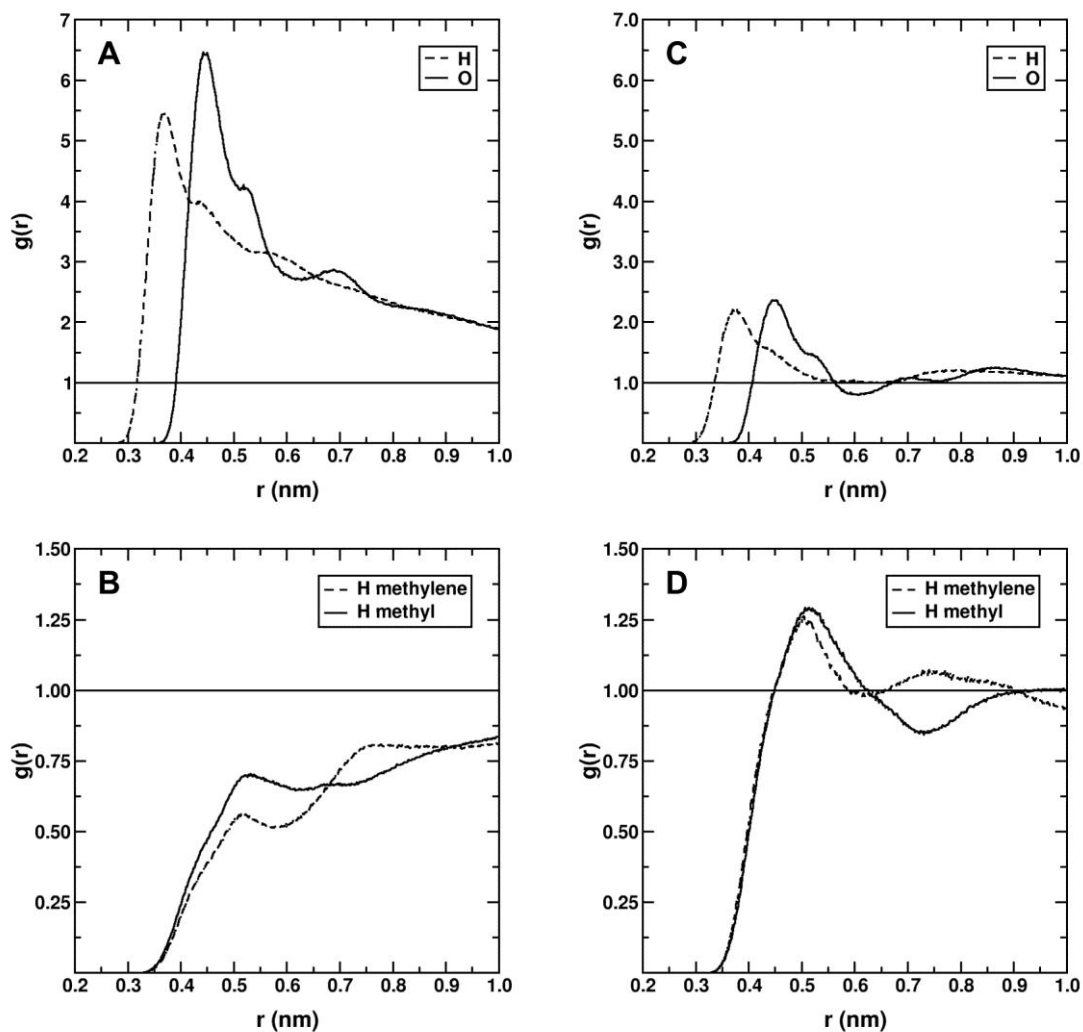


**Figure 4.10** Partial Pt–X radial distribution functions for different sites of (a) water and (b) 1,2-dimethoxyethane (indicated in legend) from simulations of  $[\text{PtCl}_6]^{2-}$  in an equimolar mixture of these solvents at 298 K; panels (c) and (d) show corresponding sets of functions from an identical simulation with MDEC scaled ionic charges.

integration ranges for water and hydroxyl hydrogen and oxygen atoms in these simulations are not clear at present.

Similar phenomena are observed for the simulations in the equimolar mixture of water and 1,2-dimethoxyethane, the model of which differs from that of 2-methoxyethanol in that it does not contain a highly charged hydroxyl group. Here, too, a dramatic difference in solvation shell composition is found on going from a simulation with full ionic charges to that with MDEC-scaled charges. In fact, extensive association, or clustering, of water molecules in the vicinity of the platinum complex are found in the former simulation (note the Pt–water RDF offset from unity up to  $> 1$  nm), which is greatly reduced in the MDEC

simulation, with an increase in the first maxima of the aliphatic hydrogen RDFs of 1,2-dimethoxyethane.<sup>53</sup> Here, too, differences in the positions of first maxima and minima in the RDFs of water and 1,2-dimethoxyethane complicate the quantitative interpretation of results in terms of the primary solvation shell composition. This condition is likely related to the fact that the effective atomic radii of the aliphatic (e.g. methyl and methylene) hydrogen atom types are significantly larger (~0.24 nm) than those of water and hydroxyl groups (0.04 nm) in the CHARMM force field used here;<sup>5</sup> this is also the case for the simulations in the water–2-methoxyethanol mixture discussed above. The implications of such large differences in the effective radii of atoms expected to compete for space in the primary solvation shell of a relatively small solute in the context of preferential solvation have not been investigated to our knowledge.

### 4.3.2 Rotational motion

The rotational diffusion of molecules in solution is characterised by reorientational correlation times, which may be estimated experimentally from NMR relaxation time measurements, among other techniques, or computed from MD simulation trajectories by integration of rotational correlation functions of molecular vectors, e.g. along bonds or angle bisectors.<sup>1</sup> The procedure for computing these correlation times from simulation was described in detail in Section 4.2.2. The second-order Legendre polynomial representation reorientational correlation time (hereafter simply referred to as the reorientational correlation time,  $\tau_2$ ), in particular, is determined in NMR experiments, and was computed for  $[\text{PtCl}_6]^{2-}$  in binary mixtures of water with methanol, 2-methoxyethanol and 1,2-dimethoxyethane (also in pure water) from the trajectories of the two sets (full and MDEC scaled ionic charges) of simulations described in preceding section; the results are presented in Table 4.3, along with experimentally-derived values presented previously. The relevant rotational correlation functions are plotted in Fig. 4.11.

For both sets of simulations, the computed reorientational correlation times can be seen to follow the experimental trend, i.e. in binary mixtures of water and organic solvents, these correlation times increase in the order methanol < 1,2-dimethoxyethane < 2-methoxyethanol. As discussed in the preceding chapter, this trend is not entirely consistent with that expected based on a simple hydrodynamic model (Stokes–Einstein–Debye equation),<sup>55</sup> since the experimental bulk viscosity of an equimolar mixture of water and 1,2-dimethoxyethane is lower than that of pure water, which is lower than that of an equimolar water–methanol mixture under these conditions (i.e. shorter reorientational correlation time expected). The viscosities of simulated solvent mixtures may be calculated using special non-equilibrium simulations, as shown by Wensink *et al.*<sup>35</sup> for mixtures of alcohols and water, however such simulations were beyond the scope of the current investigation; nevertheless, it seems likely that the viscosities of the solvent mixtures modelled should be significantly lower than experiment in view of the too-high mobility of TIP3P water, resulting in reorientational correlation times that are shorter than expected (i.e. solute rotates too rapidly).<sup>32</sup> Indeed, this is observed in the correlation times reported in Table 4.3, the only exception being the simulation with MDEC ionic charges in the equimolar water–2-methoxyethanol mixture, which, surprisingly, doubles on going from full to MDEC charges.

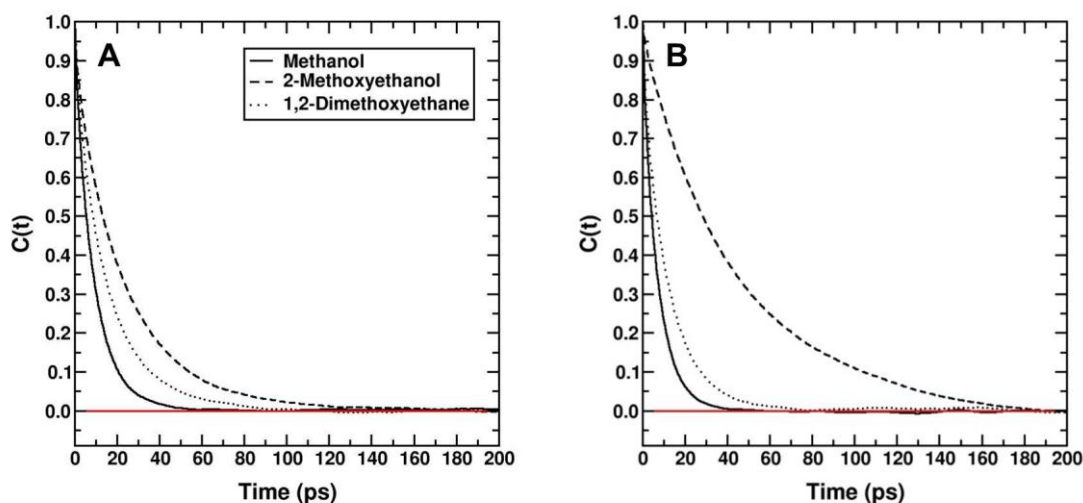


**Figure 4.11** Rotational autocorrelation functions of  $[\text{PtCl}_6]^{2-}$  in equimolar binary mixtures of water with solvent indicated: (a) full ionic charges; (b) MDEC scaled ionic charges.

Interestingly, the reorientational correlation times from simulations with full, standard ionic charges compare more favourably with experimental  $^{195}\text{Pt}$  NMR-derived values than do those from the simulations with MDEC scaled ionic charges. This is unexpected at first, considering the differences in structural results presented in the previous section: the solvation environment of the platinum complex in the latter (MDEC) set of simulations was found to more accurately reflect the primary solvation shell compositions inferred from  $^{195}\text{Pt}$  NMR chemical shift measurements reported by Westra,<sup>15</sup> i.e. preferential solvation by the organic solvent component.

**Table 4.3** Reorientational correlation times of  $[\text{PtCl}_6]^{2-}$  in equimolar binary mixtures of water and co-solvents indicated<sup>a</sup>, from simulations with full and MDEC scaled ionic charges, derived from experimental  $^{195}\text{Pt}$  NMR  $T_1$  relaxation time measurements and predicted on the basis of the Stokes–Einstein–Debye (SED) hydrodynamic continuum model.

Co-solvent <sup>a</sup>	Full charges	MDEC	$^{195}\text{Pt}$ NMR $T_1$	SED
Pure Water	5.0	–	15	28
Methanol	9.0	6.5	16	42
2-Methoxyethanol	22.1	41.7	26	86
1,2-Dimethoxyethane	14.4	11.5	18	25

However, note that the reorientational correlation times reported in Table 4.3 have not been adjusted, or scaled, to account for the too-low viscosities of the solvent mixtures simulated here, and it is expected that, following an appropriate scaling procedure, these should increase to some extent, possibly bringing the MDEC values in closer agreement with experiment (with the exception, of course of the simulation in 2-methoxyethanol, which should be investigated separately in greater detail).

### 4.3.3 Translational motion

Translational diffusion coefficients of molecules may be estimated from MD simulation trajectories by monitoring mean square displacements (MSD) or from velocity autocorrelation functions (VACF);<sup>34</sup> as discussed in Section 4.2.2, the former method was used in the present study. There, the determination of the translational diffusion coefficient of  $[\text{PtCl}_6]^{2-}$  in water was described as an example, and the results were shown to be in good agreement with the original study by Naidoo and co-workers.<sup>21</sup> The effect of the solvent model on the translational mobility of a solute is also shown in this example: the diffusion coefficient of the complex is about three times that measured experimentally, as a result of the too-high mobility of the TIP3P water model.<sup>36</sup>

The translational diffusion coefficient of the complex in equimolar binary mixtures of water with methanol, 2-methoxyethanol and 1,2-dimethoxyethane were determined from the MSD by a similar block-averaging procedure and are given in Table 4.4. An example of the MSD(t) plots used in calculating these values is given in Figure 4.12. As described in Section 4.2.2, the tabulated values are simply average diffusion coefficients of 5 ns blocks of the MD trajectory (40 ns) with corresponding standard errors. The diffusion coefficients can be seen to increase in the order of organic solvent components methanol < 1,2-dimethoxyethane < 2-methoxyethanol, and are all lower than that found in pure water. The relative magnitudes of these diffusion coefficients are qualitatively largely consistent with the experimental bulk viscosities of solvent mixtures, with the exception of the water–1,2-dimethoxyethane mixture, which, under these conditions, has a slightly viscosity lower than that of pure water. A similar trend was found for the reorientational correlation times of the platinum complex in these mixtures in the preceding section.

Naidoo and co-workers,<sup>21</sup> in their simulation study of PGM complexes in water, adopted a scaling procedure for translational diffusion coefficients of solutes at low concentration

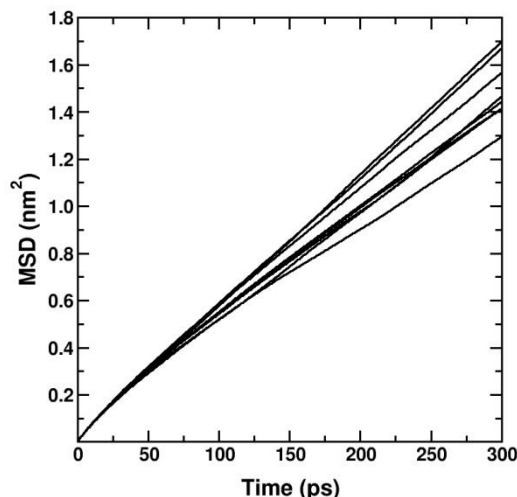


**Figure 4.12** Mean square displacement (MSD) plots over 5 ns intervals used to compute the translational diffusion coefficient of  $[\text{PtCl}_6]^{2-}$  in water–methanol mixture.<sup>21</sup>

proposed by Venable *et al.*;<sup>36</sup> these workers show that scaling of the computed translational diffusion coefficient of a solute by the ratio of the bulk viscosity of model (TIP3P) and real water leads to much improved results when compared with experiment, and also show the procedure to be valid for the range of solute concentrations over which the computed and experimental solution bulk viscosities increase in parallel (with increasing solute concentration). While this scaling procedure may be valid for the diffusion of solutes in pure water at low concentration, such studies have not been extended to binary mixtures of water and organic solvents; however, even if valid, the scaling procedure would require determination of the bulk viscosity of the simulated solvent mixtures, since these are not currently available for the solvent model combinations used here. As discussed in the previous section, this generally requires additional non-equilibrium simulations and is deemed beyond the scope of the current study; the procedure is described in detail by Wensink *et al.*<sup>35</sup> MacKerell and co-workers,<sup>41</sup> in their comparative study of CHARMM additive and Drude polarizable force fields for modelling water–methanol mixtures (the additive force field is used here), found that the diffusion coefficients of both water and methanol were overestimated in the additive model at all mixture compositions, but that the deviation from experiment increased with increasing water content as a result of the TIP3P water model. It is not clear at present how such phenomena affect the diffusion coefficients of solutes in such binary mixtures, especially when these solutes are preferentially solvated by one of the mixed solvent components.

## 4.4 Summary and concluding remarks

A number of MD simulation studies of the nature of solvation of monoatomic solutes in mixtures of water and methanol have been reported in the past two decades.<sup>16,17,56–62</sup> The majority of work in this context involves solutions of sodium chloride, and while preferential hydration of the sodium cation in such mixtures is invariably found, the results for chloride (and other halide anions) are not always consistent. Hawlicka and Swiatla-Wojcik<sup>57,59,60</sup> have reported preferential solvation of halide anions by methanol in such mixtures, while both Day and Patey<sup>16</sup> and Chowdhuri and Chandra<sup>17</sup> have found the chloride ion to be preferentially hydrated. It is important to note that these studies have made use of different combinations of ion and solvent models. MD simulations of simple polyatomic, or complex ions in solvent mixtures, on the other hand, have been rarely reported, certainly with the specific aim of studying preferential solvation phenomena.<sup>63,64</sup>

The results of classical MD simulations of the octahedral platinum complex  $[\text{PtCl}_6]^{2-}$ , described by the revised metal solution force field (MSFF) of Naidoo and co-workers,<sup>21</sup> in binary mixtures of water (TIP3P) with methanol, 2-methoxyethanol and 1,2-dimethoxyethane (CHARMM) were reported in this section.<sup>5</sup> A prominent average preferential solvation of the complex by water (hydration) over the organic component was found in all simulations, in apparent contrast with the results of experimental  $^{195}\text{Pt}$  NMR chemical shift measurements indicating the opposite effect, i.e. preferential solvation by the organic component in these solvent mixtures.<sup>15</sup> In view of recent MD simulation studies highlighting the importance of including effect of electronic polarizability in simulations of ions in solution,<sup>43,46</sup> the simulations were repeated with ionic charges scaled in a manner consistent with the MDEC theory of Leontyev and Struchebukhov.<sup>48–50</sup> This procedure is proposed to account approximately for an important aspect of electronic polarizability: the electronic dielectric screening of charges in condensed phases. The results of simulations with MDEC scaled ionic charges indicate a reduced preference for water in vicinity of the platinum complex in the mixtures studied here. Similar simulations were performed for the square-planar  $[\text{PtCl}_4]^{2-}$  in a mixture of water and methanol, yielding similar structural results, i.e. simulation with MDEC scaled charges results in enhanced competition by solvent components in the local solvation environment of the complex.

However, currently the simulations appear to be complicated by the particular choice of solvent models, within the constraints imposed by the MSFF,<sup>21</sup> which was parameterised



specifically for use in combination with CHARMM TIP3P water. While these solvent model combinations are expected to be appropriately compatible,<sup>24,25,41</sup> at least for the description of properties of their neat mixtures, differences specifically in the effective sizes of hydrogen atom types is expected to affect the average solvation environment of the platinum complex (and possibly other solutes) in a manner that is not yet fully understood. Modifications to the existing solvent models were considered to be beyond the scope of the present study, especially in view of extensive parameter testing required in the proper validation of such modifications, providing scope for future work. Nevertheless, the results presented here seem to support the recent reports of the importance of accounting for electronic polarizability in MD simulations of especially anions in solution.<sup>43,46</sup> While the simple MDEC charge scaling procedure does not account for all aspects of polarizability, and the use of a fully polarizable model is desirable (e.g. Drude model<sup>47</sup>), no such models currently exist for the description of transition metal complexes. It is also interesting to note that, as far as could be determined, no previous MD simulation studies of preferential solvation of ions in fully miscible solvent mixtures have been reported using the MDEC approach to account for the effect of dielectric charge screening.

Finally, dynamic characteristics of the platinum complex in the simulations were computed with the notion of serving as a link with experimental results presented previously, essentially as a means of validating the simulation results. Unfortunately, while the simulations show trends in rotational and translational diffusion of the complex similar to those found experimentally, both with full and MDEC scaled ionic charges, the dynamics of the mixed solvent are too rapid, most likely as a direct consequence of the use of the TIP3P water model which is known to have a too-high translational diffusion coefficient, with the effect transferred also to the solute.<sup>65</sup> Venable *et al.*<sup>36</sup> have presented a scaling procedure for solute diffusion coefficients computed from simulations in pure TIP3P water under conditions of low solute concentration; however, this procedure has not been extended to binary solvent mixtures involving TIP3P water and also requires that the viscosity of the simulated solvent mixture be determined. Moreover, it is not clear at present how discrepancies in the dynamics of solvent components in such binary mixtures affect those of the solute for systems in which the solute is preferentially solvated on the microscopic scale by one solvent component.

## References

1. Abraham, M. J.; van der Spoel, D.; Lindahl, E.; Hess, B.; and the GROMACS development team, *GROMACS User Manual version 5.0.5*, [www.gromacs.org](http://www.gromacs.org), 2015.
2. Verlet, L. *Phys. Rev.* **1967**, *159*, 98–103.
3. Hockney, R. W.; Goel, S. P.; Eastwood, J. J. *Comp. Phys.* **1974**, *14*, 148–158.
4. Cornell, W. D.; Cieplak, P.; Bayly, C. I.; Gould, I. R.; Merz, K. R. Jr.; Ferguson, D. M.; Spellmeyer, D. C.; Fox, T.; Caldwell, J. W.; Kollman, P. A. *J. Am. Chem. Soc.* **1995**, *117* (19), 5179–5197.
5. Vanommeslaeghe, K.; Hatcher, E.; Acharya, C.; Kundu, S.; Zhong, S.; Shim, J.; Darian, E.; Guvench, O.; Lopes, P.; Vorobyov, I.; MacKerell, A. D. Jr. *J. Comput. Chem.* **2009**, *31* (4), 671–690.
6. van Gunsteren, W. F.; Billeter, S. R.; Eising, A. A.; Hünenberger, P. H.; Krüger, P.; Mark, A. E.; Scott, W. R. P.; Tironi, I. G. *Biomolecular Simulation: The GROMOS96 manual and user guide*. Hochschulverlag AG an der ETH Zürich, Zürich, Switzerland, 1996.
7. Jorgensen, W. L.; Maxwell, D. S.; Tirado-Rives, J. *J. Am. Chem. Soc.* **1996**, *118*, 11225–11236.
8. Ewald, P. P. *Ann. Phys.* **1921**, *64*, 253–287.
9. Darden, T.; York, D. Pedersen, L. *J. Chem. Phys.* **1993**, *98*, 10089–10092.
10. Berendsen, H. J. C.; Postma, J. P. M.; DiNola, A.; Haak, J. R. *J. Chem. Phys.* **1984**, *81*, 3684–3690.
11. Nosé, S. *Mol. Phys.* **1984**, *52*, 255–268.
12. Hoover, W. G. *Phys. Rev. A* **1985**, *31*, 1695–1697.
13. Parrinello, M.; Rahman, A. *J. Appl. Phys.* **1981**, *52*, 7182–7190.
14. Nosé, S.; Klein, M. L. *Mol. Phys.* **1983**, *50*, 1055–1076.
15. Westra, A. N. *High Resolution NMR Studies Concerning the Solvation/Hydration and Coordination Chemistry of Pt(II/IV) Compounds*, PhD dissertation, University of Stellenbosch, 2005.
16. Day, T. J. F.; Patey, G. N. *J. Chem. Phys.* **1999**, *110* (22), 10937–10944.
17. Chowdhuri, S.; Chandra, A. *J. Chem. Phys.* **2005**, *123*, 234501-1–234501-8.
18. Lienke, A.; Klatt, G.; Robinson, D. J.; Koch, K. R.; Naidoo, K. J. *Inorg. Chem.* **2001**, *40*, 2352–2357.
19. Naidoo, K. J.; Klatt, G.; Koch, K. R.; Robinson, D. J. *Inorg. Chem.* **2002**, *41*, 1845–1849.

20. Naidoo, K. J.; Lopis, A. S.; Westra, A. N.; Robinson, D. J.; Koch, K. R. *J. Am. Chem. Soc.* **2003**, *125*, 13330–13331.
21. Matthews, R. P.; Venter, G. A.; Naidoo, K. J. *J. Phys. Chem. B* **2011**, *115*, 1045–1055.
22. Pronk, S.; Páll, S.; Schulz, R.; Larsson, P.; Bjelkmar, P.; Apostolov, R.; Shirts, M. R.; Smith, J. C.; Kasson, P. M.; van der Spoel, D.; Hess, B.; Lindahl, E. *Bioinformatics*, **2013**, *29*, 845–854.
23. Bjelkmar, P.; Larsson, P.; Cuendet, M. A.; Hess, B.; Lindahl, E. *J. Chem. Theory Comput.* **2010**, *6*, 459–466.
24. Vorobyov, I.; Anisimov, V. M.; Greene, S.; Venable, R. M.; Moser, A.; Pastor, R. W.; MacKerell, A. D. Jr. *J. Chem. Theory Comput.* **2007**, *3*, 1120–1133.
25. Lee, H.; Venable, R. M.; MacKerell, A. D. Jr.; Pastor, R. W. *Biophys. J.* **2008**, *95*, 1590–1599.
26. Hess, B.; Bekker, H.; Berendsen, H. J. C.; Fraaije, J. G. E. M. *J. Comp. Chem.* **1997**, *18*, 1463–1472.
27. Miyamoto, S.; Kollman, P. A. *J. Comp. Chem.* **1992**, *13*, 952–962.
28. Ben-Naim, A. *Pure Appl. Chem.* **1990**, *62* (1), 25–34.
29. Kusalik, P.G.; Svishchev, I. M. *Science*, **1994**, *265*, 1219–1221.
30. Laaksonen, A.; Kusalik, P. G.; Svishchev, I. M. *J. Phys. Chem. A* **1997**, *101*, 5910–5918.
31. Fu, C. F.; Tian, S. X. *J. Chem. Phys.* **2010**, *132*, 174507–174507.
32. van der Spoel, D.; van Maaren, P. J.; Berendsen, H. J. C. *J. Chem. Phys.* **1998**, *108* (24), 10220–10230.
33. Allen, M. P.; Tildesley, D. J. *Computer Simulations of Liquids*, Clarendon Press, Oxford, UK, 1989.
34. Impey, R. W.; Madden, P. A.; McDonald, I. R. *J. Phys. Chem.* **1983**, *87*, 5071–5083.
35. Wensink, E. J. W.; Hoffmann, A. C.; van Maaren, P. J.; van der Spoel, D. *J. Chem. Phys.* **2003**, *119* (14), 7308–7317.
36. Venable, R. M.; Hatcher, E.; Guvench, O.; MacKerell, A. D. Jr.; Pastor, R. W. *J. Phys. Chem. B* **2010**, *114*, 12501–12507.
37. Beret, E. C.; Martínez, J. M.; pappalardo, R. R.; Marcos, E. S.; Doltsinis, N. L.; Marx, D. *J. Chem. Theory Comput.* **2008**, *4*, 2108–2121.
38. Truflandier, L. A.; Autschbach, J. *J. Am. Chem. Soc.* **2010**, *132*, 3472–3483.
39. Bowron, D. T.; Beret, E. C.; Martin-Zamora, E.; Soper, A. K.; Marcos, E. S. *J. Am. Chem. Soc.* **2012**, *134*, 962–967.

40. Vidossich, P.; Ortuño, M. Á.; Gregori, U.; Lledós, A. *ChemPhysChem* **2011**, *12*, 1666–1668.
41. Lin, B.; He, X.; MacKerell, A. D. Jnr. *J. Phys. Chem. B* **2013**, *117*, 10572–10580.
42. Stuart, S. J.; Berne, B. J. *J. Phys. Chem.* **1996**, *100*, 11934–11943.
43. Caleman, C.; Hub, J. S.; van Maaren, P. J.; van der Spoel, D. *PNAS* **2011**, *108* (17), 6838–6842.
44. Jungwirth, P.; Curtis, J. E.; Tobias, D. J. *Chem. Phys. Lett.* **2003**, *367*, 704–710.
45. Petersen, P. B.; Saykally, R. J.; Mucha, M.; Jungwirth, P. *J. Phys. Chem. B* **2005**, *109*, 10915–10921.
46. Vazdar, M.; Pluhařová, E.; Mason, P. E.; Vácha, R.; Jungwirth, P. *J. Phys. Chem. Lett.* **2012**, *3*, 2087–2091.
47. Lemkul, J. A.; Roux, B.; van der Spoel, D.; MacKerell, A. D. Jr. *J. Comput. Chem.* **2015**, *36*, 1473–1479.
48. Leontyev, I. V.; Struchebukhov, A. A. *J. Chem. Phys.* **2009**, *130*, 085102-1–8.
49. Leontyev, I. V.; Struchebukhov, A. A. *J. Chem. Theory Comput.* **2010**, *6*, 1498–1508.
50. Leontyev, I. V.; Struchebukhov, A. A. *Phys. Chem. Chem. Phys.* **2011**, *13*, 2613–2626.
51. Pluhařová, E.; Mason, P. E.; Jungwirth, P. *J. Phys. Chem. A* **2013**, *117*, 11766–11773.
52. Pegado, L.; Marsalek, O.; Jungwirth, P.; Wernersson, E. *Phys. Chem. Chem. Phys.* **2012**, *14*, 10248–10257.
53. Lexa, K. W.; Goh, G. B.; Carlson, H. A. *J. Chem. Inf. Model.* **2014**, *54*, 2190–2199.
54. Covington, A. K.; Lilley, T. H.; Newman, K. E.; Porthouse, G. A. *J. Chem. Soc. Faraday Trans. I* **1973**, *69*, 963.
55. Dote, J. L.; Kivelson, D.; Schwartz, R. N. *J. Phys. Chem.* **1981**, *85*, 2169–2180.
56. Yoshimori, A.; Day, T. J. F.; Patey, G. N. *J. Chem. Phys.* **1998**, *109* (8), 3222–3231.
57. Hawlicka, E.; Swiatla-Wojcik, D. *J. Mol. Liq.* **1998**, *78*, 7–18.
58. Das, A. K.; Tembe, B. L. *J. Chem. Phys.* **1999**, *111* (16), 7526–7536.
59. Hawlicka, E.; Swiatla-Wojcik, D. *Phys. Chem. Chem. Phys.* **2000**, *2*, 3175–3180.
60. Hawlicka, E.; Swiatla-Wojcik, D. *J. Phys. Chem. A* **2002**, *106*, 1336–1345.
61. Keshri, S.; Sarkar, A.; Tembe, B. L. *J. Phys. Chem. B* **2015**, *119*, 15471–15484.
62. Sarkar, A.; Dixit, M. K.; Tembe, B. L. **2015**, *447*, 76–85.
63. Chaban, V. *Chem. Phys. Lett.* **2014**, *613*, 90–94.
64. Chaban, V. *J. Mol. Model.* **2015**, *21*, 172.
65. Dahlberg, M.; Laaksonen, A. *J. Phys. Chem. A* **2006**, *110*, 2253–2258.

## 5. General Discussion and Conclusions

The nature of solvation and knowledge of chemical speciation reactions of simple anionic platinum group metal (PGM) chloro-complexes in aqueous solution is of both practical importance in the PGM refining industry and more recent fundamental interest. Modern solvent extraction methods for the separation of such PGM complexes are based on the favourable distribution of these complexes between an aqueous process solution and a non-aqueous receptor phase. The development of greener, more efficient methods for the separation of PGMs is expected to benefit from a detailed knowledge of the chemical species distribution and nature of solvation of PGM complex anions in aqueous solution and organic solvent environments. In the case of platinum,  $^{195}\text{Pt}$  NMR spectroscopy has been found to be a powerful tool with which to study speciation reactions and chemical species distributions. The sensitivity of  $^{195}\text{Pt}$  NMR chemical shifts to more subtle solvent effects has also been demonstrated. Westra<sup>1</sup> recently performed a  $^{195}\text{Pt}$  NMR chemical shift-trend study of the solvation of simple octahedral platinum complex anion  $[\text{PtCl}_6]^{2-}$  in binary mixtures of water and a variety of fully water-miscible organic compounds. The results were interpreted in the context of previous NMR studies of the solvation of monoatomic cations in binary solvent mixtures, and were found to indicate *preferential solvation of the platinum complex by the organic solvent component in all mixtures*.

The first aim of this study was to develop  $^{195}\text{Pt}$  NMR techniques for unambiguous speciation commenced in an M.Sc.,<sup>2</sup> and involved the interpretation of  $^{35/37}\text{Cl}$ - and  $^{16/18}\text{O}$ -induced isotope effects in the high-resolution  $^{195}\text{Pt}$  NMR spectra of the series of hydroxido-complexes  $[\text{PtCl}_n(\text{OH})_{6-n}]^{2-}$ ,  $n = 0-5$ , present in alkaline aqueous solution. The spectra of these complexes were found to differ from those of their protonated aquo-analogues  $[\text{PtCl}_n(\text{H}_2\text{O})_{6-n}]^{4-n}$ ,  $n = 2-5$ , in the appearance of partially-resolved spectral fine structure due to isotopomers, complexes having the same chemical structure and isotopic composition, but differing in the relative positions of these isotopes. Specifically, it was found that while for the series of aquo-complexes the signals of isotopomers differing in the combination of  $^{35/37}\text{Cl}$  coordinated *trans* to aquo-ligands are partially resolved, this is not the case for the corresponding hydroxido-complexes under similar conditions. This difference was rationalised by consideration of the expected geometric effects of the Pt(IV) ligand *trans* influence series  $\text{OH}^- > \text{Cl}^- > \text{H}_2\text{O}$ ; specifically, it is proposed that shorter average Pt–Cl bond displacements *trans* to aquo-ligands facilitate the resolution of such isotopomers, while this is not the case for the longer Pt–Cl bonds *trans* to chlorido- and hydroxido-ligands. Additionally, the  $^{195}\text{Pt}$  NMR spectra of the hydroxido-complexes in  $^{18}\text{O}$ -enriched solution

contain fascinating fine structure, which is shown to be due to the partially-resolved signals of both isotopologues, differing in isotopic composition of  $^{35/37}\text{Cl}$  and  $^{16/18}\text{O}$ , as well as *isotopomers* differing in the combination of  $^{16/18}\text{O}$  coordinated in sites *trans* to chlorido-ligands. This assignment was shown to be consistent with the expected geometric effects of the *trans*-influence series given above.

Studies of the hydration (solvation by water) of a number of purely inorganic polyatomic ions using a combination of experimental and computational techniques have been reported; examples include the tetrahedral sulphate and other oxo-anions (e.g. perchlorate), and linear thiocyanate and azide anions. These studies have also been extended, to some extent, to non-aqueous solvents. The solvation of simple transition metal complexes, on the other hand, has not been studied to the same extent, despite increasing interest in the nature of hydration of PGM complexes, particularly square-planar complexes of Pt and Pd, in view of their biological activity in anticancer treatments. Non-aqueous solvents and mixed solvent solutions, in particular, have been rarely studied in this context. A further aim of this study was to obtain independent information regarding the nature of solvation of  $[\text{PtCl}_6]^{2-}$  in binary mixtures of water and selected organic solvents as studied by Westra, specifically methanol, 2-methoxyethanol and 1,2-dimethoxyethane. Experimental work included accurate measurements of  $^1\Delta^{195}\text{Pt}(^{37/35}\text{Cl})$  NMR isotope shifts,  $T_1$  spin relaxation times, to estimate reorientational correlation times of the complex in the various solution environments, and translational diffusion coefficients using  $^{195}\text{Pt}$  pulsed gradient spin-echo (PGSE) experiments. Finally, classical Molecular Dynamics (MD) computer simulations were performed with the aim of obtaining detailed microscopic information on the structure and composition of the primary solvation shell of the platinum complex in such solutions, and to determine dynamic properties for direct comparison with experimental measurements.

The effect of solvent on intrinsic NMR isotope shifts has not been studied in detail in general, but was of interest in the context of this study since the magnitude of this shift is expected to be dependent on the composition of the primary solvation shell of the platinum complex. Results presented here indicate that the  $^1\Delta^{195}\text{Pt}(^{37/35}\text{Cl})$  isotope shift in  $[\text{PtCl}_6]^{2-}$  shows a small, but systematic solvent dependence, increasing in magnitude by  $\sim 7$  ppb in the order pure water < methanol < 2-methoxyethanol < 1,2-dimethoxyethane at 293 K. The accurate measurement of these isotope shifts requires that a model function be fitted to the experimental spectrum, i.e. a signal deconvolution procedure. In equimolar binary mixtures

of water with methanol and 1,2-dimethoxyethane, the small  $^1\Delta^{195}\text{Pt}(^{37/35}\text{Cl})$  isotope shifts were found to be very similar in magnitude to those found in the respective pure *organic solvents*, methanol and 1,2-dimethoxyethane. This observation is qualitatively consistent with the proposed preferential solvation of the platinum complex by these organic compounds. The use of isotope shifts as an indicator of the solvation phenomena is clearly limited in the present case by the relatively small variations with solvent, and possibly because  $^{195}\text{Pt}$  NMR isotope shifts are fundamentally related to the paramagnetic shielding component  $\sigma_p$ , and so are most likely not independent from  $^{195}\text{Pt}$  NMR chemical shift measurements, as shown by Jameson *et al.* for  $^{51}\text{V}$  and  $^{59}\text{Co}$  in certain complexes.

The rotational and translational diffusion characteristics of  $[\text{PtCl}_6]^{2-}$  may also be expected to be influenced by the nature of its interactions with surrounding solvent molecules.  $^{195}\text{Pt}$  NMR  $T_1$  spin relaxation times of the complex in the pure solvents were found to increase in the order methanol < water < 1,2-dimethoxyethane < 2-methoxyethanol. Relaxation time measurements were explored to estimate reorientational correlations times, and interpreted by comparison to predictions of these times from available hydrodynamic models of molecular diffusion; a similar procedure was performed for solutions in equimolar binary mixtures of water with methanol, 2-methoxyethanol and 1,2-dimethoxyethane. Such hydrodynamic models, however, are not necessarily appropriate for the description of solute diffusion in solvent mixtures having complex microstructures, and, more importantly, do not provide direct, detailed microscopic information regarding the solvation environment. The results were nevertheless shown to be notionally consistent with a preferential solvation of the platinum complex by the organic solvent component as postulated. Translational diffusion measurements by  $^{195}\text{Pt}$  PGSE experiments, which have been rarely reported, were found to be demanding, and were restricted to solutions of  $[\text{PtCl}_6]^{2-}$  in pure water, methanol and their equimolar binary mixture. As expected, the results were qualitatively consistent with hydrodynamic predictions, not providing direct information on microscopic solvation phenomena. This component of the study indicated the need for a more sophisticated computational approach to the interpretation of the experimental results, specifically Molecular Dynamics (MD) computer simulations.

Finally, classical MD simulations, using the recently revised MSFF force field of Naidoo *et al.*<sup>2</sup> intended for use in combination with the CHARMM all-atom force field, were performed for  $[\text{PtCl}_6]^{2-}$  in the binary solvent mixtures described above. Initial simulations invariably



indicated a pronounced preference for water (TIP3P) in the primary coordination sphere region, in contrast with the proposed preferential solvation by the organic component inferred from  $^{195}\text{Pt}$  NMR chemical shift trends of Westra.<sup>1</sup> In view of recent reports indicating the importance of including electronic polarizability effects in accurate MD simulations of ion solvation, the series of simulations described above were repeated with *ionic charges* scaled in a manner consistent with the recent MDEC theory of Leontyev and Struchebukhov.<sup>3</sup> This procedure accounts approximately for the effect of electronic dielectric screening, which is an important aspect of polarizability particularly for charged particles in the condensed phase, by reducing the strength of electrostatic interactions. In simulations with MDEC scaled charges, a reduction in the contribution of water to the primary solvation shell of the complex was found in all solvent mixtures, particularly in the case of mixtures with 2-methoxyethanol and 1,2-dimethoxyethane, for which a strong preferential solvation effect (by these organic compounds) is indicated by the  $^{195}\text{Pt}$  NMR chemical shift results of Westra. However, the detailed interpretation of the simulation results is complicated by uncertainties in RDF integration ranges, and also conceptually since the binary solvent components differ significantly in size, with the overall solvation number unlikely to remain constant in such mixtures (compared to that in water). Moreover, polar (in water and hydroxyl groups) and aliphatic (methyl and methylene groups) hydrogen types in the CHARMM force field have different effective sizes, which further complicates interpretation of the simulation results, also since it is unclear how such differences affect the preferential solvation phenomenon in the simulation, and requires a detailed future study. Nevertheless, the results suggest that with proper inclusion of the effects of electronic polarizability, e.g. the use of fully polarizable force fields, the preferential solvation effect proposed by Westra should be more accurately recovered. Such polarizable models are not currently available for platinum, or any other transition metal complexes; the development of such models is recommended as a natural extension of the present study, e.g. as has been done for the sulphate anion. Indeed, as far as could be established, the MDEC approach has not been used for MD simulations of ions, certainly polyatomic ions, in fully miscible solvent mixtures with the specific aim of studying preferential solvation phenomena.

The dynamic properties of the  $[\text{PtCl}_6]^{2-}$  anion obtained from simulation trajectories were found to qualitatively reproduce experimental diffusion trends, but relatively large discrepancies were found which compromise the comparison between the simulation results and experimental measurements. These discrepancies are probably due to the solvent models

used, since the TIP3P water is well-known to overestimate the translational diffusion of pure water, and is expected to carry this effect over to the other solution components. Scaling procedures proposed for the correction of diffusion coefficients computed from simulations in pure TIP3P water may not be applicable in these binary solvent mixtures, particularly when preferential solvation of the solute occurs, and further requires determination of the bulk viscosity of the simulated solvent mixture by special non-equilibrium simulations.

In conclusion, the present study highlights the potential of  $^{195}\text{Pt}$  NMR spectroscopy for providing structural and dynamical information for platinum complexes in solution. Isotope effects in  $^{195}\text{Pt}$  NMR spectra, in particular, may be used for the unambiguous characterisation of such complexes, and potentially for studies of solvation phenomena. The combined experimental and computational results presented in this thesis suggest, however, that studies of preferential solvation of polyatomic anions may be non-trivial in general. Specifically, these require specialised computational work, ideally both MD simulations, using a fully polarizable force field, for obtaining average solvation shell compositions and geometries, as well as dynamic properties for comparison with experiment, in combination with direct *ab initio* computations of electronic properties studied experimentally, e.g.  $^{195}\text{Pt}$  NMR chemical shifts in the present case.

## References

1. Westra, A. N. *High Resolution NMR Studies Concerning the Solvation/Hydration and Coordination Chemistry of Pt(II/IV) Compounds*, PhD Dissertation, Stellenbosch University, 2005.
2. Engelbrecht, L.; Murray, P.; Koch, K. R. *Inorg. Chem.* **2015**, *54* (6), 2752–2764.
3. Matthews, R. P.; Venter, G. A.; Naidoo, K. J. *J. Phys. Chem. B* **2011**, *115*, 1045–1055.
4. Leontyev, I. V.; Struchebukhov, A. A. *J. Chem. Theory Comput.* **2010**, *6*, 1498–1508.

